AD-A194 101 HOT ELECTRON EMISSION IN SEMICONDUCTORS(U) INNSBRUCK 1/2
UNIV (AUSTRIA) INST OF EXPERIMENTAL PHYSICS
E GORNIK ET AL. 25 MAR 88 R/D-4410-EE-01
UNCLASSIFIED DAJA45-84-C-0052 F/G 20/12 NL

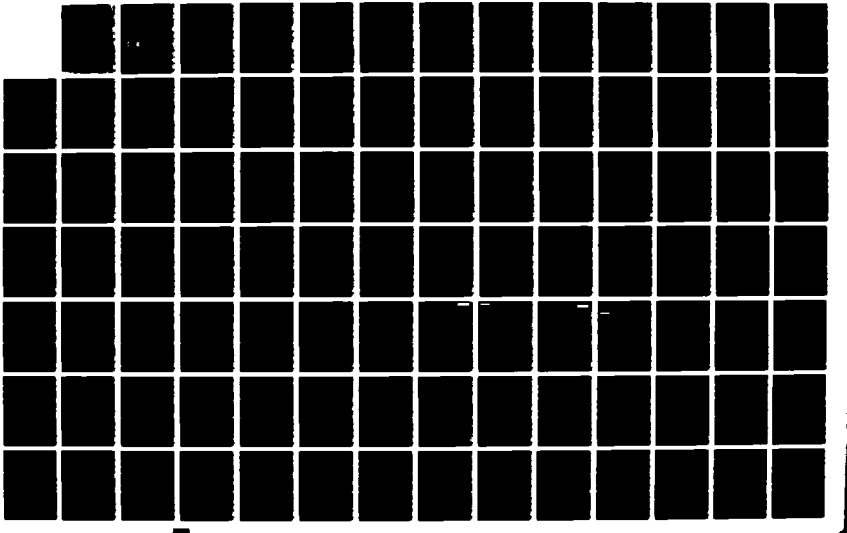

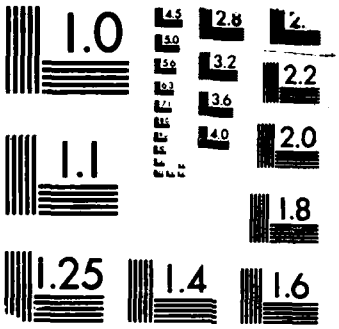

4410-EE.2

"HOT ELECTRON EMISSION IN SEMICONDUCTORS"

FINAL TECHNICAL REPORT

by

E. Gornik and K. Unterrainer
Institut für Experimentalphysik
Technikerstraße 25
A-6020 Innsbruck
AUSTRIA

March 1988

United States Army

RESEARCH & STANDARDIZATION GROUP (EUROPE)
(EUROPEAN RESEARCH OFFICE)
London England

CONTRACT NUMBER: DAJA 45-84-C-0052

Contractor: Prof. Dr. E. Gornik

unclassified

SECURITY CLASSIFICATION OF THIS PAGE (When Data Entered)

REPORT DOCUMENTATION PAGE		READ INSTRUCTIONS BEFORE COMPLETING FORM
1. REPORT NUMBER: 7	2. GOVT ACCESSION NO.	3. RECIPIENT'S CATALOG NUMBER
4. TITLE (and Subtitle): Hot Electron Emission in Semiconductors		5. TYPE OF REPORT & PERIOD COVERED: Final technical report Nov. 26, 1984 - Feb.29,1988
		6. PERFORMING ORG. REPORT NUMBER
7. AUTHOR(s): Prof. Dr. Erich Gornik Dr. Manfred Helm Mag. K. Unterrainer		8. CONTRACT OR GRANT NUMBER(s): DAJA 45-84-C-0052
9. PERFORMING ORGANIZATION NAME AND ADDRESS: Institut für Experimentalphysik A-6020 Innsbruck, Austria		10. PROGRAM ELEMENT, PROJECT, TASK AREA & WORK UNIT NUMBERS
11. CONTROLLING OFFICE NAME AND ADDRESS: USARDSG-UK Box 65, FPO NY 09510		12. REPORT DATE: March 25, 1988 13. NUMBER OF PAGES
14. MONITORING AGENCY NAME & ADDRESS (if different from Controlling Office)		15. SECURITY CLASS. (of this report): unclassified 15a. DECLASSIFICATION/DOWNGRADING SCHEDULE

16. DISTRIBUTION STATEMENT (of this Report)

17. DISTRIBUTION STATEMENT (of the abstract entered in Block 20, if different from Report)

18. SUPPLEMENTARY NOTES

19. KEY WORDS (Continue on reverse side if necessary and identify by block number)

novel tunable FIR sources,
hot electron emission in GaAs/GaAlAs heterostructures,
hot carrier distribution in crossed fields,
stimulated emission from p-Ge in crossed fields

20. ABSTRACT (Continue on reverse side if necessary and identify by block number)

see reverse side

DD FORM 1 JAN 73 1473 EDITION OF 1 NOV 65 IS OBSOLETE

SECURITY CLASSIFICATION OF THIS PAGE (When Data Entered)

The spectrum of the stimulated far infrared emission from p-Germanium in crossed electric and magnetic fields is studied by means of a tunable narrow-band GaAs-detector. A multimode spectrum is observed from polished high parallel samples. The mode spectrum is quantitatively explained in terms of internal waveguide-like modes.

With the help of an external resonator the number of modes was drastically reduced. The external resonator has a confocal configuration. For the first time a single mode operation is demonstrated.

The problem of the electron distribution in crossed electric and quantizing magnetic dields is treated for free electrons in a parabolic band. The master equation for the diagonal elements of the density matrix is solved including the k_z-dependence of the electron distribution. It is shown that population inversion between Landau levels can be achieved if scattering by optical phonons and a quasi-elastic scattering process are taken into account.

The energy relaxation of 2D electrons in GaAs/GaAlAs structures has been investigated by analysing the electric field dependence of Shubnikov-de Haas oscillations, the far infrared emission and photoluminescence spectra. A quite general behavior of the electron heating $\Delta T = T_e - T_L$ as a function of the input power per electron P_e is found: $T \propto \sqrt{P_e}$. The corresponding energy relaxation times in the range of nsec are independent of the electron temperature up to 30 K and inversly proportional to the electron density. At higher electron temperatures the energy relaxation is governed by optical phonon emission. However, the onset depends on electron concentration and is different for heterostructures and quantum wells. From intensity dependent cyclotron resonance transmission experiments Landau level lifetimes between 0.2 ns and 1 ns depending on the electron density are found in agreement with data from time-resolved photoluminescence.

Smith Purcell radiation is coupled out from a drifting 2D-carrier gas with the help of sinusoidal gratings. From the emitted radiation the form of the distribution function can be determined. As a result a drifted Fermi-distribution with rather low temperatures is found at the saturated drift velocity of 2×10^7cm/s.

"HOT ELECTRON EMISSION IN SEMICONDUCTORS"

Principal investigator and contractor

Prof. Dr. Erich Gornik
Institut für Experimentalphysik
Technikerstraße 25
A-6020 Innsbruck
AUSTRIA

Contract Number: DAJA 45-84-C-0052

Final Technical Report
26 November 1984 - 29 February 1988

"The research reported in this document has been made possible through the support and sponsorship of the US Government through its US Army Research and Standardisation Group (Europe). ~~This report is intended only for the internal management use of the contractor and the US Government~~"

CONTENTS

HOT ELECTRON EMISSION IN SEMICONDUCTORS

FINAL REPORT

SUMMARY OF THE SCIENTIFIC WORK

The aim of the project was twofold:

a) A detailed investigation of various emission processes in the far infrared with the technical goal to develope a narrowband and powerful solid state source.

b) The study of the hot electron emission spectra in MOS-type devices to obtain information on the electron distribution function in the 2D channel

Several methods and techniques have been suggested in the proposal. Not all of them have been persued in detail. However, we can state that both claims have been achieved within the project.

The final results are the following:
We were able to repeat as the first group in the western world the findings by a Russian group (Andronov et al.): the generation of stimulated emission from streaming carriers in p-Ge. Our main contribution to this field was the explanation of the multimode structure of the lasing process and the first demonstration of a single mode operation with external mirrors. In addition a fundamental theoretical study was perf.med to explain the electron

distribution under streaming conditions for a single band case.

The also suggested method of generating far infrared emission from 2-dimensional plasma oscillations was not continued further due to requirements which we could not fulfill. It would have been necessary to produce gratings with periods below 1000 A which is beyond the possibilities of our technology. However, we have done an important step forward in this direction by demonstrating for the first time Smith-Purcell radiation from a drifting carrier gas under a periodic grating. The continuation of this work has the potential to produce Bloch-type oscillations in the future.

The analysis of the far infrared emission from MOS-type devices was restricted to GaAs/GaAlAs heterostructures since this system is considered as the candidate for the highest speed devices. We have studied the energy loss rate in GaAs/GaAlAs heterostructures as a function of the electrical input power to get information on the dominant scattering mechanisms at low temperatures. As a result from an analysis of the black body emission we found a sample independent energy loss rate over the input power. This is only valid for electron temperatures up to 40 K where acoustic deformation potential scattering is dominant. For higher electron temperatures optical phonon emission dominates the energy loss. However, there is still some controversy left about the importance of hot phonon effects in the electron temperature range between 50 K and 100 K. The results from the black body emission indicate the influence of hot phonon effects while our most recent work using the analysis of the Smith-Purcell radiation indicates considerably lower electron temperatures and no evidence for hot phonon effects.

One of the main achievements of the project is the observation of the Smith-Purcell radiation from drifting carriers over a periodic grating as mentioned before. We have used the emitted spectrum to determine the hot electron distribution function and the drift velocity in extremely high mobility GaAs/GaAlAs heterostructures. This is the first measurement of the drift velocity in a semiconductor by a purely optical technique. The observed drift velocities are about 10 % lower than derived from current measurements. The electron temperatures at drift velocities close to the saturation velocity are about 50 K, and thus considerably lower than obtained from black body emission experiments ($\approx$ 100 K). As a result we find a drifted Fermi-Dirac distribution function with a large drift energy and low electron temperature.

The final report will consist of two parts:

In Part I the results on stimulated emission from p-Ge will be presented together with a quantum mechanical calculation of the hot carrier distribution function under crossed field conditions.

In Part II the far infrared black body emission from GaAs/GaAlAs heterostructures will be discussed together with the analysis of the Smith-Purcell radiation from drifting carriers under a periodic potential.

Published papers within the project

1. R.A. Höpfel, G. Weimann
Electron heating and free carrier absorption in GaAs/AlGaAs single heterostructures, Appl.Phys.Lett. 41, 291(1985)

2. R.A. Höpfel, E. Gornik, G. Weimann

FIR-Emission from free carrier plasma in GaAs/AlGaAs heterostructures Proceedings of the 17th Int. Conf. on the Physics of Semiconductors, ed. J.D. Chadi and W.A. Harrison, Springer Verlag (1985) p. 579

3. M. Helm, E. Gornik, A. Black, G.R. Allan, C.R. Pidgeon, K. Mitchell

Hot electron Landau level lifetime in GaAs/AlGaAs heterostructures, Physica 134B, 323(1985)

4. M. Helm, E. Gornik

Landau level population inversion in crossed electric and quantizing magnetic fields, Phys.Rev.B34, 7459(1986)

5. E. Gornik

Energy relaxation phenomena in GaAs/GaAlAs structures, NATO ASI series B: Physics Vol.152, p.167, Plenum Press

6. M. Helm, K. Unterrainer, E. Gornik, E.E. Haller

New results on stimulated emission from p-Ge in crossed fields, Solid-State Electronics 31, 759 (1988)

7. K. Unterrainer, M. Helm, E. Gornik, E.E. Haller, J. Leotin

Mode structure of the p-Ge far infrared laser with and without external mirrors: Single line operation, Appl.Phys.Lett. 52, 564 (1988)

8. M. Helm, K. Unterrainer, E. Gornik

Hot carrier quantum distribution function in crossed electric and magnetic fields, Phys.Rev B (to appear in 1988)

9. E. Gornik, R. Christanell, R. Lassnig, W. Beinstingl, K. Berthold, G. Weimann

Analysis of carrier distribution function through Smith-Purcell effect in GaAs/GaAlAs heterostructures, Solid-State Electronics 31, 751 (1988)

Participating Scientific Personal

Prof.Dr. Erich Gornik (Principal Investigator)

Dr. Ralph A. Höpfel

Dr. Manfred Helm (earned Ph.D. during report period)

Mag. Karl Unterrainer (earned Master degree during report period)

Mag. Robert Christanell (earned Master degree during report period)

Dr. Rudolf Lassnig

Dr. Reinhard Berger

Gottfried Strasser

Part I

A) STIMULATED FAR INFRARED EMISSION FROM p-GERMANIUM

Introduction

The distribution function in momentum space is of particular interest in the investigation of hot carriers in external fields. This widely used expression 'hot carrier' implicitly assumes that the distribution function is of quasi - Maxwellian type, characterized by an electron temperature higher than that of the thermal bath. This model corresponds to a quite isotropic distribution function and is justified if scattering events can be regarded as quasi elastic processes. On the other hand, a quite different type of high field phenomena characterized by a highly anisotropic distribution can be obtained, when optical phonon emission predominates over all other scattering mechanisms. In fact, in pure semiconductors at low lattice temperatures it is possible to accelerate a carrier up to an energy equal to the optical phonon energy $\hbar\omega_{op}$. Provided that the optical phonon interaction is adequately strong, the carriers having reached $\hbar\omega_{op}$ will emit almost immediately an optical phonon by dissipating all of its kinetic energy. The carrier, thereby scattered near to the ground state, will be accelerated again to $\epsilon=\hbar\omega_{op}$ and will repeat thereafter the same process until this is interrupted by some other scattering event. Such a repeated motion is called 'streaming motion' and it results in a non - Maxwellian type distribution function /1/.

By applying a magnetic field perpendicular to the electric field a

carrier accumulation in a limited area of the momentum region can occur, which leads to a population inversion /2/. For such a hot carrier system, fascinating effects are theoretically predicted, such as negative differential conductivity in d.c. fields and amplification in the range from mm-wave to far infrared./3/

Several experimental investigations of the streaming effect have been performed in different materials /4/. Hall and current measurements showed a clear evidence for streaming motion and for carrier accumulation /5/. In the p-Ge system it was possible to observe far infrared emission /6/. This opened up the possibility of directly probing the distribution function of the population inverted hot carriers, but also encouraged further seeking for far infrared amplification.

The first report on 'laser like' from p-Ge was reported by a Russian group /7/. Shortly after this report also Komiyama et al. /8/ observed stimulated emission from p-Ge. The observed spectra showed a broad band emission without structure but with a clear threshold behavior. The most recent investigations were devoted to the study of the real mode structure of this new laser process /9/,/10/. At present several groups are persuing the extraction of one single narrow line from the broad band emission spectrum. Since only a single line laser can be used for spectroscopy.

In the first two sections of this report a model for the explanation of the population inversion in p-Ge within the streaming motion picture will be discussed. The experimental methods are explained in the following sections. In the final sections the results are discussed and our recent explanation of the mode structure is presented.

Streaming Motion

Streaming motion is expected under the condition that the optical phonon interaction predominates over all other scattering processes. We will show that such a situation is realized in pure crystals at low temperatures. In ionic crystals the optical phonon scattering is determined by very strong polar optical coupling. In covalent materials ,such as Ge, the carriers interact with the optical deformation potential, which is expressed in the form

$$\tau_{op} = \frac{(D_t K)^2 (m^*)^{3/2}}{\pi\hbar^2 \rho\sqrt{(2\hbar\omega_o)}} \left\{ N_{op} \left[\frac{\epsilon}{\hbar\omega_{op}} + 1\right]^{1/2} + (N_{op} + 1)\left[\frac{\epsilon}{\hbar\omega_{op}} - 1\right]^{1/2} \right\} \quad (1)$$

where the coupling strength $D_t K$ is $9 \cdot 10^8$ eV/cm, the density of the crystal ρ is 5.32 g/cm^3, the effective mass $m^* = 0.043 \cdot m_0$ for the ligth holes and $m^* = 0.35 \cdot m_0$ for the heavy holes. The optical phonon energy is $\hbar\omega_{op}$ = 37 meV. Figure 1 shows the scattering probabilities for a heavy hole in p-Ge at 4.2 K. The interaction is not so strong as in the polar optical case, but the probability of optical phonon emission at kinetic energies equal to the optical phonon energy is still much higher than that due to ionized impurity scattering and acoustical phonon scattering. N_{op} is supposed to be very low at 4.2 K and therefore only the second term (emission term) in eq.1 contributes to the rate. Carrier-carrier scattering is supposed to be unimportant at carrier densities lower than $5 \cdot 10^{14}$ cm^3.

Let us now imagine that a free carrier with an effective mass m^* is at rest at time t = 0. With an electric field applied, the carrier is accelerated in the direction of the electric field with an acceleration rate $\dot{v} = e \cdot E/m^*$.

The velocity of the carrier reaches the critical velocity v_{op}

$$\tfrac{1}{2}m^{*}\cdot v_{op}^{2} = \hbar\omega_{op} \qquad (2)$$

which corresponds to the kinetic energy equal to the optical phonon energy $\hbar\omega_{op}$, at time $t = t_{op}$

$$t_{op} = (2m^{*}\cdot\hbar\omega_{op})^{1/2}/(e\cdot E) \qquad (3)$$

Supposed that E is not too high the carrier will almost immediately emit an optical phonon and return to about the ground state. The carrier will perform a streaming motion with emitting optical phonons after the time interval t_{op}. The drift velocity of an ideally streaming carrier is

$$v_{d} = \tfrac{1}{2}v_{op} \qquad (4)$$

In an actual experimental situation, streaming motion is only possible if the carrier suffers no other scatterings before reaching t_{op}. Therefore the condition

$$t_{op} < \left[\frac{1}{\bar{\tau}_{imp}} + \frac{1}{\bar{\tau}_{ac}}\right]^{-1} \qquad (5)$$

must be fullfilled, where $\bar{\tau}_{imp}$ and $\bar{\tau}_{ac}$ are scattering rates for impurity and acoustical phonon scattering, averaged for energies smaller than the optical phonon energy. From eg.3 and eq.4 the condition for the lower limit of the electric field E_{min} results. On the other hand, to justify the expression 'immediatly scattering' the electric field should not exceed a maximum limit E_{max}, which Komiyama /11/ tried to estimate in the following rough measure

$$t_{op} = \tau_{op}(1.1\cdot\hbar\omega_{op}) \qquad (6)$$

where $\tau_{op}(\epsilon)$ is the optical phonon scattering probability for the energy ϵ. Thus streaming motion is expected in the range $E_{min} < E < E_{max}$. Table 1 shows characteristic quantities for streaming motion in different materials.

When a transverse magnetic field $\vec{B} = (0,0,B)$ is applied to an ideally streaming carrier in an electric field $\vec{E} = (E,0,0)$, the trajectory of

streaming is curved due to the Lorentz force. The free motion of the carriers is described by the classical equation

$$m\frac{d}{dt}\vec{v} = e\cdot(\vec{E} + \vec{v} \times \vec{B}) \qquad (7)$$

The motion of the carriers is a cyclotron orbit with the center at C = (0,-E/B,0) in velocity space (see Fig. 1). The motion in real space is a 'cycloid motion' with a mean drift velocity v_d = -E/B in y-direction. To take into account for the interaction with the optical phonon interaction it is useful to introduce the normalized field ξ

$$\xi = v_{op}\cdot B/E \qquad (8)$$

which specifies the position of the center of the cyclotron orbit relative to the circle $|\vec{v}| = v_{op}$. At this circle the motion of the carrier is interrupted by optical phonon emission and scattered back to $\vec{v}$ = (0,0,0). The trajectory of the ideally streaming carriers is called the 'main trajectory'

If $\xi < 1$, point C is situated outside the circle $|\vec{v}| = v_{op}$. For $\xi > 1$, the point C lies inside the circle. For $\xi > 2$, the main trajectory is closed within the circle $|\vec{v}| = V_{op}$ and streaming motion becomes prohibited. In the last two cases a round area is formed around C (indicated by the shaded area in Fig. 1), in which the trajectories of the cyclotron oscillation do not cross the circle $|\vec{v}| = v_{op}$: A carrier in this area, if present, performs a sustained cyclotron oscillation and drifts along the y-direction in real space. In the case of ideally streaming for $1 < \xi < 2$ this 'passive' region is expected to be empty, as the main trajectory is outside of this area. In a real experiment, however, a few carriers may be occasionally scattered into this area by optical phonon emission after an adequately penetration into the high energy range $|\vec{v}| > v_{op}$. Carriers, once scattered into this region, stay there till removed by other scattering processes; as a consequence a carrier accumulation is formed in this area. In an early theoretical paper Meada and

Kurosawa /2/ obtained a significant accumulation of heavy holes in this region for p-Ge.

Population Inversion and Far Infrared Emission

In p-type Ge the ligth and heavy lole bands are degenerate at the band edge. In the case of a carrier accumulation far infrared emission can be expected in a wide frequency range(Fig. 2). Under the special condition $\xi^h < 1 < \xi^l$ (h for heavy, l for ligth hole band) an accumulation takes place only in ligth hole band and streaming in the heavy hole band. The light hole accumulation is addionally increased by scattering induced redistribution of carriers from the heavy hole band. This accumulation can lead to a population inversion between the ligth and heavy hole bands in momentum space. In thermal equilibrium the ratio of the populations is $n^l/n^h = (m^l/m^h)^{3/2}$. In the above situation this is changed to $n^l/n^h = (m^l/m^h)^{3/2} \cdot (\bar{\tau}^l/t^h_{op})$, where $\bar{\tau}^l$ is the life time of the holes in the accumulation area and t^h_{op} is the optical phonon scattering time of the heavy holes. For the situation $\xi^h < 1 < \xi^l$, the life time of the ligth holes is assumed to be larger then the heavy hole scattering time. Therefore a population inversion is built up. Far infrared emission is expected due to transitions between the ligth and heavy hole bands. Assuming parabolic bands the maximum energy ϵ_{max} of the emission is given when the light hole energy reaches the optical phonon energy.

$$\epsilon_{max} = (1/2m^l - 1/2m^h)(k^l_{op})^2\hbar^2 \qquad (9)$$

$$(1/2m^l)(k^l_{op})^2\hbar^2 = \hbar\omega_{op} \qquad (10)$$

Fig. 1

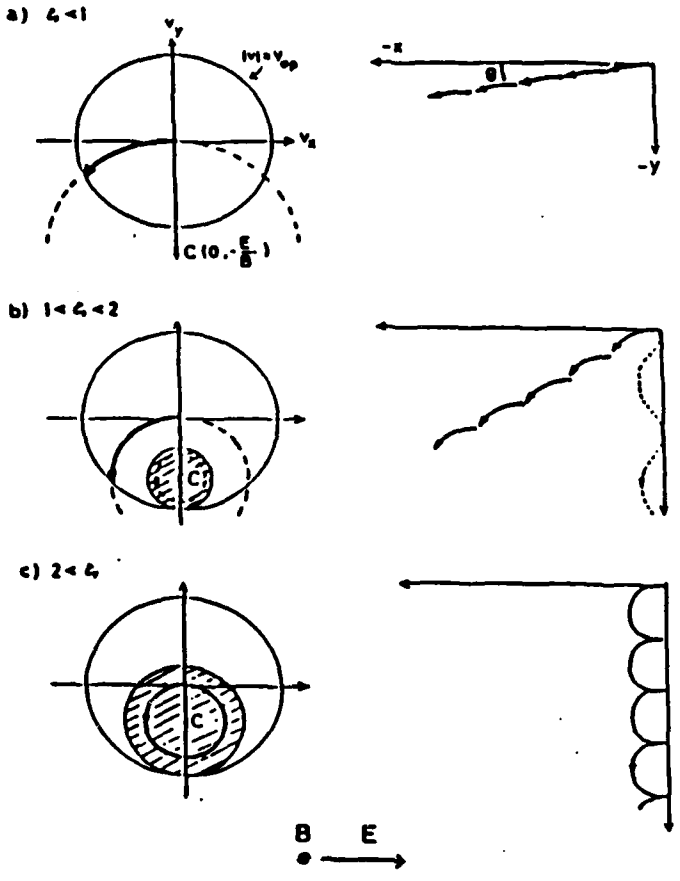

Fig. 2

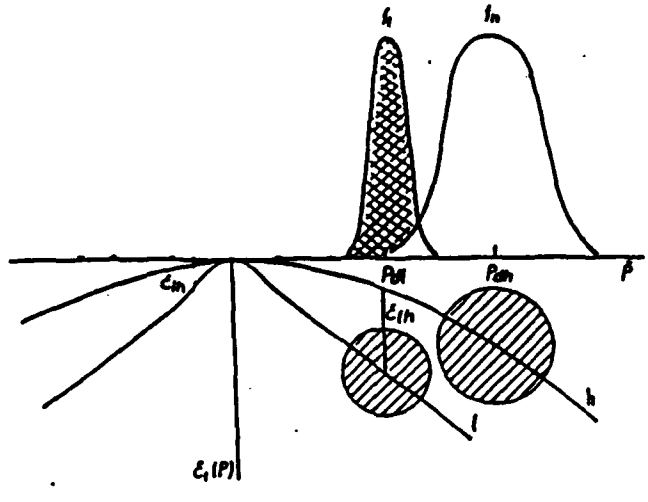

Fig. 1: Classical motion of carriers in crossed fields in velocity and real space for different values of ξ.

Fig. 2: Valence bandstructure of Ge and drifted distribution functions of heavy and light holes.

For p-Ge the maximum energy ϵ_{max} = 32.5 meV. This type of population inversion is of particular interest, since it occurs in the continuum of the energy bands, in contrast to the usual population inversion realized between discrete energy levels in many existing laser systems.

For a calculation of the gain for far infrared amplification it is necessary to know the distrubtion functions of both carrier types. In addition other absorption processes have to be considered, e.g. free carrier absorption. Pozhela et al./12/ used Monte Carlo simulations to get realistic distribution functions and from them, he calculated the emission and reabsorption to get a gain of about 0.05 cm^{-1}. This is a rather low gain. This implies a high quality factor of the resonator to achieve stimulated emission.

Experimental Methods

The crystals of p-Ge used in this work are Ga doped having a concentration $p = |N_A - N_D| = 1.1 \cdot 10^{14}$ cm^{-3}. The resistivity at room temperature is 25 Ωcm. The sample parameters have to be choosen to achieve high gain. For a too high concentration streaming motion becomes impossible as impurity scattering will become dominant. The concentration $p = 1.1 \cdot 10^{14}$ cm^{-3} seems to compromise with both requirements. The samples are cut from the crystal with a wire saw, cleaned with triclorethylene, acetone and propanol and finally etched with CP4.

The sample dimensions are about 5 × 1 × 0.5 mm^3. For making contacts In is evaporated to the end faces and thereafter alloyed at 400 °C for 5 min.

The experiments are performed in a helium cryostat with two superconducting magnets with the sample placed in the middle of the upper magnet. For the current and spontaneous emission measurements the electric

field is applied by a cable discharge pulser with 50 Ω impedance and a maximum output voltage of 1000 V. The pulselength is 1 μsec to avoid sample heating, the repetition rate is tunable between 10 and 100 Hz. The current through the sample is measured by a series resistance, which is also immersed in liquid helium. For the emission experiments the far infrared is guided by a 10 mm bore brass ligth pipe to different detectors, which are placed in the same cryostat in the middle of the lower magnet. A Ga doped Ge-detector is used as a broad band detector with a peak sensitivity around 100 μm. The spectra of the emission are investigated with a GaAs-detector. The energy of the $1s \rightarrow 2p_+$ impurity transition is linearly tunable in a wide range by a magnetic field, the linewith is 0.25 cm^{-1} /13/. An InSb-cyclotron resonance detector is addionally used for spectroscopy. All detectors are driven in a constant current operation, the photoconductive signal is preamplified and thereafter integrated by the Boxcar integrator.

For stimulated emission the sample dimensions have to be larger and the side faces have to be paralell within 30". This processing is done by a comercial company for infrared lenses. Contacts are made in the same way as described above. For lowering the surface resistance and to secure the homogenity of the electric field copper plates are soldered to the contact sides. Copper wires are connected to these plates. The copper plates serve also as sample holder to keep the sample in an upright position and in the center of the magnet. The angle of total reflection for Ge (n=4) is only 15^o. As a result a resonator is formed by internal total reflections at the sample surfaces if the side faces are polished. The laser mode will be similar to wave guide like mode. The sample dimensions have to be quite big

($50 \times 5 \times 5$ mm^3) for this type of laser. As a consequence the sample impedance is very low (about 2Ω): The current denisity is $j = n \cdot e \cdot v_d \simeq 200$ A/cm^2, for $n = 1.1 \cdot 10^{14}$ cm^{-3} and $v_d = 1 \cdot 10^7$ cm/s. For a contact area of 5×0.5 cm^2 the current through the sample is about 300 A. To realize an electric field $E > E_{min}$ we have to apply voltages of about 1000 V. This means for a sample resistance of about 2 Ω a required electrical power of 200 kW. We use a specially designed thyratron tube pulse generator which supplies 5000 V into 25 Ω. An impedance transforming network is used in connection with a triax cable operated between outer and inner shielding (impedance $\simeq$ 10 Ω) to match the low impedance of the sample. The pulse length is 1 μs and the repetiton rate about 10 Hz, for heiger rates lasing breaks down due to sample heating.

To enhance a longitudinal mode two approaches have been used:

a) evaporation of metal films to the end faces of the sample so that they can serve as mirrors

b) attachment of external mirrors with controlled reflectivity

In the first case we evaporated CaF_2 as an insulation layer and thereafter 1000 A Au for the 100% reflective mirror and 150 A Ni-Cr for the semitransparent one. In the second case external mirrors are used in a confocal geometry: One mirror is plane and coated with 1000 A Au on one side to serve as 100% reflectivity mirror. The second mirror is plano convex and its curved surface is coated with different thicknesses of Cr. The different mirror reflectivities were measured with a CO_2 pumped FIR-gas laser and a Golay - detector to be between 80% and 97%. The external mirrors are attached to the sample with silicone oil and fixed with nail enamel.

Results and Discussion

The measurements of the current through the samples show the expected behavior: For a constant applied voltage magnetic field the current increases sligthly with increasing magnetic field until $\xi^h = 1$, where a small maximum occurs; for $\xi^l > 1$ the current decreases as the carriers start to accumulate. This behavoir is a clear proof that our concentration is low enough to enable streaming motion.

Fig. 3 shows typical results of the spontaneous far infrared emission, investigated with a Ge(Ga)-detector. The magnetic field is varied, the different traces belong to different applied fields. The signal increases, as the ligth holes start to accumulate ($\xi^l = 1$). The maximum is between $\xi^h = 1$ and $\xi^h = 2$, where the heavy holes are in a situation between streaming motion and accumulation. For higher magnetic fields the signal decreases as an increasing amount of heavy holes are in the passive region.

Encouraged from the streaming behavior evident from the spontaneous emission data, a Russian group /7/ and Komiyama et al./8/ observed stimulated emission with rather long samples without mirrors. The observed spectra showed a clear threshold behavior for lasing. However the spectra were quite broad and showed many unexplained peaks. The mode of the lasing was not clear at this point. At this stage we also tried to obtain lasing in samples which showed clear evidence for streaming. However we could not observe lasing. The reason was that the reflectivity was too low.

In experiments with larger samples (50 × 5 × 5 mm) we were able to observe stimulated emission even without mirrors. Fig. 4 shows the magnetic

Fig. 3

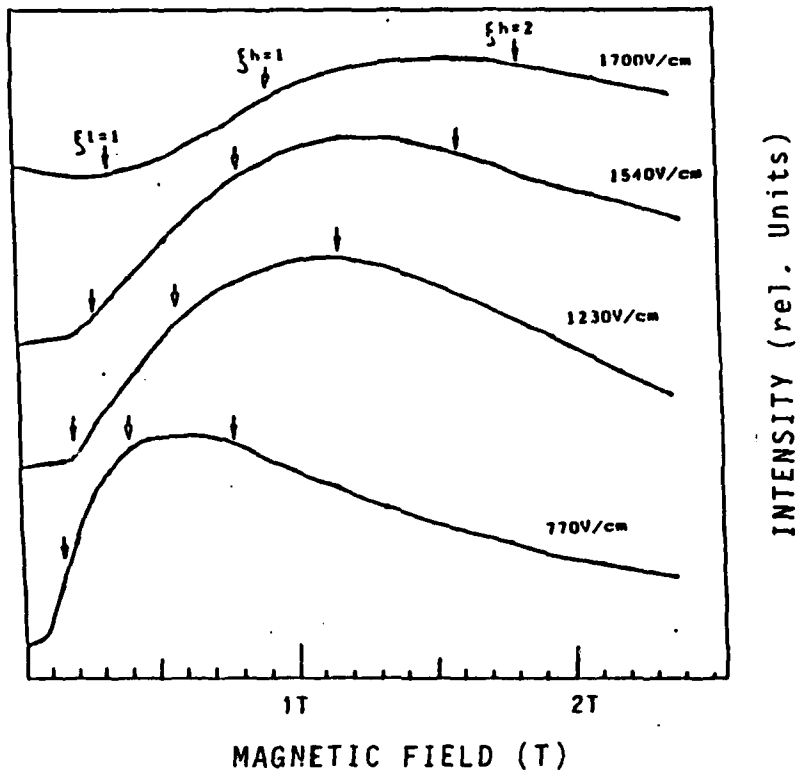

Fig. 4

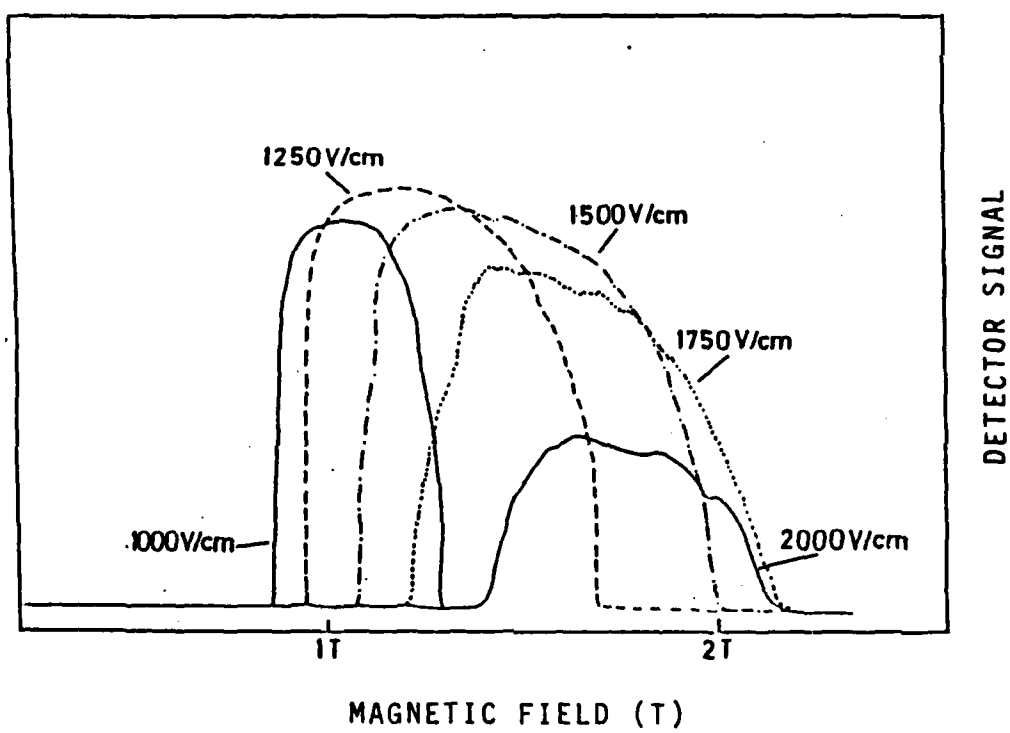

Fig. 3: Magnetic field dependence of the spontaneous emission signal of a p-Ge sample for different values of the electric field recorded with a Ge:Ga - detector.

Fig. 4: Magnetic field dependence of the stimulated emission signal from sample 1 for different electric fields detected with a Ge:Ga - detector.

field dependence of the detector signal for different electric fields. For certain magnetic fields the signal increases for two orders of magnitude (from 0.5 mV to 50 mV for Ge-detector current of $4 \cdot 10^{-5}$ A). This range shifts for higher electric fields to higher magnetic fields, similar to the maximum of the spontaneous emission. Emission occurrs for electric fields E between 1000 V/cm < E < 2000 V/cm and magnetic fields B between 1 T < B < 2 T. Expressed by the the normalized field ξ, stimulated emission is observed between $1.3 < \xi^h < 1.9$. These data agree quite well with the results of other authors /7/,/8/. The small differences in the onset position of the induced emission can be explained by the sligthly different carrier concentration and an other crystal orientation. A different carrier concentration influences the far infrared absorption (free carrier absorption) and a different crystal orientation parallel to the magnetic field can change the distribution function. For two of our samples the orientation of the long axis (this is the axis parallel to the magnetic field) is (1,0,0). For a third sample the orientation of the long axis is perpendicular to the (1,0,0) direction. This sample shows no lasing activity. For maximum output power in the literature the orientation parallel to the magnetic field is reported to be the (1,1,1)-direction. The power of the emitted far infrared radiation is estimated by a comparision with other FIR-sources (CO_2 pumped gas laser , InSb-cyclotron resonance emitter) to be about 300 mW. This is lower than Andronov /10/ reported for his samples with the crystal orientation (1,1,1) parallel to the magnetic field.

A detailed analysis of the emission spectra was performed with a GaAs-detector. The GaAs-detector can be used as a high sensitivity

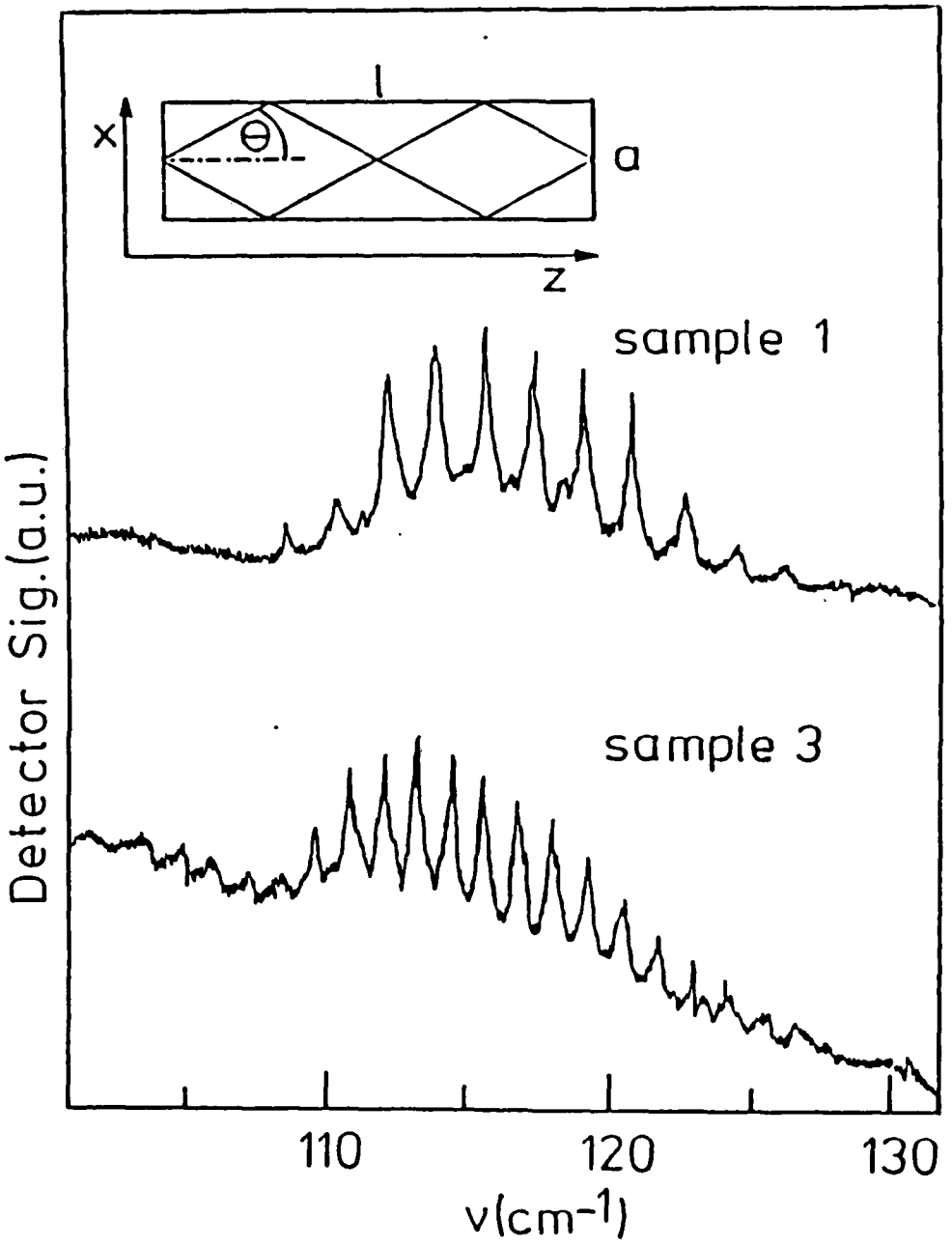

Fig. 5: Spectrum of stimulated emission for different electric and magnetic fields.

Sample 1: E= 1.8 kV/cm, B= 1.4 T

Sample 3: E= 1.9 kV/cm, B= 1.7 T

The insert schematically shows the ray path in the Ge-crystal.

pectrometer when tuned with the magnetic field. Fig. 5 shows emission spectra (intensity versus frequency) from two samples for different values of the electric and magnetic fields. The decreasing background level is due to the variation of the detector characteristic with magnetic field. The spectra consist of 10-20 lines with a regular mode spacing. Their positions remain fixed for changed applied fields. The measured linewidth is about 0.4 cm^{-1}. We conclude that the real width of the emission is of the same order as the detector linewidth (0.25 cm^{-1}). By varying the electric and magnetic fields it is possible to obtain lasing between 75 μm and 110 μm. There is a general trend towards emission at shorter wavelength for both higher electric and higher magnetic fields. In contrast to Andronov et al /10/ and Komiyama et al./9/, no long wavelength lasing (150-250 μm) could be found in our samples, which is probably because of the somewhat higher carrier concentration. Andronov et al./7/ and Komiyama et al./8/ suggested that the lasing modes are due to total reflections at the sample surfaces, since without mirrors the quality factor of the cavity is far too low to allow longitudinal or transverse modes (the Ge surface has 36% reflectivity at normal incidence). According to Fig.5 the observed mode spacings are 1.74 cm^{-1} and 1.20 cm^{-1} for samples 1 and 3, respectively, and 1.40 cm^{-1} for sample 2 (not shown). Comparing the spacings with the dimensions of the samples, it appears to be very likely that the width, a, is the crucial parameter determining the mode spacing (see Table I).

The mode spacings can be explained by considering an electromagnetic wave in the germanium crystal (see insert in Fig.5) propagating with components of the wavevector in the direction of l (z-direction) and a (x-direction)/14/: $\vec{k} = k_x\vec{e}_x + k_z\vec{e}_z$, where $\vec{e}_x$ and $\vec{e}_z$ are the respective unit vectors. The

transverse resonance condition is given by /15/ $k_x n = k\, n \sin\theta = M\pi/a$, where n is the refractive index, M is an integer, and θ is the angle between $\vec{k}$ and the longitudinal axis of the crystal. The analogous longitudinal resonance condition is not considered, because it would yield a very narrow mode structure which is not observed in the experiment. In addition, we have the geometrical condition $\tan\theta = Na/l$ (N integer), which ensures that the path of the ray is closed within the sample. This leads to a mode spacing (in wavenumbers) $\Delta\nu = (2a\, n \sin\theta)^{-1}$. θ must satisfy the condition $14.5^\circ < \theta < 75.5^\circ$, because 14.5° is the angle of total reflection for germanium. One can assume that modes with the smallest possible θ have the lowest losses, because they undergo the fewest reflections. Thus, for each sample the mode spacing is determined first by choosing the angle, θ, with the smallest possible N, and then this angle is used in the expression for $\Delta\nu$. This procedure gives a mode spacing, $\Delta\nu$, of 1.77 cm^{-1} (N=6), 1.41 cm^{-1} (N=5), and 1.14 cm^{-1} (N=4), for sample 1,2 and 3, respectively, in good agreement with the measured values. This interpretation is confirmed by the work of Andronov et al./10/, who reported emission of a single line by using a very thin (a = 0.7 mm) sample, where the mode spacing is as wide as the gain region.

After attaching external mirrors to sample 3 (see insert in Fig.6), the region of electric and magnetic fields where lasing occurs stays roughly the same. The detector signal is also of the same order of magnitude with and without mirrors. The observed spectra, however, exhibit a dramatic change. Fig.6 shows spectra of sample 3 for different electric and magnetic fields, recorded with the GaAs-detector. A considerably reduced number of lines appears with wider mode spacing and higher amplitude, accompanied by some other less dominant structure. Varying the electric and magnetic field allows

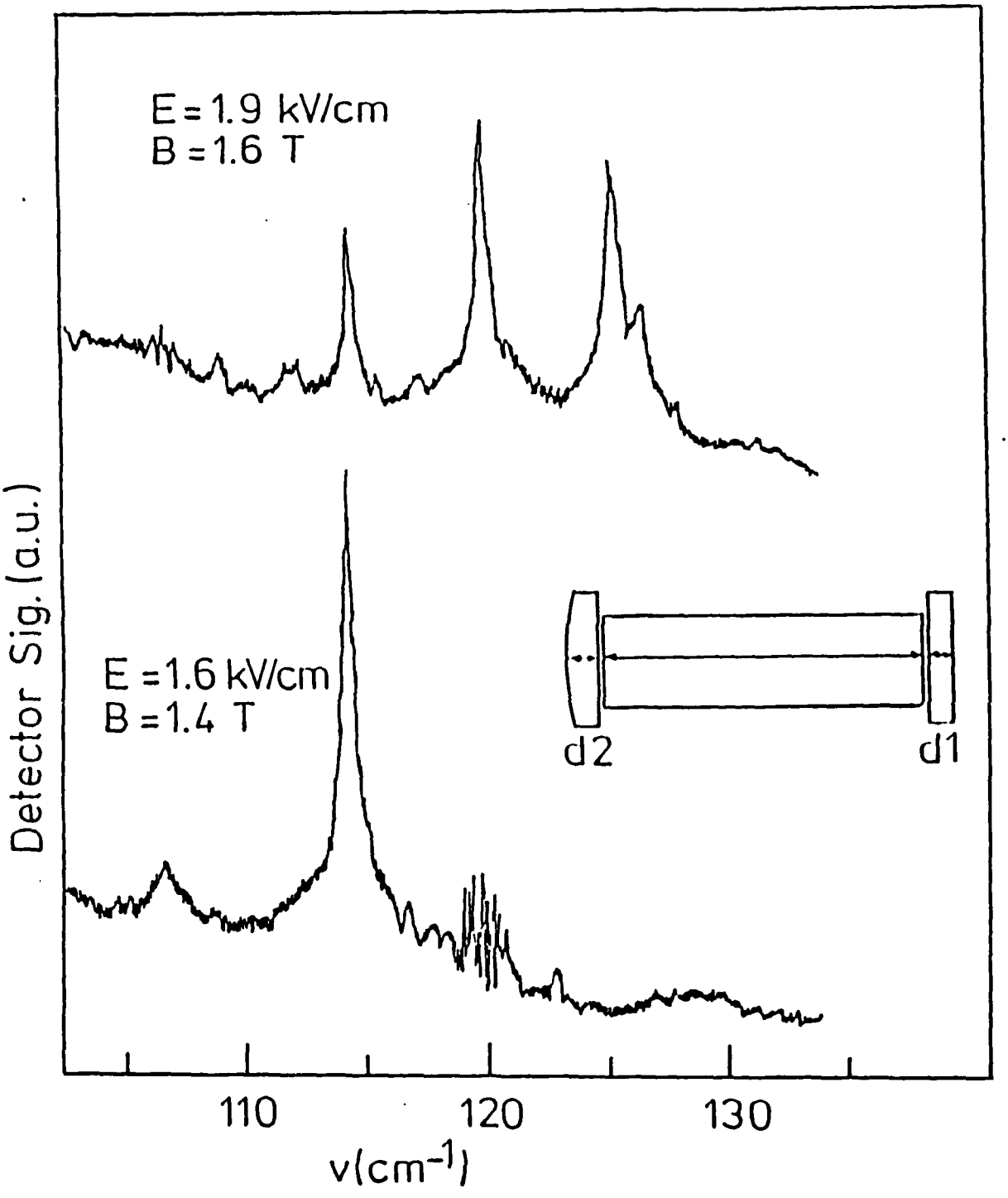

Fig. 6: Emission spectra from sample 3 after attaching external mirrors for different electric and magnetic fields. The insert shows the cavity configuration.

to switch on and off lines on the long- or short- wavelength side of the spectrum due to a change in the gain spectrum. In this way it was possible to obtain operation of a single line (lower part of Fig.6) /16/. This was the first report on forcing a multimode p-Ge laser to oscillate on a single line by attaching external mirrors. The emission wavelength is 87.3 μm (114.5 cm^{-1}), the adjacent line at 83.3 μm (120.0 cm^{-1}) is just at threshold. As seen from Fig.6 the single line contains approximately the same total intensity as the three lines together. However one cannot exclude the coexistence of several cavity modes within this line, because their spacing would be below the resolution of the detector. The spectra observed by Andronov et al./10/ from samples with external mirrors showed a very irregular and complicated structure. Komiyama et al./17/ reported some changes in the spectrum and were able to reduce the number of oscillating lines by sandwiching a thin layer of poly-4-methylpent-1-ene (manufactured under the trade name TPX by Imperial Chemical Industries) between the sample and one mirror.

The mode spacing in Fig.6 is equal to $\Delta\upsilon = 5.5\ cm^{-1}$, which is too large for fundamental longitudinal or transverse cavity modes. A possible explanation is the formation of an intracavity interference filter by the two Ge-plates: Since they are not subject to the electric field like the sample, they are expected to have a slightly different index of refraction and also the thin layer between sample and mirror induces a change of the refractive index, which provides the possibility of Fabry-Perot like reflections. A thickness of $d_1 = 0.9$ mm and $d_2 = 1.1$ mm (the slight curvature of the convex plate is neglected) would give a spacing of only 1.4 cm^{-1} and 1.1 cm^{-1}, respectively. If, however, the combined resonance condition for both plates is considered, the spacing is calculated to 5.5 cm^{-1}. This result is based upon a ratio of d_2/d_1 equal to 5/4. Considering an uncertainty of the measured

thicknesses of 0.05 mm and a low finesse of the Fabry-Perots, one gets spacings between 4 cm^{-1} and 6 cm^{-1}. A definitive explanation of the present spectra would require knowledge about the refractive index of the lasing sample as well as the influence of the thin layer between sample and mirrors. The investigation of different mirror configurations, especially with different thicknesses, appears necessary.

We also checked the emission when the plane mirror had a reflectivity of only 90%. In this case no lasing was achieved, which confirms the interpretation as waveguide-like modes in the mirrorless configuration: These modes are destroyed by attaching mirrors, which prevents total reflection on both end faces. Considering only the mirror output and no other losses the gain is calculated to be about $5 \cdot 10^{-3}$ cm^{-1}.

Table I: Sample dimensions and observed mode spacings: l is the sample length ((111)-direction), d is the distance between the electrical contacts, a is the width and $\Delta\nu$ is the measured mode spacing.

Sample	l	d	a (mm)	$\Delta\nu$ (cm^{-1})
1	46.9	3.7	2.4	1.74
2	43.1	4.2	3.15	1.40
3	48.4	5.2	3.75	1.20

References:

/1/ W. Shockley, Bell Syst.tech.J., 30, 990(1951)

/2/ H. Meada, T. Kurosawa, Proc. 11th Int.Conf.Phys.Semicond.,

Warsaw (New York; Elsevier), p.602(1972)

/3/ A.A. Andronov et al., JETP Lett., 30, 551(1979)

/4/ S. Komiyama, T. Masumi, K. Kajita, Phys.Rev. B, 20,5192(1979)

/5/ S. Komiyama, R. Spies, Phys.Rev. B, 23, 6839(1981)

/6/ S. Komiyama, Phys.Rev.Lett., 48, 271(1982)

/7/ A. A. Andronov, I. V. Zverev, V. A. Kozlov, Yu. N. Nozdrin, S. A. Pavlov and V. N. Shastin, Sov. Phys.-JETP Lett. 40, 804 (1984)

/8/ S. Komiyama, N. Iizuka, and Y. Akasaka, Appl. Phys. Lett. 47, 958 (1985)

/9/ S. Komiyama, Proc. 18th Int. Conf. Phys. Semiconductors, World Scientific Publishing, Singapore, 1987, p. 1641

/10/A. Andronov, A. Muravjev, I. Nefedov, Y. Nozdrin, S. Pavlov, V. Shastin, Y. Mityagin, V. Murzin, S. Stoklitsky, I. Trofimov, and A. Chebotarev, Proc. 18th Int. Conf. Phys. Semiconductors, World Scientific Publishing, Singapore, 1987, p. 1663

/11/S. Komiyama, Adv.Phys., 31, 255(1982)

/12/Y.K. Pozhela et al., Phys.Lett.Solidi(b), 128, 653(1985); Proc.17th Int.Conf.Phys.Semicond., San Francisco 1984, p.1333

/13/E. Gornik, Physica 127B, 95(1984)

/14/M. Helm, K. Unterrainer, E. Gornik and E.E. Haller, Solid-State Electronics 31, 759 (1988)

/15/M. J. Adams, An Introduction to Optical Waveguides, J. Wiley & Sons, New York, 1981

/16/K. Unterrainer, M. Helm, E. Gornik, E.E. Haller, J. Leotin, Appl.Phys.Lett.,52, 564(1988)

/17/S.Komiyama and S. Kuroda, Jap. J. Appl. Phys. 26, L71 (1987)

B) CALCULATION OF THE HOT CARRIER QUANTUM DISTRIBUTION FUNCTION IN CROSSED ELECTRIC AND MAGNETIC FIELDS

In this chapter we want to discuss the most important ideas from a theoretical point of view for the build-up of an inversion in the crossed field configuration and review calculations of the distribution function. The main part will be devoted to a new approach for the calculation of the distribution function in crossed fields which explicitly considers the LL structure of the energy spectrum. Only one type of carriers population inversion is considered within this carrier system.

The existence of an inverted distribution in crossed fields was first predicted by Maeda and Kurosawa in 1972 /1/. They performed Monte Carlo calculations and also tried to understand the situation by qualitative arguments: They found out the importance of the optical phonon scattering for the generation of a non thermal distribution. Their model was refined by other authors /2/,/3/ and became famous under the name "streaming motion and accumulation". This concept is based on the classical motion of carriers in crossed fields considering a sufficiently strong interaction with optical phonons. In crossed fields, the carriers move on circles in velocity space with central point $v_d = -(E/B)$. The energy of optical phonons $\hbar\omega_{op}$ corresponds to another circle $v = v_{op} = \sqrt{2\hbar\omega_{op}/m^*}$ centered at the origin $v = 0$. When the trajectory of a carrier crosses the circle $v = v_{op}$, the carrier can emit an optical phonon and is scattered back near the origin.

In the limit of large electric fields, $E/B \gg v_{op}$, all trajectories are open, i.e. they cross the circle $v = v_{op}$. In this case the motion is only slightly influenced by the magnetic field and is called "streaming motion" because of the successive acceleration and phonon emission. In the other limiting case $E/B \ll v_{op}$ most of the trajectories are closed and the carriers are not affected by optical phonon scattering. In the intermediate range a fraction of the carriers performs streaming motion, while another part moves on closed trajectories. The streaming carriers have a finite probability of being scattered into the area of closed trajectories, the so called passive region, where they can accumulate. They can only be removed from there by acoustic phonon or impurity scattering, which are both much slower than the optical mode scattering. As a consequence, the carriers get accumulated (or bunched) in a limited area of momentum space.

Calculations showed that for $\xi < 2$ a torus-type distribution function can arise in this accumulation area, which corresponds to a population inversion between Landau levels. Analytical approaches based on the Boltzmann equation have been performed for this situation /4/ as well as Monte Carlo calculations /5/, mostly applied to n-InSb, n-GaAs and the heavy holes of p-Ge. Very recently, Abou El Ela and Ridley /6/ made a Monte Carlo simulation for n-GaAs, including electron-electron scattering and intervalley transfer.

Experimentally, the accumulation of carriers was proved in different materials /7/, but it was not clear, if a population inversion between Landau levels could be achieved. A short time ago, strong far infrared emission signals have been observed in p-Germanium /8/, which were ascribed to a LL inversion of light holes.

Obviously, the most important application of an inverted distribution function is the generation and amplification of coherent radiation, in this case caused by transitions between Landau levels. According to this, the main drawback of the theoretical work mentioned above is the fact that it does not account for the discrete structure of the energy spectrum, i.e. the Landau levels.

All these studies were performed in the limit of nonquantizing magnetic fields, that means the use of a classical distribution function smeared out over the Landau levels and the use of the zero-magnetic field scattering rates. These classical approaches are not suited to yield information about the population of different Landau levels.

In this work we treat the problem of carriers in crossed fields in a quantum mechanical frame, i.e. the Landau levels are automatically incorporated in the calculation.

We consider the Hamiltonian for a carrier with charge e and effective mass m^* in crossed electric and magnetic fields interacting with phonons /9/,/10/:

$$H = \frac{1}{2m^*} (\vec{p}-e\vec{A})^2 - e\vec{E}\cdot\vec{r} + H_{ph} + H_{el-ph} \qquad (1)$$

Here H_{ph} is the free phonon term:

$$H_{ph} = \sum_{\vec{q}} \hbar\omega_q \, (b_q^+ \, b_q + \tfrac{1}{2}) \qquad (2)$$

where the b_q^+ and b_q are the phonon creation and destruction operators,

respectively, and H_{el-ph} is the electron- (hole-) phonon coupling:

$$H_{el-ph} = i \sum_{\vec{q}} C(\vec{q}) \; (b_q \; e^{i\vec{q}\vec{r}} - b_q^+ \; e^{-i\vec{q}\vec{r}}) \qquad (3)$$

C(q) depends on the specific nature of the electron-phonon coupling. Eigenvalues and eigenfunctions of the electronic part of the Hamiltonian ($\vec{B}$ in z-direction, $\vec{E}$ in x-direction) are given by

$$E_\upsilon = (n+\tfrac{1}{2})\,\hbar\omega_c + \hbar^2 k_z^2/2m^* - eEX + \tfrac{1}{2}\, m^*(E/B)^2 \qquad (4)$$

where the index υ summarizes the quantum numbers n, k_y, and k_z, $\omega_c = |e|B/m^*$, and $X = (\hbar k_y/eB + m^*E/eB^2)$.

$$\Psi_\upsilon(\vec{r}) = e^{ik_y y}\; e^{ik_z z}\; \Phi_n\left(\frac{x-X}{l}\right) \qquad (5)$$

where $l = \sqrt{\hbar/|e|B}$ and $\Phi_n\left(\frac{x-X}{l}\right)$ is the n-th harmonic oscillator wave function. The basic quantum transport equation is the equation of motion for the density operator, the Liouville - von Neumann equation

$$i\hbar \frac{\partial \rho}{\partial t} = [H,\; \rho] \qquad (6)$$

Here, ρ is the density operator of the total electron - phonon system. The electron distribution function is given by the diagonal elements of the reduced density operator, f , which is obtained by taking the trace over the phonon states:

$$f_\nu = Tr_{ph}\langle\nu|\rho|\nu\rangle \qquad (7)$$

Assuming no correlation between electron and phonons in the diagonal elements of ρ and a weak electron - phonon coupling the Pauli master equation can be derived for the diagonal elements of the reduced density operator (neglecting the Pauli exclusion principle)/10/,/11/,/12/

$$\frac{\partial f}{\partial t}\nu = \sum_{\nu'} f_{\nu'} W_{\nu'\nu} - f_\nu W_{\nu\nu'} \qquad (8)$$

The $W_{\nu\nu'}$ are the scattering probabilities from state ν to state ν' according to Fermi's golden rule :

$$W_{\nu\nu'} = \frac{2\pi}{\hbar}\sum_{\vec{q}} |\langle\nu|C(\vec{q})\, e^{i\vec{q}\vec{r}}|\nu'\rangle|^2 \left[N_q\delta(E_\nu - E_{\nu'} + \hbar\omega_q) + (N_q+1)\delta(E_\nu - E_{\nu'} - \hbar\omega_q)\right]$$

N_q is the Planck distribution for the phonons, the matrix elements are given by (see e.g. Ref. 13)

$$|\langle\nu|e^{i\vec{q}\vec{r}}|\nu'\rangle|^2 = |J_{nn'}(q_x,q_y)|^2\, \delta_{k_z',k_z-q_z}\, \delta_{k_y',k_y-q_y} \qquad (9)$$

with $|J_{nn'}(\xi)|^2 = \frac{n!}{n'!}\xi^{n'-n}\, e^{-\xi}\, [L_n^{n'-n}(\xi)]^2 \qquad (n \leq n')$,

and $\xi = l^2(q_x^2 + q_y^2)/2$. The $L_n^{n'-n}$ are associated Laguerre polynomials /14/. It is worth noting that the electric field only appears in the energy conserving δ-function and not in the squared matrix elements.

We now proceed to get a steady state solution of the master equation (8) which then reads

$$0 = \sum_{\upsilon'} f_{\upsilon'} W_{\upsilon'\upsilon} - f_{\upsilon} W_{\upsilon\upsilon'} \qquad (11)$$

In the following we want to consider the situation where the current through the sample is constant. Therefore we assume a spatially homogeneous distribution function. Thus, the f_{υ} have to be independent of X, and therefore of k_y /9/,/19/. This enables us to perform the summation over k_y directly and we are left with a system of N coupled integral equations (for N LL) in the variable k_z:

$$0 = \sum_{n'} \int dk_z' f_{n'}(k_z') W_{n'n}(k_z',k_z) - f_n(k_z) W_{nn'}(k_z,k_z') \qquad (12)$$

The rates $W_{nn'}(k_z,k_z')$ are now also k_y-integrated. The distribution functions for the different LL's can be expressed as

$$f_n(k_z) = \frac{1}{\sum_{n'} W_{nn'}(k_z)} \sum_{n'} \int dk_z' f_{n'}(k_z') W_{n'n}(k_z',k_z) \; , \qquad (13)$$

where $W_{nn'}(k_z) = \int dk_z' W_{nn'}(k_z,k_z')$.

The proper normalization condition is $\sum_n \int dk_z f_n(k_z) = 1$.

Our first attempt to solve this equation was done by dropping the k_z-dependence. Then Eq. (13) becomes a system of algebraic equations. Physically, this approximation contains an overestimation of transitions due to a change in the spatial variable X, and an underestimation of transitions

due to a change in the quantum number k_z. This approach is shown in Ref. /15/ for 3 Landau levels, including polar optical and acoustic deformation potential phonon scattering, which is adequate for electrons in GaAs or InSb. For the first time, the possibility of a population inversion between Landau levels is demonstrated theoretically in a quantum mechanical frame.

Recently, we have extended this approach by taking into account the k_z-dependence and solving the coupled integral equations (13) for 3 Landau levels. This work is contained in Ref. /16/, for optical and acoustic deformation potential scattering (adequate e.g. for the light holes in Germanium).

A population inversion is predicted also for this case. In addition, the one-dimensional distribution functions in the different Landau levels are discussed, and special attention is paid to a comparison of the quantum mechanical picture with the classical picture of streaming motion.

The most important feature for a further development of our model is the inclusion of the influence of the heavy hole band to the population of the light hole band in p-Ge. As the redistribution of carriers from the heavy hole band can enhance the inversion in the light hole band.

References:

/1/ H.Maeda and T.Kurosawa, in "Proceedings of the 11th Int. Conf. on the Physics of Semiconductors, Warsaw, 1972", Ed. Polish Academy of Sciences (PWN-Polish Scientific Publishers, Warsaw, 1972), p.602

/2/ Ya.I.Al'ber, A.A.Andronov, V.A.Valov, V.A.Kozlov, and I.P.Ryazantseva, Solid State Commun. 19, 955 (1976)

/3/ A.A.Andronov, V.A.Kozlov, L.S.Masov, V.N. Shastin, Sov.Phys.-JETP Lett.30, 551(1979)

/4/ F.Brosens and J.T.Devreese, Solid State Commun.44, 597 (1982)

/5/ P.Warmenbol, F.M.Peeters, and J.T.Devreese, Phys.Rev.B 33, 1213 (1986)

/6/ F.Abou El-Ela and B.K.Ridley, at the "5th Int Conf. on Hot Carriers in Semiconductors, Boston 1987", to be published in Solid State Electronics

/7/ S.Komiyama, Adv.Phys. 31, 255 (1981)

/8/ Yu.B.Vasil'ev and Yu.L.Ivanov, in "Proceedings of the 18th Int Conf. on the Physics of Semiconductors, Stockholm, 1986", Ed. O.Engström (World Scientific Publishing, Singapore, 1987) p.1659

/9/ H.F.Budd, Phys.Rev.175, 271 (1968)

/10/ D.Calecki, C.Lewiner, and P.Nozieres, J.Phys. (Paris) 38, 169 (1977)

/11/ L. Van Hove, Physica 21, 517 (1955); 23, 441 (1957)

/12/ D.Calecki, in "Physics of Nonlinear Transport in Semiconductors", Ed. D.K.Ferry, J.R.Barker, and C.Jacoboni (Plenum Press, New York, 1980), p.289

/13/ J.R.Barker, J.Phys.C 5, 1657 (1972)

/14/ I.S.Gradsteyn and I.M.Ryzhik, "Tables of Integrals, Series and Products" (Academic Press, New York, 1965)

/15/ M.Helm and E.Gornik, Phys.Rev.B 34, 7459 (1986)

/16/ M. Helm, K. Unterrainer, E. Gornik, Phys.Rev B (to be published)

Part II

A) ENERGY RELAXATION

The mechanism of the energy relaxation and the form of the distribution function are of fundamental interest for the understanding of electric field effects in two-dimensional electron systems. At low temperatures where lattice scattering is weak, hot electron phenomena can be produced by fields as low as V/cm in Si as well as GaAs inversion layers.

In the present report, two different methods are used to determine the elctron temperature and the energy relaxation time:

a) The electron gas is heated up by electric field pulses and the emitted broadband far infrared radiation is analyzed in terms of a black body source with a temperature T_e. The derived electron temperatures are independent of sample parameters when plotted against the input power per electron ($P_e = e\mu E^2$). A nearly linear dependence of T_e over P_e is found for electron temperatures between 10 K and 40 K. At higher T_e-values a weaker increase is found which tends to saturate at $T_e \approx 100$ K. From an energy balance consideration energy relaxation times are obtained which decrease linearly with increasing electron density /1/,/2/.

As a dominant energy relaxation mechanism acoustic deformation potential scattering is found for electron temperatures up to 40 K. At higher electron temperatures optical phonon emission dominates the energy relaxation. However, the obtained relaxation times are longer than the

theoretically expected times for a bulk like phonon process. This is an indication for a possible influence of hot phonon effects.

b) A direct way to obtain the energy relaxation rate is the measurement of the incoherent saturation of the cyclotron resonance transition. This is done under the assumption that a magnetic field does not change the relaxation rates significantly. The relaxation times derived are comparable to the values found in the case without magnetic field /3/. As the CR-saturation is a direct technique, these experiments can be used as a prove for the validity of the black-body emission analysis.

Both techniques give energy relaxation times between 1 ns and 0.2 ns depending on the 2-dimensional carrier density. These times agree with values obtained in the bulk if compared with the equivalent 3-dimensional density.

B) ANALYSIS OF THE CARRIER DISTRIBUTION FUNCTION THROUGH SMITH-PURCELL EFFECT IN GaAs/GaAlAs HETEROSTRUCTURES

The two-dimensional electrons in selectively doped GaAs/GaAlAs heterojunctions exhibit extremely high mobilities at low temperatures /4-6/. The electrons are easily heated up in an external electric field leading to a rapid rise in electron temperature /1,7,8/ and a reduction of electron mobility /9/. No detailed analysis of the form of the distribution function has been performed for extremely high mobilities. In this case normal Fermi distributions cannot be used since drift energies comparable with the Fermi energy can be achieved

already at low electric fields.

In the present paper a direct analysis of the electron distribution function for extremely high mobility samples as a function of the external electric field is presented. The Smith-Purcell effect /10/ is measured in a semiconductor for the first time: A periodic potential of period L induces an energy loss of a drifting carrier distribution via photon emission. The angle between the drift and the grating momentum is varied by using different sample geometries. The geometry-dependent emission spectra are momitored through a magnetic-field-tuned InSb-detector /11/.

Through the selective momentum transfer ($\pm q = 2\pi/L$) the spectral analysis of the energy loss yields detailed information on the drifted electron distribution function. For a momentum transfer much smaller than the electron momentum, the frequency ω of the emitted light is directly proportional to the particle wavevector k:

$$\omega \simeq hkq/m^* = v_k q \qquad (q \ll k). \tag{1}$$

m^* is the electron mass. Thus the emitted spectra reflect directly the distribution of the carrier velocities v_k. In the following analysis the electron distribution function will be described as a shifted Fermi function:

$$f(E) = 1/(1 + \exp(h^2(k - k_D)^2/2m^* - \mu)/T_e). \tag{2}$$

introducing the drift momentum k_D and the drift-dependent electron temperature T_e as phenomenological parameters. Our model assumes that the distribution

function is stationary, depending only on the electric field and the sample mobility. The FIR coupling represents only a neglibible cooling process.

Theory of the emission process

FIR emission from a free electron system requires a second scattering process for momentum conservation, which can be either impurity or phonon scattering /12/. An electromagnetic calculation of the FIR emission from heated carriers through a grating was recently performed in ref. 1. For the electric field driven electrons, the lateral potential modulation $U_o\cos(qx)$ represents a coherent scattering source (the lattice vector has been taken in the x direction). Formally, it can be described as one "extended" impurity, scattering the electrons by $\pm q$. The emission spectrum of a drifted electron distribution depends on the angle between the lateral structures and the electric field and thus the current direction.

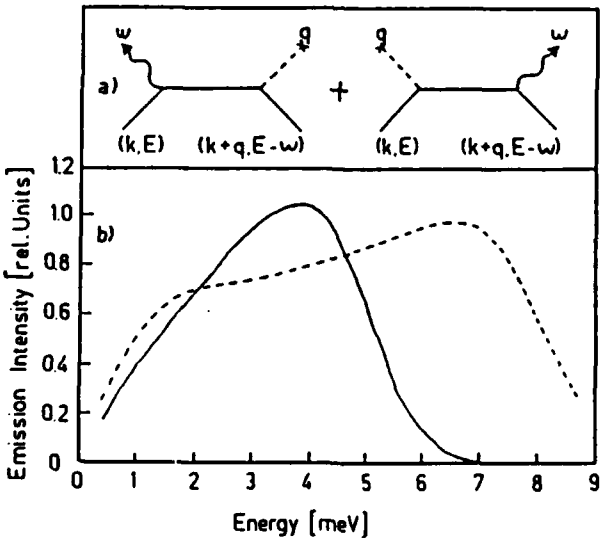

Fig. 1:
(a) Scattering diagrams used for the theoretical calculation.
(b) Calculated emission intensity versus frequency from drifted electron distributions with a temperature of 35 K, comparing $j_\perp q$ (full curve) with $j/\!/q$ (broken curve). The spectra are weighted by ω to account roughly for the detector sensitivity.

We calculate the emission rate in the lowest order, including only the scattering processes shown in Fig. (1a). This diagrammatic approximation can be controlled analytically also for "badly" shaped electron distributions. Static screening is included in the impurity potential. Evaluating the diagrams Fig. (1a) and performing the sum over the photons the energy loss rate is obtained as:

$$\frac{dW}{dt} = \frac{e^2 U_0^2 q^2}{4\pi^2 m^* c^3 \hbar^5} \sum_{\pm} \frac{1}{|\ \pm\ |} \int_{-\infty}^{\infty} dk_y f(k_x^{\pm}, k_y)\ \{1 - f(k_x^{\pm} \pm q, k_y)\}\ ,$$

$$k_x^{\pm} = \pm\left(\frac{q}{2} + \frac{\omega m^*}{\hbar q}\right)\ . \qquad (3)$$

The sum over (±) describes the two possible momentum transfers, and the k_x-integration has already been performed by exploiting the delta function for energy conservation. The influence of the electron distribution $f(k_x,k_y)$ is contained in the k_y sum, which is evaluated numerically.

Fig. (1b) shows the calculated energy-dependent emission intensity for the parameters of the sample described below, for an electron temperature of 35 K. The curves are weighted by ω in order to account roughly for the detector sensitivity. The full curve describes a carrier distribution which is heated by an electric field normal to the grating wavevector q. In this direction the result is independent of the drift velocity if a shifted Fermi distribution is used. In contrast, the broken line shows the result for the electric field parallel to q, with $v_D = 0.7\ v_F$: A substantial change of the emission characteristics is obtained. The spectrum splits into two broad structures. The shifts to higher and lower energies demonstrate the transition from normal free carrier emission to the Smith-Purcell regime (the low energy side disappears for still higher drift velocities). While the lower part of the spectrum is out of the range of our detector, the change on the high energy

side should be observable when changing the orientation of the current with respect to the grating.

Experiment

We have plasma etched a periodic grating with lattice constant L into the top layer of a GaAs/GaAlAs heterostructure as shown in Fig. (2a). The height of the modulation was of the order of 200 A and the electron density is 2.8 x $10^{11}/cm^2$. The modulation induces a periodic potential acting on the 2D electrons, which is evident from Shubnikov-de Haas (SdH) oscillations. At 4.2 K the samples had a zero field mobility of 2.0 x $10^6 cm^2/Vs$ before plasma etching, and very narrow minima in σ_{xx}. After etching the mobility was only reduced to 1.5 x $10^6 cm^2/Vs$, however the minima became much broader. We interpret this broadening as the appearance of a sinusoidal potential, leading to a local variation of the electron density. From the width increase of the SdH oscillation we estimate the size of the periodic potential to be of the order of 1 meV.

Fig. 2

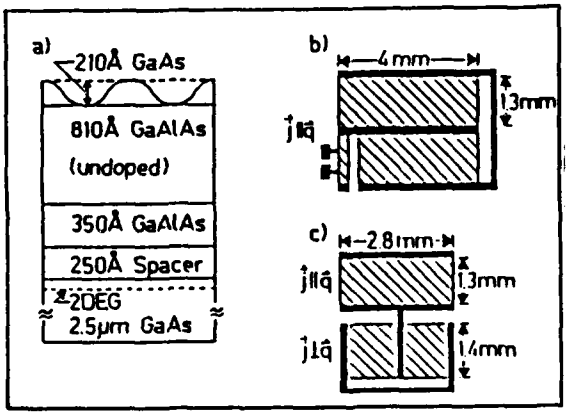

Fig. 3

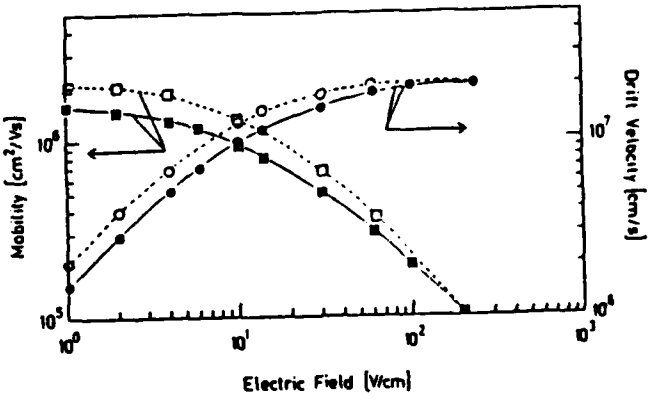

Fig. 2:
Schematical drawing of the GaAs-GaAlAs structures with periodic grating used in the experiments (a). Sample 1 with the contacts parallel to the grating (b) and sample 2 with contacts both parallel and normal to the grating wavevector (c).

Fig. 3:
Mobility and drift velocity of the electrons as a function of the electric field. Open symbols: Before plasma etching. Full symbols: After plasma etching. Due to the high sample mobility the drift velocity saturates already at low electric fields.

Two different sample geometries were realized: Sample 1 had the grating grooves parallel to the contacts (Fig. 2b), and as a result q//j. In sample 2 both geometries (q//J and q⊥j) are realized. The drift velocity and mobility versus the external electric field as derived from direct conductivity measurements of the small sample structure (Fig. 2b) at 4.2 K before and after the plasma etching are shown in Fig. (3). It is evident that the saturation drift velocity is already obtained for electric fields in the order of 100 V/cm. The observed dependences of v_D and μ are in good agreement with the theoretical calculation of Lei et al. /13/ based on a non-Boltzmann balance equation approach and using a drifted Fermi/Dirac distribution with temperature T_e.

The analysis of the emitted radiation in the presence of a periodic potential allows us to answer the question whether the drift velocities are realistic and what is the average temperature of the carrier distribution. Emission spectra for a plasma etched sample 1 (Fig. 2b) for several electric fields are shown in Fig. (4). For the lowest electric field the detector response is only due to broad band thermal emission from the heated electron distribution /1/. Above an electric field of 30 V/cm the emission spectra start to show a structure around a magnetic field of 0.3 T, which develops to a clear but broad peak at 100 and 150 V/cm. The spectra show a clear shift between 50 and 100 V/cm, indicated by the arrow which marks the decay of the signal.

For samples without a grating the spectra show a similar form as the curve for 10 V/cm for all electric fields, but the broad peak around 0.3 T is missing. Consequently the additional structure can be directly attributed to

Smith-Purcell type emission.

To demonstrate that the observed emission is due to the grating induced potential we prepared a sample where the grating wavevector q is oriented both parallel and normal to the current direction. In Fig. (5) a comparison of the emission for q//j (dashed curve) and q⊥j (full curve) is shown for an electric field of 100 V/cm. In both orientations radiation due to the Smith-Purcell effect is observed. It is evident that the spectrum for q//j is shifted to higher energies. In the q⊥j case the scattering depends essentially on the carrier temperature, independent of the drift velocity. The emission comes mainly from carriers moving with the Fermi velocity perpendicular to the current direction.

Fig. 4

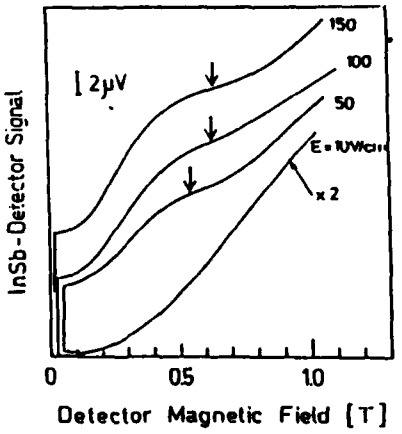

Fig. 5

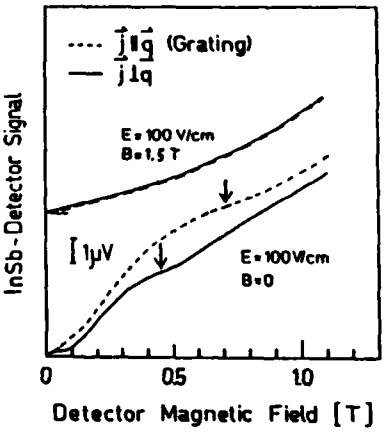

Fig. 4:
Emission spectra from drifted electron distributions with j//q, for different electric field strengths. The broad structure appearing at high fields is a consequence of the grating-induced emission.

Fig. 5:
Emission spectra from drifted electron distributions, comparing geometries with j//q and j⊥q. A magnetic field normal to the interface destroys the selective emission.

From this experiment it is directly evident that the shift of the spectra is due to the drift of the carriers. The spectra thus show the behaviour

predicted by the theory (Fig. 1b). For the given situation the shift can be converted into the drift velocities, although we have to keep in mind that the detector has a rather limited resolution of 1 meV and that the emitted spectrum is quite broad.

As an additional proof that the emission is due to the high carrier velocity we reduced the carrier velocity with an applied magnetic field perpendicular to the 2D-plane. The selective emission and the difference in the spectra between $j//q$ and $j\perp q$ disappeared as shown in Fig. (5) for a magnetic field of 1.5 T.

As a rough estimate we obtain a drift velocity of 1.5×10^7 cm/s for 100 V/cm. This drift velocity is somewhat smaller than that derived from current measurements. In addition we can estimate the carrier temperature: It has to be in the order of $\simeq$ 50 K from a fit of the decaying part of the spectra which are marked by arrows. Our calculations show that for considerably higher temperatures ($T_e > 80$ K) the spectra become extremely broadened and it would not be possible to observe well-defined structures with the given resolution of the InSb detector.

C) SUMMARY.

A significant difference in electron temperatures is found from the black-body emission analysis and the Smith-Purcell effect. In both cases samples with mobilities higher $1 \times 10^6 cm^2/Vs$ at 4.2 K were used. In the Smith-Purcell case a rather significant drift velocity is found which results in a shifted Fermi-Dirac distribution. In the hot electron emission experiment a

thermodynamic equilibrium distribution was assumed, which is not a good description of the real situation. In the case of the emission experiments we can therefore conclude that the electron temperature model gives problematic electron temperatures ($T_e \simeq 100K$) if a significant drift energy is present.

The obtained drifted Fermi-Dirac distribution and the rather low electron temperatures derived from the Smith-Purcell effect are well explained with the theory of Lei et al. /13/.

References:

/1/ R.A. Höpfel, G. Weimann, Appl.Phys. Lett 46 (3), 291 (1985).

/2/ E. Gornik, NATO ASI Series, Ed. C.M. Sotomayor Torres, Series B: Physics Vol. 152, p.167, Plenum Press 1986.

/3/ M. Helm, E. Gornik, A. Black, G.R. Allan, C.R. Pidgeon, K. Mitchell, G. Weimann, Physica 134B, 323 (1985), Springer-Verlag.

/4/ H.L. Störmer, R. Dingle, A.C. Gossard, W. Wiegmann, M.D. Sturge, Solid State Commun. 29, 705 (1979).

/5/ K. Hirakawa, H. Sakaki, Phys.Rev. B33, 8291 (1986).

/6/ J.J. Harris, C.T. Foxon, D.E. Lacklison, K.W.J. Barnham, Superlattices and Microstructures 2, 563 (1986).

/7/ H. Sakaki, K. Hirakawa, J. Yoshino, S.P. Svensson, Y. Sekiguchi, T. Hotta, S. Nishii, N. Miura, Surf.Sci. 142, 306 (1984).

/8/ J. Shah, A. Pinczuk, H.L. Störmer, A.C. Gossard, W. Wiegmann, Appl.Phys.Lett. 42, 55 (1983).

/9/ J. Shah, A. Pinczuk, H.L. Störmer, A.C. Gossard, W. Wiegmann, Appl.Phys.Lett. 44, 322 (1984).

/10/S.J. Smith, E.M. Purcell, Phys.Rev. 92, 1069 (1953).

/11/E. Gornik, W. Müller, F. Kohl, IEEE Transactions on Microwave Theory and Techniques MTT 22, 991 (1974).

/12/G.D. Mahan, in Many Particle Physics, Plenum Press 1981, p. 707.

/13/X.L. Lei, J.Q. Zhang, J.L. Birman, C.S. Ting, Phys.Rev. B33, 4382 (1986)

Electron heating and free-carrier absorption in GaAs/AlGaAs single heterostructures

R. A. Höpfel[a)]
Institut für Experimentalphysik, Universität Innsbruck, A-6020 Innsbruck, Austria

G. Weimann
Forschungsinstitut der Deutschen Bundespost, beim Fernmeldetechnischen Zentralamt, Am Kavalleriesand 3, D-6100 Darmstadt, Germany

(Received 12 October 1984; accepted for publication 14 November 1984)

We observe far infrared broadband emission from the hot two-dimensional electron plasma in GaAs/AlGaAs single heterostructures grown by molecular beam epitaxy. The radiation is analyzed in two different frequency regimes (around 35 and 100 cm^{-1}). From the relative dependence of the intensities on the applied longitudinal electric field the hot-electron temperatures are determined. From the absolute emission intensities values of the free-carrier absorption coefficient (down to 10^{-5} in ultrahigh mobility samples) are measured.

The topic of carrier heating in the lateral transport of two-dimensional (2D) systems along semiconductor interfaces and heterojunctions has attracted much interest in the last years, especially due to the applications of these systems for fast field-effect transistors[1] and, recently, for hot carrier and real space transfer devices.[2] There are several theoretical papers[3] on the problem of carrier heating in GaAs/AlGaAs heterojunctions. Two main experimental approaches, namely, hot-carrier photoluminescence[4] and magnetotransport,[5] have been made to measure the carrier distribution function or the carrier temperature, respectively.

In this letter we report on far infrared (FIR) emission experiments that were performed by passing a lateral current through the 2D electron system of GaAs/AlGaAs single heterojunctions. This heats up the carriers to a carrier temperature T. It has been shown in the experiments of Shah *et al.*[4] and in femtosecond studies of the intraband relaxation by Erskine *et al.*[6] that the carriers thermalize very fast to a thermal distribution characterized by the carrier temperature T_e via carrier-carrier interaction within less than 100 fs.[6] Since this is by orders of magnitude less than the energy relaxation time (10^{-10}–10^{-9} s) the carrier system itself represents a system in thermal equilibrium.

The FIR emission therefore can be described by thermodynamical considerations. In equilibrium the spectral emission intensity $I(\omega,T)$ of electromagnetic radiation from a system with temperature T is given by

$$I(\omega,T) = I_{BB}(\omega,T)\,A(\omega), \tag{1}$$

where I_{BB} is the spectral emission intensity of a black body and A is the spectral absorptivity of the system, in a 2D system for normal incidence

$$A(\omega) = \frac{4\,\mathrm{Re}\,F}{|\sqrt{\epsilon}+1+F|^2}, \tag{2}$$

with $F = \sigma(\omega)/\epsilon_0 c$ and ϵ being the dielectric constant of the substrate. A Drude form of the dynamical conductivity $\sigma(\omega)$ in n-Si inversion layers has been confirmed by microwave and FIR transmission experiments by Allen *et al.*[7] up to frequencies of 40 cm^{-1}. This allowed the determination of T_e from the absolute FIR emission intensity at one frequency as shown in Ref. 8. In GaAs/AlGaAs heterostructures, however, the free-carrier absorption has not been measured yet. In order to eliminate the unknown free-carrier absorption and, furthermore, to avoid the problem of measuring absolute FIR intensities, a *relative* method is applied in this work. The signals of two FIR detectors (high-purity n-type GaAs at 35 cm^{-1}, Ga-doped Ge around 100 cm^{-1}) are measured as a function of the applied electric field. The signals of the two detectors are evaluated in the following way: at a field E_i (corresponding to a carrier temperature T_i) the detector signal from the nth detector is given by

$$U_{n,i} = \int_0^\infty R_n(\omega)\,A(\omega)\,I_{BB}(\omega,T_i)\,d\omega. \tag{3}$$

The detector responsivity $R_n(\omega)$ can be written as $R_n(\omega) = R_n^0\,r_n(\omega)$ as well as $A(\omega)$ as $A(\omega) = A_n^0\,a_n(\omega)$. This means that the responsivity $R_n(\omega)$ and the absorptivity of the electron system $A(\omega)$ are mathematically expressed by a product of the relative frequency dependent functions $r_n(\omega)$, $a_n(\omega)$ and absolute factors A_n^0 and R_n^0 at the detector peak frequencies. The following assumptions can be made. (a) A Drude-type relative frequency behavior of $a_n(\omega)$ within the frequency interval of each detector n is assumed, which is a good approximation even if the dynamical conductivity deviates from Drude behavior over a wide range of frequency. (b) The field dependence of $A(\omega)$ is assumed to follow the field dependence of the momentum relaxation time τ via the dynamical conductivity. This change of the dynamical conductivity plays a role at high electric fields where the mobility changes with electric field. Then Eq. (3) contains two unknown parameters, namely, the carrier temperature T_i and the product $A_n^0 R_n^0$, since the relative detector response $r_n(\omega)$ is well known.[9] Measuring the detector signals $U_{n,i}$ of the two detectors with two different applied electric fields, gives a numerically soluble set of four equations for the four unknown variables. Measurements at more values of the electric field yield more data than unknown variables and thus allow us to prove the consistency of the assumptions. Thus a determination of the electron temperature can be made from the relative emission signals, without knowing the absolute detector response and the optical properties of the system.

[a)] Present address: AT&T Bell Laboratories, Holmdel, New Jersey 07733.

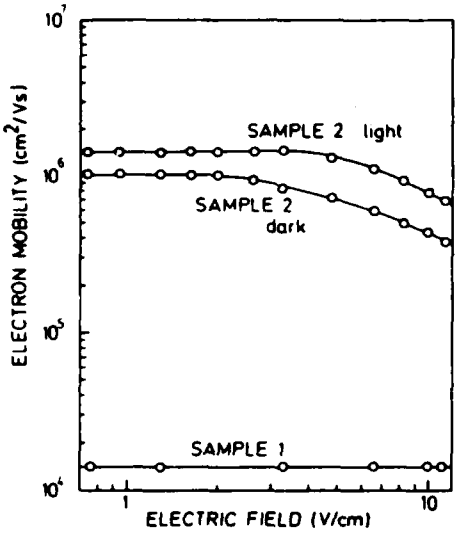

FIG. 1. Carrier mobility as a function of lateral electric field for the two samples: the high mobility sample (sample 2) is measured before (dark) and after (light) illumination with visible light.

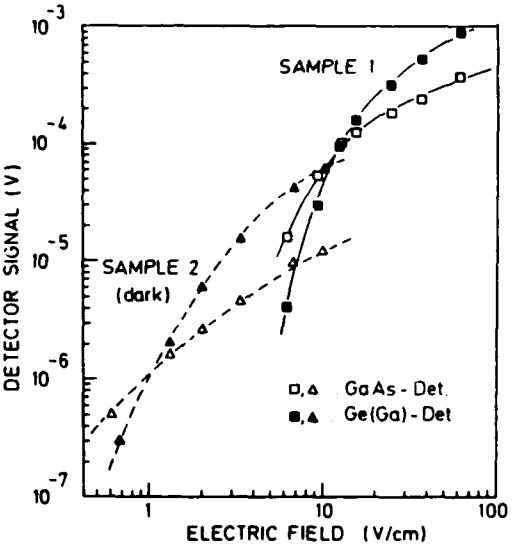

FIG. 2. Detector signals as a function of applied electric field for two samples (sample 1 and sample 2, dark) and two different detectors: GaAs detects the radiation of longer wavelength (35 cm $^{-1}$) than Ge (Ga) (around 100 cm^{-1}, full symbols).

The samples used in the experiments are modulation-doped GaAs/$Al_{0.35}$ $Ga_{0.65}$As single heterostructures grown by molecular beam epitaxy. The electron mobilities are 1.0×10^6 cm^2/Vs at electron concentration $n_s = 2.4\times10^{11}$ cm^{-2} at 4.2 K (sample 2). By illumination the electron concentration and mobility can be changed persistently to $n_s = 3.8\times10^{11}$ cm^{-2} and $\mu = 1.3\times10^6$ cm^2/Vs as a consequence of the persistent photoeffect found by Störmer *et al.*[10] Ohmic contacts, which must be of extremely low resistance in order to avoid FIR emission from the contacts, were made by alloying evaporated Au/Ge films of 1000-Å thickness at 400 °C. For comparison also a low mobility sample (1) with $n_s = 8.7\times10^{11}$ cm^2/Vs and $\mu = 1.6\times10^4$cm^2/Vs was used. All experiments were performed at liquid helium temperatures. The electric field was pulsed in order to avoid sample heating and to allow the use of correlation techniques. The current through the device and the detector signals are measured simultaneously. The geometry of the waveguide and the detectors favors the detection of the radiation emitted in the direction normal to the surface of the sample. The radiating area is 2 mm × 3 mm.

Figure 1 displays the carrier mobility of both samples as a function of the longitudinal electric field. With increasing electric field the mobility of sample 2 decreases due to electron heating and increased phonon scattering. The low mobility sample (1) does not show a significant field dependence of the mobility since it is dominated by impurity scattering. In Fig. 2 the obtained values of the detector signals as a function of the applied electric field are plotted. Here the characteristic feature of this experiment can be seen very clearly: the signals of the two detectors have remarkably different *slopes*, the increase of the Ge(Ga) detector signal (full symbols) with electric field is much stronger than that of the GaAs detector signals. This is a consequence of the exponential dependence of the Bose quantum statistics on the quantity $\hbar\omega/k_BT$. Therefore, at different frequencies the temperature dependence of the emission intensity is different.

From Eqs. (1)–(3) quantitative values of the electron temperature are determined using numerical fitting procedures. The results are shown in Fig. 3, where the electron heating $\Delta T = T - 4.2$ K is plotted versus the input power per electron: the electron heating increases with the input power and reaches 100 K when the input power exceeds 10^7 eV. s^{-1} per electron. The values of heating for the three different values of carrier concentration and mobility are surprisingly close together, although the electron concentration varies by a factor of 3 and the mobility by a factor of 100. Also the slopes of the curves are similar except sample 2 (light) which shows a somewhat stronger increase of heating with input power. The change of slope, however, is too weak and almost within the error bars, so there can be no conclu-

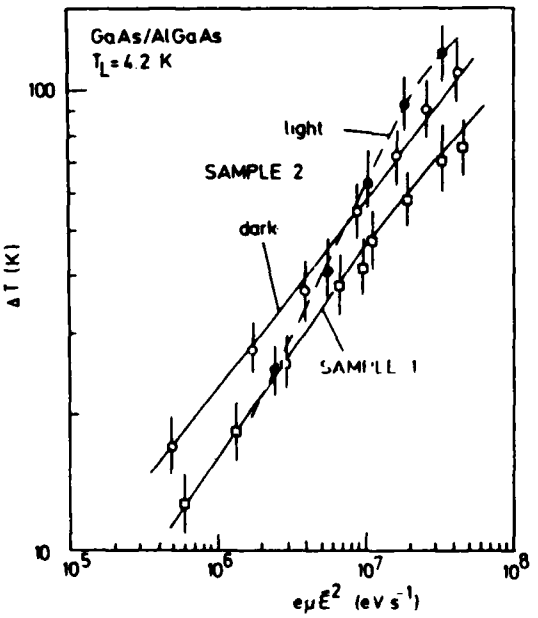

FIG. 3. Electron heating $\Delta T = T - 4.2$ K as obtained from the evaluation of the emission intensities at the two frequencies of the detectors. The abscissa is the input power per electron. The lines (dashed for sample 2 light) are drawn only to guide the eye.

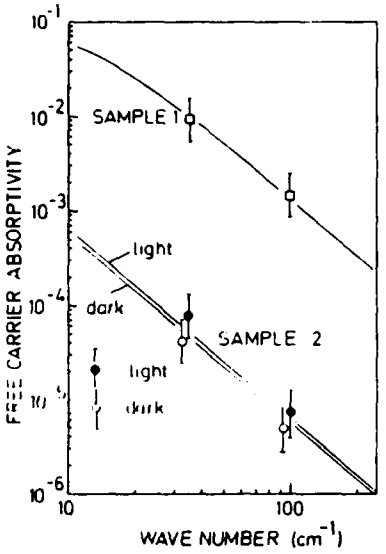

FIG. 4. Measured values of the free-carrier absorptivity vs far infrared wave number. The full curve is calculated assuming Drude behavior with momentum relaxation times taken from the dc mobility.

sions drawn from this behavior. These results show that the heating in GaAs/AlGaAs heterostructures in this range of lattice temperature and carrier heating is a function of the input power per carrier rather than an explicit function of carrier density and mobility. This observation is similar to the results obtained in Si MOSFET's[8] and is also consistent with magnetoconductivity data of Sakaki *et al.*[5] showing also only a small dependence on carrier concentration and mobility. This behavior is expected when acoustic phonon scattering determines the energy loss of the carriers to the lattice.[5,11] The absolute values obtained by this optical emission method are in good quantitative agreement with the results of photoluminescence experiments by Shah *et al.*[4] at high electron temperatures and the values obtained by Sakaki *et al.*[5] from magnetoconductance measurements at low electric fields.

A comparison of the detector signals with those of *n*-InSb cyclotron emission at saturation electron temperatures[12] allows an absolute determination of the emission intensity as described in Ref. 8. Detector responsivities of $\sim 1\times 10^{7}$ V/W (GaAs) and $\sim 2\times 10^{7}$ V/W (Ge) with an accuracy of 30% are obtained for the used detectors. The emitted power from the GaAs/AlGaAs heterostructures therefore ranges from 10^{-14} W, which represents the noise level of the detector arrangement, up to 10^{-10} W within the detector intervals. Knowing the absolute emission intensity and the electron temperature, we can separate the product $A_n^0 R_n^0$ and give values of the absorptivity of the 2D carrier system at the detector frequencies. The results are shown in Fig. 4. The absorptivity of the carrier plasma is plotted for the different samples at the two detector frequencies. The free-carrier absorption (evaluated for low electric fields) strongly depends on the carrier mobility; the absorption varies by two orders of magnitude from the low mobility sample (high absorptivity = emissivity) to the high mobility sample which reveals a very low absorptivity of below 10^{-3} at 100 cm^{-1}. Note that these low values of absorption are measurable without gate modulation techniques as usually applied for absorption measurements in 2D systems.[7] The full curve in Fig. 4 displays the theoretical frequency and mobility dependence assuming Drude conductivity with the values of the relaxation time τ taken from the dc mobility. The agreement (within the experimental error range coming from the uncertainty in measuring the absolute detector responsivity) obviously shows that the FIR absorption in the 2D plasma is determined by the same scattering processes as the dc transport. This means that Coulomb scattering by residual impurities, which is the dominant scattering process in these structures, also provides the momentum transfer for the free-carrier optical transitions.

In conclusion, we have observed broadband far infrared radiation from the hot-carrier plasma in GaAs/AlGaAs heterojunctions with ultrahigh as well as low electron mobility. A relative method of determining the carrier heating in the electric field is introduced, which allows the measurement of T over a wide range of carrier heating ($10\,\mathrm{K} < T < 150\,\mathrm{K}$). The method can be also applied to investigate carrier heating in small devices and integrated circuits. At room temperature, however, one has to work in the near infrared range in order to obtain a similarly strong dependence of the emission intensity on carrier heating. Furthermore, the FIR absorption of the 2D plasma could be estimated for the first time, showing a strong dependence on the amount of impurity scattering which permits the momentum transfer for the optical transition.

One of us (R.A.H.) acknowledges support of this work by the Jubiläunsfonds der Österrdichischen Nationalbank and by the European Research Office of the U. S. Army, London. Valuable discussions and permanent collaboration with Professor E. Gornik are gratefully acknowledged. Thanks are extended to G. Strasser for expert help in making the ohmic contacts. The samples were grown at the Forschungsinstitut der Deutschen Bundespost, Darmstadt, in collaboration with W. Schlapp.

[1]For a review see T. P. Pearsall, Surf. Sci. 142, 524 (1984).
[2]S. Luryi, A. Kastalsky, A. C. Gossard, and R. Hendel, Appl. Phys. Lett. 45, 1294 (1984), and references therein.
[3]For example, P. J. Price, Proceedings of 17th International Conference on The Physics of Semiconductors, San Francisco 1984 and references therein.
[4]J. Shah, A. Pinczuk, H. L. Störmer, A. C. Gossard, and W. Wiegmann, Appl. Phys. Lett. 44, 322 (1984).
[5]H. Sakaki, K. Hirakawa, J. Yoshino, S. P. Svensson, Y. Sekiguchi, T. Hotta, and S. Nishii, Surf. Sci. 142, 306 (1984).
[6]D. J. Erskine, A. J. Taylor, and C. L. Tang, Appl. Phys. Lett. 45, 54 (1984).
[7]S. J. Allen, D. C. Tsui, and F. DeRosa, Phys. Rev. Lett. 35, 1359 (1975).
[8]R. A. Höpfel, E. Vass, and E. Gornik, Solid State Commun. 49, 501 (1984).
[9]R. K. Williardson, and A. C. Beer, eds., *Semiconductors and Semimetals* (Academic, NY, 1975), Vol. XII.
[10]H. L. Störmer, A. C. Gossard, W. Wiegmann, and M. D. Sturge, Solid State Commun. 49, 705 (1979).
[11]E. Vass, R. A. Höpfel, and E. Gornik, Solid State Commun. (to be published.
[12]E. Gornik, J. Magn. Magn. Mater. 11, 39 (1979).

Reprint from

Proceedings of the 17th
International Conference
on the Physics of Semiconductors

Edited by J.D. Chadi and W.A. Harrison

Springer-Verlag
New York Berlin Heidelberg Tokyo

FIR-EMISSION FROM FREE CARRIER PLASMA IN GaAs/AlGaAs HETEROSTRUCTURES

Ralph A. Höpfel*, E. Gornik
Institute of Experimental Physics
Schöpfstraße 41, A-6020 Innsbruck
AUSTRIA

G. Weimann
Forschungsinstitut der Deutschen Bundespost
D-6100 Darmstadt
GERMANY

The far infrared (FIR) broadband emission from the two-dimensional (2D) electron plasma in GaAs/AlGaAs heterostructures is investigated for the first time by means of narrowband detectors. The carrier heating in the electric field and the free carrier optical properties are measured. In low mobility samples the free carrier absorption can be described by a Drude behaviour calculated from the DC electrical conductivity, in high mobility samples the free carrier absorption extremely decreases as expected, deviations from the Drude behaviour, however, are observed. Free carrier optical transitions in an external periodical potential (periodic gate structure) are calculated, experimental attempts on FIR emission from such structures are discussed.

I. FIR Broadband Emission from a "warm" 2D Plasma

In the thermodynamical equilibrium the spectral emission intensity $I(\omega)$ of electromagnetic radiation of a system with temperature T is given by

$$I(\omega) = I_{BB}(\omega) \cdot A(\omega) \qquad (1)$$

where I_{BB} is the spectral emission intensity of a black body and $A(\omega)$ is the spectral absorptivity of the system, in a 2D system given by

$$A(\omega) = \frac{4 \cdot \mathrm{Re}F}{|\sqrt{\varepsilon} + 1 + F|^2}\ , \qquad (2)$$

with $F = \sigma(\omega)/\varepsilon_o c$ and ε being the dielectric constant of the substrate. A Drude form of the dynamical conductivity $\sigma(\omega)$ in n-Si inversion layers has been confirmed by microwave and FIR transmission experiments performed by Allen et al. /1/ up to frequencies of 40 cm^{-1}. In GaAs/AlGaAs heterostructures, however, the free carrier absorption has not been measured yet. In order to evaluate FIR emission intensities from the free carrier plasma - as it has been performed in Si-MOSFET structures in ref. /2/ - a relative method is applied in this work. The signals of two narrowband detectors (high purity n-type GaAs at 35 cm^{-1}, Ga-doped Ge at

*present address: AT&T Bell Laboratories, Holmdel, New Jersey 07733, USA.

100 cm^{-1}) are measured as a function of the electric field. From the relative signals the electron temperature is determined using a fit to equation (1), from the absolute intensities the values of the free carrier absorption coefficient can be obtained.

The samples used in our experiments are MBE grown GaAs-AlGaAs single heterostructures with mobilities of 1×10^6 cm^2/Vs at electron concentration $n_s = 2.4 \times 10^{11} cm^{-2}$ at 4.2 K. By LED illumination the electron concentration and mobility changes persistently to $n_s = 3.8 \times 10^{11} cm^{-2}$ and $\mu = 1.3 \times 10^6 cm^2/Vs$. Ohmic contacts, which are important to be of extremely low resistance in order to avoid FIR emission from the contacts, were made by alloying Au/Ge evaporated films of 1000 Å at 400°C. All experiments were performed at liquid helium temperatures, experimental details are contained in ref. /2/, the detectors' spectral responsivities are described in ref. /3/.

The experimental results are shown in fig. 1 and fig. 2. With increasing electric field the mobility decreases due to electron heating and increased phonon scattering. The evaluation of mobility data for electron temperatures - as shown in ref. /4/ by Shah et al. in comparison to photoluminescence experiments - is somewhat problematic due to sample dependent effects. Therefore this decrease of mobility with carrier heating is not quantitatively evaluated.

The values for electron heating as a function of the input power $e\mu|\vec{E}|^2$ per electron, as obtained from the relative FIR emission intensities at two frequencies, is plotted in figure 2 for two values of the carrier concentration. It is emphasized that no absolute intensities have to be known in order to evaluate the carrier heating from the relative signals of the GaAs- and Ge-detector, respectively. The carrier heating above liquid helium temperature is in the same range as measured by photoluminescence by Shah et al. /4/, where the carrier distribution in multiquantum wells is directly measured. At low electric fields the carrier heating is more effective for the lower electron concentration - which also can be seen in the mobility behaviour qualitatively (fig. 1). At higher fields the behaviour changes and the two lines cross.

From the absolute emission intensities ($10^{-13} - 10^{-12}$ W), which were estimated by comparison with InSb cyclotron emission at saturation electron temperatures - see ref. /2/ for details - first informations about the free carrier optical properties can be obtained: The experiments show that the free carrier absorption in low mobility samples ($\mu \sim 10^4 - 10^5 cm^2/Vs$, A (at $\tilde{\nu} = 35\ cm^{-1}$) $\sim 10^{-3}$) can be quantitatively described by a Drude behaviour using the τ-values from DC electrical transport. The extremely high mobility samples (fig. 1 and 2) reveal extremely low absorptivity

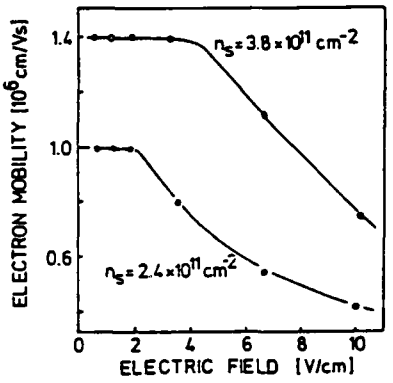

Fig. 1: Electron mobility determined from DC transport as a function of the electric field.

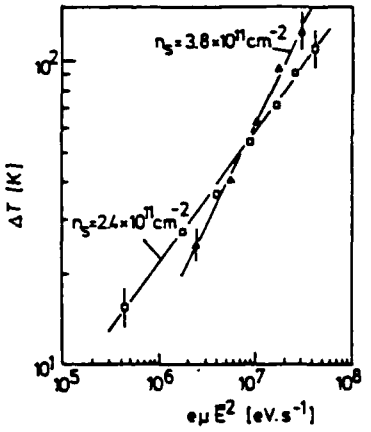

Fig. 2: Electron heating $\Delta T = T_e - 4.2\,K$ determined from relative FIR emission as a function of the input power $e\mu|\vec{E}|^2$ per electron.

values below 10^{-4} (at $\tilde{\nu} = 35\ cm^{-1}$) and below 10^{-5} (at $\tilde{\nu} = 100\ cm^{-1}$). Note, that these low values of absorption are measurable in emission experiments without using gate modulation techniques! The dependence of the emission intensity on the electric field, however, cannot be described by a Drude form of $\sigma(\omega)$ with the relaxation time τ taken from the field-dependent mobility. A quantitative fit is obtained only, when a constant, not field-dependent value of τ (in this case the low-field momentum relaxation time τ_m) is used. The decrease of τ_m at higher electric fields, as seen in mobility data, is not relevant for the free carrier emissivity. From this we conclude that free carrier optical transitions are made possible mainly by impurity scattering, which enables the momentum transfer.

II. Free carrier optical transitions in an external periodic potential

Two-dimensional electron systems represent ideal systems for observing optical transitions due to periodically accelerated motion ("Smith-Purcell-effect" /5/): (1) The carriers are confined near the surface and can be brought close to a periodic gate potential; (2) the carrier system is extremely degenerate and high Fermi velocities are present at simultaneously high mobilities giving extremely long mean free paths up to more than 1 μm at the Fermi surface.

In the following the emission intensity of a GaAs/AlGaAs heterostructure due to the free-carrier radiation by the motion of the electrons with velocity v near the Fermi surface along a periodic potential with amplitude ΔU and period (a) is estimated in a semi-classical model using the dipole radiation theory and Fermi-statistics for the transition probability.

The emission frequency is given by $\omega = (2\pi/a)\cdot v\cdot\cos\phi$, for the estimation of the spectral emission intensity the following assumptions are made: (a) The drift of the carriers along the grating is neglected, only the thermal velocity is considered, (b) only the part of the carriers within the polar angle interval $(-\pi/4, +\pi/4)$ with nearly angle-independent emission frequency ($\cos\phi \sim 1$) is taken into account. Thus the spectral emission intensity per unit area is given by

$$I(\omega)\, d\omega = \frac{e^4 (\Delta U)^2 \cdot \omega \cdot f(\varepsilon)\,[1 - f(\varepsilon - \hbar\omega)]}{6\varepsilon_o\, c^3 h^2}\, d\omega \quad . \tag{2}$$

In fig. 3 the spectral absolute intensity of FIR emission from a real GaAs/AlGaAs heterostructure is plotted ($n_s = 4 \times 10^{11}\,cm^{-2}$, $a = 2200$ Å). The spectral intensity per frequency interval is for a realistic periodic potential of $\Delta U = 1$ mV in the order of some $10^{-11}\,W/cm^2cm^{-1}$ and should therefore be observable. The intensity is proportional to the square of the periodic potential, and thus may reach values of up to $\mu W/cm^2cm^{-1}$. By assuming only carriers with $\vec{k}$-orientation near to the grating orientation, we neglect the low-frequency emission of carriers moving in small angles along the grating. Thus the real emission intensity should be higher than estimated here. A classical treatment of this contribution would give higher values than the black-body emission in the low-frequency regime and thus break the thermodynamic equilibrium model.

Experimentally the system is realised by evaporating a semitransparent (NiCr) gate electrode upon a sinusoidal photoresist structure and applying small voltages and a "compensation" voltage along the gate in order to avoid pinch-off effects during the electric field heating of the 2D system as described in ref. /2/. Experimental results on this new source will be published in a forthcoming paper.

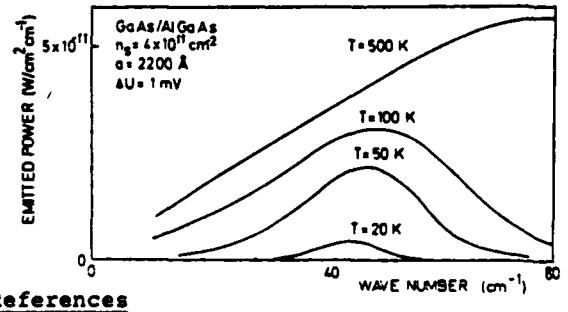

Fig. 3: Spectral emission intensity of "Smith-Purcell"-radiation in GaAs/AlGaAs assuming a periodic potential $\Delta U = 1$ mV and taking only into account electrons in the interval $(-\pi/4, +\pi/4)$ in respect to the grating orientation. Frequency interval 1 cm^{-1}.

References

/1/ S.J. Allen, D.C. Tsui, F. DeRosa, Phys.Rev.Lett. 35 (1975) 1359.
/2/ R.A. Höpfel, E. Vass, E. Gornik, Solid State Commun. 49 (1984) 501.
/3/ "Semiconductors and Semimetals" (R.K. Williardson, A.C. Beer, ed.) Vol. 12, Academic Press, New York 1977.
/4/ J. Shah, A. Pinczuk, H.L. Störmer, A.C. Gossard, W. Wiegmann, Appl. Phys.Lett. 44 (1984) 322.
/5/ S.J. Smith, E.M. Purcell, Phys.Rev. 92 (1953) 1069.

Physica 134B (1985) 323-326
North-Holland, Amsterdam

HOT ELECTRON LANDAU LEVEL LIFETIME IN GaAs/GaAlAs HETEROSTRUCTURES

M. HELM and E. GORNIK

Institut für Experimentalphysik, Universität Innsbruck, A-6020 Innsbruck, Austria

A. BLACK, G.R. ALLAN, C.R. PIDGEON and K. MITCHELL

Physics Department, Heriot-Watt University, Edinburgh, U.K.

G. WEIMANN

Forschungsinstitut der Deutschen Bundespost beim Fernmeldetechnischen Zentralamt, D-6100 Darmstadt, Germany

We report the first measurement of inter-Landau level lifetimes in GaAs/GaAlAs-heterostructures. Saturation cyclotron resonance has been measured using a high intensity optically pumped far infrared laser. The results are analyzed on the basis of a three level model. The obtained lifetimes vary from 0.18 to 1.2 ns for samples with different carrier concentration.

1. INTRODUCTION

In the recent past high power far infrared spectroscopy has been used to determine the lifetimes of impurity and Landau states in semiconductors[1-3]. Up to now these investigations have been restricted to bulk material. Another method to determine energy relaxation times was employed by Bauer and Kahlert[4] for degenerate bulk material and recently by Sakaki et al[5] for GaAs/GaAlAs-heterostructures: The energy relaxation time in a magnetic field was deduced from the strength of the Shubnikov-de Haas (SdH) oscillations as a function of the electric field.

It was found by Gornik et al.[1] and Allan et al.[3] that in bulk material electron-electron scattering plays a dominant role for the inter-Landau level (LL) lifetime. A connection between electron density in the excited level and lifetime was established.

The aim of the present paper is to find out whether a similar mechanism controls the relaxation in 2D-layers as present in heterolayers. We have performed cyclotron resonance (CR) absorption saturation measurements on GaAs/GaAlAs-heterostructures. This technique is a direct method for probing the inter-LL lifetime. The absorption process is described on the basis of a three level model. By comparison with the experimental data the lifetime is deduced and found to vary from 0.18 ns to 1.2 ns for samples with different carrier concentrations indicating the influence of an electron-electron scattering process also in the 2D situation. A direct comparison with theoretical calculations is difficult, since most of the calculations concerning energy relaxation in 2D-systems do not include a magnetic field[6-8].

2. EXPERIMENTAL

The samples were grown by molecular beam epitaxy, their mobilities vary between 10^5 and 10^6 cm^2/Vs, their carrier concentrations between 1.2 and $3 \cdot 10^{11}$ cm^{-2}. A high power quasi cw optically pumped FIR laser was used in the pulsed mode. The pulse duration (0.3 ms) was adjusted to be much longer than the expected relaxation time, ensuring steady-state conditions during optical excitation. In the present work only the

0378-4363/85/$03.30

118.8 μm methanol line was used, because it yielded the highest intensities. Moreover, at the corresponding energy of 10.43 meV the nonparabolicity and polaron effect are large enough to enable saturation. The FIR intensity in the sample was determined by a calibrated pyroelectric detector taking into account the losses of the light pipe and the reflection at the substrate surface. Due to the light pipe optics the sample was subjected to unpolarized radiation. Therefore the effective intensity in the sample was one half of the total intensity in the sample as the geometry was rather a Faraday geometry. An n-type InSb photoconductive detector was used, situated below the sample in the liquid He-bath. The electron concentration was determined from SdH-measurements.

3. THEORETICAL MODEL

Saturation of cyclotron resonance transitions is not possible in a equidistant Landau ladder. However, if a sufficient amount of nonparabolicity and polaron contribution to the effective mass is present, the level shifts can be larger than the linewidth of the individual transitions. In this case saturation can be achieved. Recent experiments[9] have shown that the influence of the LO-phonon ($\hbar\omega \simeq 36$ meV) on the energy levels in GaAs/GaAlAs-heterostructures is negligible below 25 meV, but becomes strong above this value. In the present situation the photon energy is $\hbar\omega = 10.43$ meV, which means that the LL $n = 0$, 1 and 2 undergo small polaron shifts, whereas the $n = 3$ LL is shifted considerably. Thus for a not too broad absorption line the analysis has to include up to three levels. If the absorption linewidth is smaller than the nonparabolicity ($\Gamma < (\hbar\omega_c)^2/\varepsilon_g$), only two levels need to be considered.

The rate equations can, therefore, be written as:

$$\rho_o \frac{df_o}{dt} = -\frac{I}{\hbar\omega} A_o + f_1(1 - f_o)\frac{\rho_o}{\tau} \quad (1)$$

$$\rho_o \frac{df_1}{dt} = \frac{I}{\hbar\omega}(A_o - A_1) + [f_2(1 - f_1) - f_1(1 - f_o)]\frac{\rho_o}{\tau} \quad (2)$$

$$\rho_o \frac{df_2}{dt} = \frac{I}{\hbar\omega} A_1 - f_2(1 - f_1)\frac{\rho_o}{\tau} \quad (3)$$

with I the effective laser intensity in the sample, $\rho_o = eB/\pi\hbar$ the electron concentration per LL, and τ the relaxation time. τ is chosen to be the same for both the $n = 1$ and the $n = 2$ LL since the experimental information is not enough to distinguish a separate τ_1 and τ_2. A_n is the absorptivity of a 2D electron gas given by

$$A_n \simeq \frac{4\sqrt{\varepsilon}\,\mathrm{Re}\,\sigma^{(n)}/\varepsilon_o c}{(\sqrt{\varepsilon} + 1 + \mathrm{Re}\,\sigma^{(n)}/\varepsilon_o c)^2} \quad (\mathrm{Im}\,\sigma \ll \mathrm{Re}\,\sigma \text{ assumed}) \quad (4)$$

with $\mathrm{Re}\,\sigma^{(n)}/\varepsilon_o c =$

$$C \cdot \hbar\omega_c (f_n - f_{n+1})(n+1)\frac{\Gamma}{(\varepsilon_{n+1} - \varepsilon_n + \hbar\omega)^2 + \Gamma^2}$$

the real part of the dynamical conductivity. C is a dimensionless constant determined from the value of the low-intensity absorption. The $\sqrt{\varepsilon}$ in the numerator of Eq. (4) is due to the experimental set-up since the laser beam passes the GaAs substrate prior to the 2D system. The usual expansion of A_n for $\mathrm{Re}\,\sigma^{(n)}/\varepsilon_o c \ll 1$ is not employed, because the changes in transmission reach 65 % in the CR-active polarization. In steady state, Eq. (1) - (3) are solved numerically together with the condition

$$f_o + f_1 + f_2 = \nu \quad (5)$$

where ν is the number of (spin degenerate) filled LL, $\nu = \pi n_s h/eB$. For a comparison with the experiment the normalized transmission change $1 - T/T(\sigma = 0)$ is calculated, with

$$T \simeq \frac{4\sqrt{\varepsilon}}{(\sqrt{\varepsilon}+1+\mathrm{Re}\,\sigma^{(0)}/\varepsilon_0 c+\mathrm{Re}\,\sigma^{(1)}/\varepsilon_0 c)^2} \quad (6)$$

4. RESULTS AND DISCUSSION

Typical experimental traces are shown in Fig. 1 for sample 1433 ($n_s = 1.2 \cdot 10^{11}\mathrm{cm}^{-2}$) and sample 1360 ($n_s = 3 \cdot 10^{11}\mathrm{cm}^{-2}$).

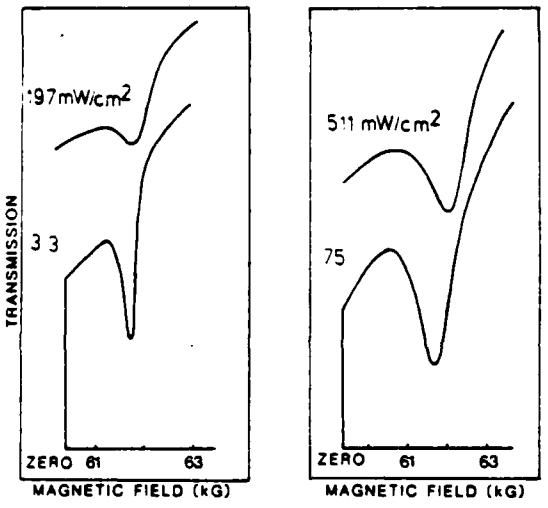

FIGURE 1
Cyclotron resonance absorption for two different GaAs/GaAlAs-heterostructures at 118.8 μm for several laser intensities.
(a) sample 1433 (b) sample 1360
The transmission zero corresponds to CR-active polarization.

Two features can be clearly seen: In both samples saturation has been achieved, but more easily in the low concentration sample. Furthermore, a shift of several hundred Gauss is observed only in Fig. 1b, indicating a transfer of electrons to the n = 2 LL, which also makes the saturation more difficult. This clearly shows the requirement of including this level into the analysis as described before. In Fig. 1a the linewidth is so small that there is no overlap between the two transitions and accordingly no shift.

In Fig. 2 the intensity dependence of the relative transmission change is plotted together with the best fit from Eq. (1) - (5) for sample 1360.

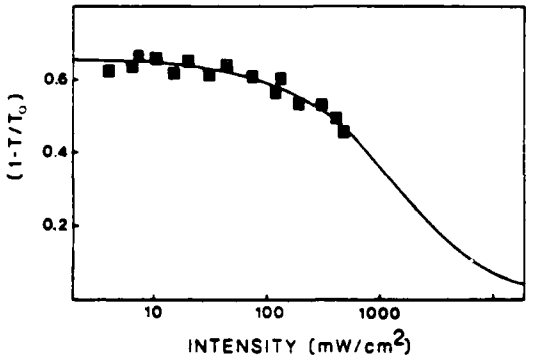

FIGURE 2
Intensity dependence of the relative transmission change for a laser line of 118.8 μm for sample 1360. The solid line represents the best fit from Eq. (1) - (5).

An onset of saturation is observed with a reduction of $1 - T/T_0$ up to 30 %. A further increase in intensity was limited by the experimental system.

Table 1 gives the resulting lifetimes for all samples investigated:

TABLE 1

sample	$n_s(10^{11}\mathrm{cm}^{-2})$	τ(ns)
1360	3.0	0.18
1355	3.0	0.25
1234	2.0	0.65
1395	1.5	0.55
1433	1.2	1.20

The lifetimes were all obtained under conditions, where the n = 0 LL is just filled or partially filled.

Within the experimental error the lifetime increases with decreasing carrier concentration. In an earlier paper Sakaki et al.[5] reported somewhat larger τ-values, but the same depen-

dence on carrier concentration. This was explained by a concentration dependent acoustic phonon rate. His experiment, however, was performed in the weak heating regime ($T < 30$ K) and with small magnetic fields ($B < 3$ T). In the present work a considerable part of electrons is excited to higher LL, corresponding to intersubband temperatures well above 100 K. In addition, for a LL separation of 10 meV the acoustic phonon emission is most likely not the dominant relaxation process. The influence of an electron-electron scattering process similar to that found in bulk material[1,3] seems to be evident for the observed density dependence. To examine this process in detail the excited level carrier concentration has to be determined. Up to now there are not enough data available reaching out in the strong saturation regime to make a meaningful evaluation about the density dependence.

We found that the obtained lifetimes depend strongly on the analysis of the data. The factor $(1 - f_i)$ in Eq. (1) - (3) gives rise to a much slower decrease in the saturation curve (Fig. 2) and to an earlier threshold for saturation, especially in the case of a filled LL. Neglecting this factor would result in a longer lifetime up to a factor of five. From this we conclude that a reliable evaluation needs more data and data to higher power levels, where this factor plays a less important role.

A large uncertainty is found in the evaluation for the low density samples 1395 and 1433 caused by experimental problems: The magnitude of the low-power absorption was not well reproducible according to the unstable experimental conditions. This seems to come from the flat inversion channel in these samples. Similar effects have been observed with DC fields[10]. It was, therefore, difficult to determine the constant C in Eq. (4) accurately.

In summary, we have used FIR saturation spectroscopy to determine inter-Landau level lifetimes in GaAs/GaAlAs-heterostructures. We have found clear evidence for an electron concentration dependent lifetime ranging from 0.18 ns to 1.2 ns. This suggests that electron-electron scattering is playing a dominant role in the energy loss mechanism. A detailed description of the process needs more experimental and theoretical work.

ACKNOWLEDGEMENTS

This work was partly supported by the Jubiläumsfonds der Österreichischen Nationalbank, the European Research Office of the US-Army, London, and by the Science and Engineering Research Council (SERC) of the United Kingdom. The collaboration between the Heriot Watt University, Edinburgh, and the University of Innsbruck was made possible by the British Council.

REFERENCES

1. E. Gornik, T.Y. Chang, T.J. Bridges, V.T. Nguyen, I.D. McGee, and W. Müller, Phys.Rev. Lett. 40 (1978) 1151.
2. C.R. Pidgeon, A. Vass, G.R. Allan, W. Prettl, and L.A. Eaves, Phys.Rev.Lett. 50 (1983) 1309.
3. G.R. Allan, A. Black, C.R. Pidgeon, E. Gornik, W. Seidenbusch, and P. Colter, Phys.Rev. B 31 (1985) 3560.
4. G. Bauer and H. Kahlert, Phys.Rev. B 5 (1972) 566.
5. H. Sakaki et al., Surf.Sci. 142 (1984) 306.
6. K. Hess and C.T. Sah, Phys.Rev. B 10 (1974) 3375.
7. T. Neugebauer and G. Landwehr, Phys.Rev. B 21 (1980) 702.
8. E. Vass, this volume.
9. M. Horst, U. Merkt, W. Zawadzki, J.C. Maan, and K. Ploog, Solid State Commun. 53 (1985) 403.
10. W. Seidenbusch, private communication.

PHYSICAL REVIEW B VOLUME 34, NUMBER 10 15 NOVEMBER 1986

Landau-level population inversion in crossed electric and quantizing magnetic fields

Manfred Helm and Erich Gornik
Institut für Experimentalphysik, Universität Innsbruck, A-6020 Innsbruck, Austria
(Received 8 September 1986)

The problem of the electron distribution in crossed electric and quantizing magnetic fields is treated for free electrons in a parabolic band. The master equation for the diagonal elements of the density matrix is solved, neglecting the k_z dependence of the electron distribution. It is shown that population inversion between Landau levels can be achieved if scattering by optical phonons and a quasielastic scattering process are taken into account.

It is well known that in crossed electric and magnetic fields the electron distribution function can be inverted,[1-9] when the interaction between electrons and optical phonons is strong enough. The electron motion is usually described in the picture of "streaming motion":[4-9] The electrons are assumed to be accelerated until they have enough energy to emit an optical phonon; after that they return into the so-called passive region (inside the circle $v < v_{op} = \sqrt{2\hbar\omega_{op}/m^*}$). If they are scattered into the part of the passive region where the trajectories are closed (accumulation area), they will stay there until they are removed by acoustic-phonon or impurity scattering. The motion is characterized by the parameter $\zeta = v_{op}B/E$. For $\zeta < 1$ all electrons are streaming, and for $\zeta > 2$ all electrons are accumulated (more precisely, the main trajectory through the point $|v| = 0$ is closed), while for $1 < \zeta < 2$ the electrons are partly streaming and partly accumulated.

It was shown that for $\zeta \lesssim 2$ a torus-type distribution function can arise in the accumulation area, which corresponds to a population inversion between Landau levels (LL's).[2,3,6,7] Theoretical studies based on Monte Carlo calculations[7] as well as analytical approaches based on the Boltzmann equation,[6] were carried out. The accumulation of carriers in this area was proved experimentally in different materials,[4] but it was not clear if a population inversion between LL's could be achieved. Very recently, Chebotarev and Murzin reported the observation of a strong emission signal in n-type Ge, which was ascribed to a LL inversion.[10]

Up to now, to our knowledge, all theoretical studies were performed in the limit of nonquantizing magnetic fields; that means the use of a classical distribution function smeared out over the LL's and the use of the zero-magnetic-field scattering rates. On the other hand, if one wants to study optical transitions between (inverted) LL's, the discrete structure of the energy levels is of fundamental importance. In this Rapid Communication we treat the problem of electrons in crossed fields in a fully quantum mechanical frame, which means that we start from the Liouville equation for the density operator.[11,12]

We consider the Hamiltonian (with obvious notations)

$$H = H_{el} + H_{ph} + H_{el\text{-}ph} , \tag{1}$$

where the electric field is incorporated in H_{el}. The electronic eigenvalues and eigenfunctions (B in z direction, E in x direction) are given by[12]

$$E_\nu = (n+\tfrac{1}{2})\hbar\omega_c + \frac{\hbar^2 k_z^2}{2m^*} + eEX_\nu + \tfrac{1}{2}m^*\left(\frac{E}{B}\right)^2 , \tag{2}$$

where

$$\omega_c = \frac{eB}{m^*}, \quad X_\nu = -\left(\frac{\hbar k_y}{eB} + \frac{m^*E}{eB^2}\right) .$$

$$\Psi_\nu(\mathbf{r}) = \text{const} \times e^{ik_y y} e^{ik_z z} \Phi_n\left(\frac{x - X_\nu}{l}\right) , \tag{3}$$

where $l = \sqrt{\hbar/eB}$ and $\Phi_n[(x - X_\nu)/l]$ is the nth harmonic oscillator wave function. The index ν summarizes the quantum numbers n, k_y, k_z. The stationary equation for the density operator is

$$[H, \rho] = 0 . \tag{4}$$

The electron distribution function corresponds to the diagonal matrix elements $\rho_\nu = \mathrm{Tr}_{ph}\langle\nu|\rho|\nu\rangle$, where the trace is taken over the phonon states. In the case of weak electron-phonon coupling it is possible to express the nondiagonal elements by diagonal elements, which then obey the master equation[12]

$$\sum_{\nu'} \rho_{\nu'} W_{\nu'\nu} - \rho_\nu W_{\nu\nu'} = 0 . \tag{5}$$

The $W_{\nu\nu'}$ are the transition probabilities from state ν to state ν' induced by the electron-phonon interaction. Equation (5) is a system of n coupled integral equations (when n LL's are taken into account) for the density-matrix elements. As we look for a homogeneous distribution function, we assume that the ρ_ν are independent of X_ν and, therefore, of k_y.[11,12] Then the k_y integration can be performed directly, and we are left with k_z as the only integration variable.

At this point we make a crude but not unrealistic approximation to enable a simple solution. We drop the quantum number k_z, which means that all electrons are concentrated at $k_z = 0$ (according to the peak in the density of states). This assumption is justified by an experiment of Eaves *et al.*[13] who showed that in high electric fields, transitions with a change in k_z become less important than transitions associated with a change of the spatial coordinate x (see below and Fig. 1). However, we want to point out that the aim of this paper is not a de-

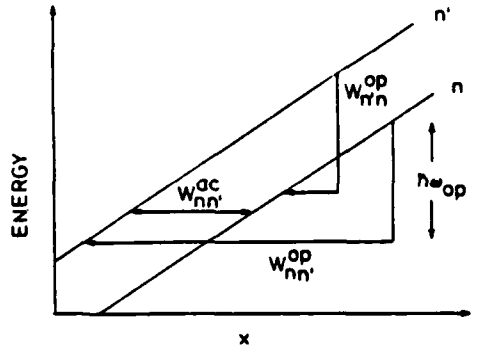

FIG. 1. Two LL's are plotted vs the direction of the electric field. The mechanism of acoustic- and optical-phonon transitions is illustrated.

tailed quantitative study, but rather the first attempt to get information about the qualitative behavior of the distribution function when the magnetic field is quantizing. As a result, Eq. (5) is changed into a system of purely algebraic equations.

In the following we want to deal with three LL's, which is the minimum number necessary to study streaming motion and population inversion: two "unbroken" LL's ($n=0,1$) inside the circle $v=v_{op}$ and the $n=2$ LL, which is broken by the emission of an optical phonon. The system of three linear equations is solved and yields ρ_0, ρ_1, ρ_2 as a function of the k_y-integrated transition rates $W_{nn'}$. We take into account polar optical-phonon scattering and acoustic deformation potential scattering; thus $W_{nn'}=W^{ac}_{nn'}+W^{op}_{nn'}$. The transition probabilities are given by Fermi's golden rule.[11,12] It should be noted that the electric field only appears in the energy δ function and not in the squared matrix elements.

In order to enable an analytical evaluation of the scattering rates we consider only spontaneous emission of optical phonons ($N_{op}\cong 0$) and apply the equipartition approximation for acoustic phonons ($1\ll N_{ac}\cong k_BT/\hbar\omega_q$). Further, we regard the scattering by acoustic phonons as elastic. These approximations can be assumed to be valid at intermediate temperatures ($T\cong 20$–80 K). The explicit transition rates are then given by

$$
\begin{aligned}
&W^{ac}_{10}=W^{ac}_{01}=A^{ac}[8+8\bar{\omega}_c^2]e^{-\bar{\omega}_c^2/2}\,,\\
&W^{ac}_{20}=W^{ac}_{02}=A^{ac}[6+4(2\bar{\omega}_c)^2+2(\bar{\omega}_c)^4]e^{-(2\bar{\omega}_c)^2/2}\,, \qquad (6)\\
&W^{ac}_{21}=W^{ac}_{12}=A^{ac}[7+9\bar{\omega}_c^2-5\bar{\omega}_c^4+\bar{\omega}_c^6]e^{-\bar{\omega}_c^2/2}\,,\\
&W^{op}_{10,01}=A^{op}\cdot 8e^{-(\bar{\omega}_{LO}\mp\bar{\omega}_c)^2/2}\,,\\
&W^{op}_{20,02}=A^{op}[2+2(\bar{\omega}_{LO}\mp 2\bar{\omega}_c)^2]e^{-(\bar{\omega}_{LO}\mp 2\bar{\omega}_c)^2/2}\,, \qquad (7)\\
&W^{op}_{21,12}=A^{op}[11-6(\bar{\omega}_{LO}\mp\bar{\omega}_c)^2\\
&\qquad\qquad +(\bar{\omega}_{LO}\mp\bar{\omega}_c)^4]e^{-(\bar{\omega}_{LO}\mp\bar{\omega}_c)^2/2}\,,
\end{aligned}
$$

where

$$
\bar{\omega}_c=\hbar\omega_c/eEl,\quad \bar{\omega}_{LO}=\hbar\omega_{LO}/eEl\,,
$$

$$
A^{ac}=\frac{D^2k_BTB}{16\sqrt{2\pi}d\rho c_s^2\hbar^2El},\quad A^{op}=\frac{\sqrt{2\pi}e^2\omega_{LO}Bl}{16d\hbar E4\pi\varepsilon_0}\left(\frac{1}{\varepsilon_\infty}-\frac{1}{\varepsilon_{st}}\right)
$$

(D ... deformation potential, ρ ... mass density, c_s ... sound velocity, ω_{LO} ... LO-phonon frequency, $\varepsilon_{st},\varepsilon_\infty$ ... static and high frequency dielectric constant, respectively). d is the thickness of the two-dimensional slab (it cancels out in the final expressions for ρ_i).

Obviously, the acoustic rates depend critically on the ratio $\hbar\omega_c/eEl$. This quantity characterizes the possibility of phonon transitions:[13] As long as $eEL\ll\hbar\omega_c$, the spatial overlap between wave functions of different LL's and same energy is too small to enable transitions ($W_{nn'}\to 0$). Instead of this, transitions associated with a change in k_z, which are not included in our model, would become relevant. However, no population inversion is expected in this regime, but we must be aware of the fact that for $eEl<\hbar\omega_c$ our model is no longer valid. When $eEl>\hbar\omega_c$, the exponential in (6) tends to unity, and direct transitions between the bottom of different LL's become possible. In Fig. 1 this mechanism of phonon-induced transitions between LL's is shown. Transitions caused by optical phonons also yield a vertical contribution in this scheme, corresponding to $\hbar\omega_{LO}$. The required overlap depends on the values of ω_{LO} and ω_c and is much larger for transitions to a higher LL. Hence, $W^{op}_{n'n}>W^{op}_{nn'}$ ($n'>n$) as expected for thermodynamic reasons. In a realistic situation $\omega_c\ll\omega_{LO}$, so the optical-phonon-induced transitions set in at higher electric fields than the acoustic transitions.

At this point it is meaningful to analyze the physical situation based on a three-level scheme. Population inversion should build up between the two lower levels, so the system has to be pumped from $n=0$ to $n=2$. The main requirements for the transition rates are $W_{21}>W_{20}$, and W_{02} as large as possible in order to ensure a fast depletion of the lowest level (more precisely, the expression $W_{21}W_{01}W_{02}/W_{12}W_{10}W_{20}$ must be large).

A central result of our calculation is that no population inversion can be achieved when only optical phonons are taken into account, and no additional quasielastic scattering mechanism comes into play. This stands in contrast to previous calculations performed in the limit of nonquantizing magnetic fields[6,7] and is probably a consequence of the discrete structure of the energy spectrum. The usual explanation for the inversion between the $n=0$ and $n=1$ LL is that the transition probability W^{op}_{21} is larger than W^{op}_{20} (in other words, after emission of an optical phonon the streaming electron rather returns into a state near $v=0$,[3] which corresponds to the $n=1$ LL in the present case). This argument turns out to be correct in terms of the explicit phonon rates. An inversion, however, is prohibited, because the rates W^{op}_{02},W^{op}_{01} are too small compared to W^{op}_{20},W^{op}_{10}.

The situation changes dramatically when an elastic process is also considered ($W^{ac}_{nn'}=W^{ac}_{n'n}$). In Fig. 2 optical and acoustic rates are plotted versus the electric field for two different magnetic field strengths. The parameters are chosen suitable for GaAs [$\hbar\omega_{LO}=36$ meV, $m^*=0.066m_0$, $D=16$ eV, $c_s=5000$ m/s, $\rho=5.3$ g/cm^3, $\varepsilon_{st}=12.5$, $\varepsilon_\infty=10.9$ (Ref. 14)]. In order that only three LL's are relevant, the magnetic field has to be relatively large, which in turn requires quite high electric fields. Figure 3 shows the population difference $\rho_1-\rho_0$ corresponding to the rates of Fig. 2. It is clearly seen that inversion can be

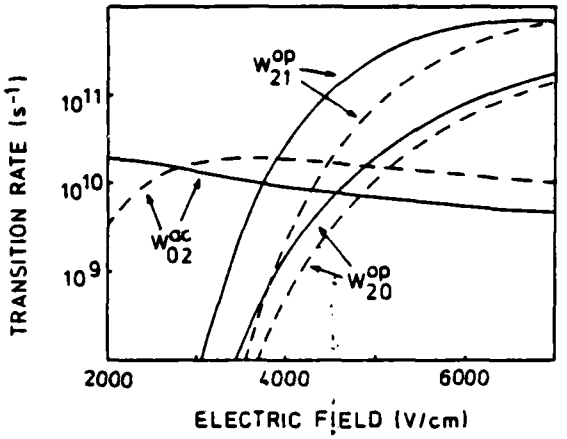

FIG. 2. Transition rates W_{21}^{op}, W_{20}^{op}, and W_{02}^{ac} as a function of the electric field for $B=2$ T (solid line) and $B=3$ T (dashed line). All parameters are chosen suitable for GaAs. d is taken 100 Å, $T=30$ K.

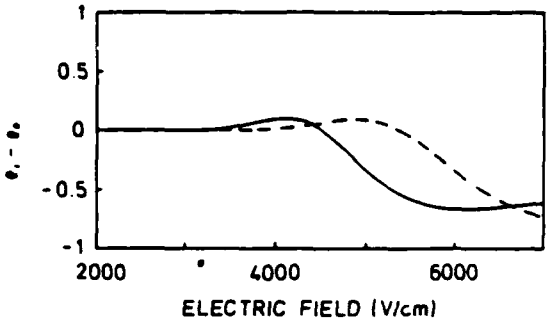

FIG. 3. Population difference $\rho_1-\rho_0$ vs electric field for $B=2$ T (solid line) and $B=3$ T (dashed line). For $B=2$ T the maximum occurs at 4100 V/cm ($\zeta=2.15$, $eEl=2.1\hbar\omega_c$, $\rho_1=0.48$, $\rho_0=0.37$) and for $B=3$ T at 4900 V/cm ($\zeta=2.7$, $eEl=1.4\hbar\omega_c$, $\rho_1=0.48$, $\rho_0=0.38$).

achieved when W_{21}^{op} and W_{20}^{op} come into the same order of magnitude as W_{02}^{ac}; more exactly when $W_{21}^{op} > W_{02}^{ac} > W_{20}^{op}$. Hence the mechanism of inversion can be described as follows: The system is pumped by the transition rate W_{02}. Since $W_{21} > W_{20}$, an overpopulation is built up in the $n=1$ level. To maintain the inversion in a steady state the $n=0$ level has to be depleted by the rate W_{02}, which in turn is identical to the pump. The inversion is, therefore, induced by the selective interplay of different scattering processes.

The relative strengths of the acoustic- and optical-phonon coupling influence the regime of inversion: When the acoustic-phonon interaction increases, the inversion region is shifted towards higher electric fields and vice versa. Consequently, inversion is not restricted to $-1.5<\zeta<2$ as stated in the literature,[4] but can also occur at somewhat smaller or larger values of ζ. It can disappear completely when the relative coupling strengths differ too much. In addition, the absolute value of the magnetic field has an influence on the regime of inversion: A higher magnetic field results in a shift towards higher ζ (see Fig. 3).

An increase of the electric field beyond the maximum value of $\rho_1-\rho_0$ destroys the inversion, because the $n=1$ LL starts streaming ($\rho_1-\rho_0\sim-1$). At still higher electric fields, when all LL's are in a streaming state, the electrons are distributed equally between the LL's ($\rho_l=\frac{1}{3}$). The opposite case of low electric fields also leads to an equidistribution, but this stems from the assumption of totally elastic acoustic-phonon scattering and has no physical significance. The region of very low and very high fields must be regarded with caution anyway, because more than three LL's become relevant.

At this point we have to discuss the validity of our approximations at different magnetic fields. Our calculation is restricted to a regime where only three LL's participate in the pumping process. We have neglected transitions involving a change of k_z; however, these transitions become more important for $eEl<\hbar\omega_c$, which is a range sufficiently below the inversion regime (see Fig. 3). These transitions tend to flatten the steep rise of the optical-phonon rates, leading to a small shift of the inversion maximum to lower electric fields. But as long as $W_{02}^{ac} > W_{20}^{op}$ the inversion will probably still hold.

Experiments have been performed at rather low magnetic fields to fulfill the condition $\zeta\lesssim 2$ for reasonable electric fields. In this case a large number of LL's would have to be considered in our analysis. This makes an explicit evaluation very difficult. On the other hand, eEl becomes much larger than $\hbar\omega_c$ (if E/B is kept constant) in this situation. Consequently, the scattering process considered in this work becomes clearly dominant due to the increasing overlap of the wave functions with decreasing magnetic field. This is further evidence that this process gives an essential contribution to the electron distribution function between LL's.

In summary, we have treated the problem of the electron distribution in crossed electric and quantizing magnetic fields with approximations allowing an explicit solution. The possibility of LL inversion has been demonstrated when polar optical-phonon scattering and another quasielastic scattering process are taken into account.

A treatment which is directly comparable to an experimental situation, however, should include up to 5 or 6 LL's. Furthermore, the finite energy of acoustic phonons should be considered and the solution of the coupled integral equations (k_z dependence) is necessary. But also, the present simple approach reveals the qualitative behavior of the system.

We gratefully acknowledge helpful discussions with Professor W. Zawadzki and Dr. R. Lassnig. This work was supported by the European Research Office of the U.S. Army.

[1]H. Maeda and T. Kurosawa, in *Proceedings of the Eleventh International Conference on the Physics of Semiconductors, Warsaw, 1972*, edited by The Polish Academy of Sciences (PWN-Polish Scientific Publishers, Warsaw, 1972), p. 602.

[2]Ya. I. Al'ber, A. A. Andronov, V. A. Valov, V. A. Kozlov, and I. P. Ryazantseva, Solid State Commun. 19, 955 (1976).

[3]T. Kurosawa, Solid State Commun. 24, 357 (1977).

[4]S. Komiyama, Adv. Phys. 31, 255 (1982).

[5]S. Komiyama, in *Polarons and Excitons in Polar Semiconductors and Ionic Crystals*, edited by J. T. Devreese and F. M. Peeters (Plenum, New York, 1984), p. 41.

[6]F. Brosens and J. T. Devreese, Solid State Commun. 44, 597 (1982).

[7]P. Warmenbol, F. M. Peeters, and J. T. Devreese, Phys. Rev. B 33, 1213 (1986).

[8]R. Brazis, Physica B 134, 201 (1985).

[9]A. A. Andronov *et al.*, Physica B 134, 210 (1985).

[10]A. P. Chebotarev and V. N. Murzin, Pis'ma Zh. Eksp. Teor. Fiz. 40, 234 (1984) [JETP Lett. 40, 1005 (1984)].

[11]D. Calecki, C. Lewiner, and P. Nozières, J. Phys. (Paris) 38, 169 (1977).

[12]D. Calecki, in *Physics of Nonlinear Transport in Semiconductors*, edited by D. K. Ferry, J. R. Barker, and C. Jacoboni (Plenum, New York, 1980), p. 289.

[13]L. Eaves, P. S. S. Guimaraes, J. C. Portal, T. P. Pearsall, and G. Hill, Phys. Rev. Lett. 53, 608 (1984).

[14]*Semiconductors*, edited by O. Madelung, M. Schulz, and H. Weiss, Numerical Data and Functional Relationships in Science and Technology, Landolt-Börnstein Series, Group III, Vols. 17a and 17b (Springer, Berlin, 1982).

Optical Properties of Narrow-Gap Low-Dimensional Structures

Edited by

C. M. Sotomayor Torres

University of St. Andrews
St. Andrews, Scotland

J. C. Portal

CNRS-INSA
Toulouse, France
and CNRS-SNCI
Grenoble, France

J. C. Maan

Max-Planck-Institut für Festkörperforschung
Grenoble, France

and

R. A. Stradling

Imperial College of Science and Technology
London, England

Plenum Press
New York and London
Published in cooperation with NATO Scientific Affairs Division

ENERGY RELAXATION PHENOMENA IN GaAs/GaAlAs STRUCTURES

Erich Gornik

Institut für Experimentalphysik, Univ. Innsbruck
A-6020 Innsbruck, Austria

The energy relaxation of 2D electrons in GaAs/GaAlAs structures has been investigated by analysing the electric field dependence of Shubnikov-de Haas oscillations, the far infrared emission and photoluminescence spectra. A quite general behavior of the electron heating $\Delta T = T_e - T_L$ as a function of the input power per electron P_e is found: $T \propto \sqrt{P_e}$. The corresponding energy relaxation times in the range of nsec are independent of the electron temperature up to 30 K and inversly proportional to the electron density. At higher electron temperatures the energy relaxation is governed by optical phonon emission. However, the onset depends on electron concentration and is different for heterostructures and quantum wells. From intensity dependent cyclotron resonance transmission experiments Landau level lifetimes between 0.2 ns and 1 ns depending on the electron density are found in agreement with data from time-resolved photoluminescence.

INTRODUCTION

The mechanism of energy relaxation is of fundamental interest for the understanding of electric field effects in two-dimensional (2D) electron systems. At low temperatures, where lattice scattering is weak, hot electron phenomena can be produced by fields as low as V/cm in Si as well as GaAs inversion layers.

The first investigations of energy relaxation in 2D systems were performed by Hess et al.[1]. The energy loss was determined from Shubnikov-de Haas (SdH) experiments as a function of electric field for temperatures up to 20 K in p-Si inversion layers. Similar investigations were performed by Englert and Landwehr[2] for Si-n-inversion layers. Sakakai et al.[3] investigated with the same technique n-GaAs inversion layers in heterostructures. For temperatures below 30 K a dominance of acoustic phonon relaxation is found for both materials.

Emission techniques including the analysis of the broad-band hot electron emission[4,5], subband emission[6] and the plasmon emission[7,8] have been used to determine the energy loss rate as a function of input power. It was found that this rate

is sample-independent as long as acoustic phonon scattering is dominant. A theoretical description of this phenomenon was given by Vass[9,10] and Price[11,12].

Very fundamental information on the hot electron distribution and energy loss rate is obtained from time resolved photoluminescence experiments performed by Shah et al.[13,14]. Over a wide range of electric fields a hot electron temperature-like distribution function was found. For temperatures above 50 K the energy loss rate is dominated by the emission of longitudinal optical (LO) phonons. Evidence for screening of the electron LO phonon interaction[15,16] and for hot phonon effects[17,18] is found.

The energy relaxation in the presence of a strong magnetic field has been studied only recently. The saturation behavior of the cyclotron resonance (CR) absorption as a function of laser power yields an electron density dependent energy relaxation time[19]. From time dependent luminescence experiments in GaAs/GaAlAs quantum wells a decrease in the relaxation rate with magnetic field is found for fields below 10 T[20] and an increase for fields of 20 T[21].

In the present paper a summary on experimental techniques to determine the energy relaxation in GaAs/GaAlAs heterostructures in the temperature range up to 100 K is given. The results will be compared with recent theoretical results. In the presence of a magnetic field a qualitative description of the experimental findings will be presented due to the lack of theoretical work.

ENERGY RELAXATION AT ZERO AND LOW MAGNETIC FIELDS

The electron heating and the energy relaxation in 2D GaAs was first investigated by analysing Shubnikov-de Haas (SdH) oscillations at low magnetic fields ($B < 3$ T) as a function of the input power. Optical techniques as photoluminescence and far infrared (FIR) emission at zero magnetic field followed. The classical technique evaluating the time dependence of the hot electron current following a small step variation in electric field[22] has not been applied to a 2D system so far.

a) Electric field dependence of SdH oscillations

A damping of SdH oscillations in magneto-resistance is observed when the 2D electron gas (2DEG) is heated in an electric field. To determine the electron temperature T_e from the temperature and electric field dependent oscillations, the Dingle temperature must be constant[23]. If that is the case the change in amplitude can be described by one parameter T_e. Fig. 1 shows a typical result of SdH measurements after Sakaki et al.[3] at 4.2 K. The decay in SdH amplitude is clearly observed with increasing current (corresponding to increasing electric field). Significant differences in the heating behavior are found as a function of zero field mobility. However, a very general behavior is obtained when T_e is plotted against the input power per electron. The weakness of this technique lies in the fact that $P_e = e\mu E^2$ is calculated using the electric field dependent mobility at zero magnetic field while the T_e values are determined from SdH oscillations at finite B.

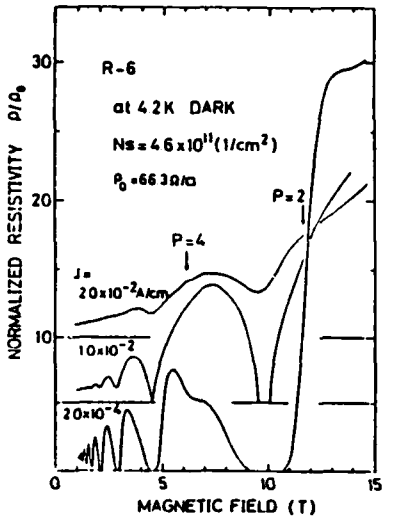

Fig. 1: Shubnikov-de Haas oscillations of Sample R-6 after Ref. 3. The sample has a mobility of $2.05 \times 10^5 cm^2/Vs$.

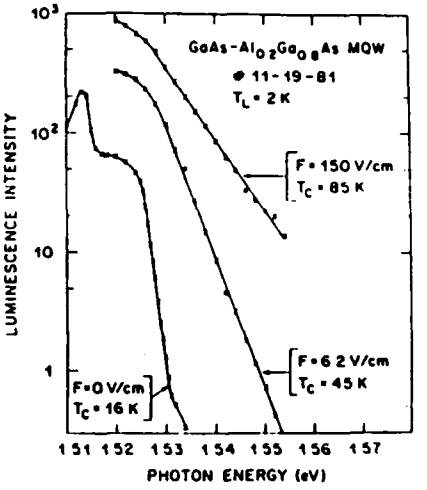

Fig. 2: Photoluminescence spectra of GaAs/AlGaAs heterostructures for three in-plane electric fields. The electron temperatures deduced from the high-energy slope are indicated. Relative intensities of curves are arbitrary (after Ref. 13).

The results from Sakaki et al.[3] will be shown in Fig. 4 together with the data from the other techniques. Similar results were obtained by other authors studying the mobility and electron temperature as a function of electric field[24,25,26].

b) Hot electron luminescence analysis

Luminescence experiments on GaAs/GaAlAs multiple quantum well (MQW) structures were performed by Shah et al.[13,14]. A cw infrared dye laser (7700 Å < λ < 7900 Å, P = 2 mW) was used to weakly excite carriers in the GaAs across the gap. Luminescence spectra as a function of electric field were analysed with a double monochromator. Typical spectra after Shah et al.[14] are shown in Fig. 2 for three different electric fields. The high energy tail is attributed to electron hole recombination. This tail can be well fitted by a single exponential (see Fig.2) at all fields up to the highest field (150 V/cm). The spectra are fitted with a Maxwell-Boltzmann type distribution with a temperature T_e higher than T_L.

The obtained electron heating ΔT is also plotted in Fig.4 over the input power derived from I-V measurements. In a steady state situation the power input must be equal to the power loss to the lattice. This technique gives direct means to determine energy loss rates at zero magnetic field. It is found that the electron heating shows a somewhat weaker dependence on input power than the previous technique and that there is also practically no dependence on the carrier concentration.

The disadvantage of this technique is the simultaneous excitation of holes which can influence the total energy loss rate. In addition we have to be aware of the fact, that the experiments were performed on MQW which may give a somewhat different behavior than heterostructures. A comparison will only be meaningful for rather wide wells (as in the present case: well thickness 250 Å).

c) Far infrared (FIR) emission

The basic idea of this experiment is to heat up the 2D carrier gas by electric field pulses and to measure the spectrum and intensity of the emitted broadband FIR light and to correlate it with an electron temperature.

FIR broadband emission has first been used in Si-MOSFETs to determine the energy loss of 2D carriers[4]. The electron temperature T_e was determined from the absolute value of the emitted power. For 2D electrons in GaAs a somewhat different experimental technique based on a relative intensity measurement was applied. The signals of two narrowband FIR detectors (n-GaAs at 35 cm^{-1}, Ga doped Ge at 100 cm^{-1}) are measured as a function of the applied electric field and calculated for each detector according to

$$U = \int_0^\infty R(\omega)A(\omega)I_{BB}(\omega,T_e)\cdot d\omega \qquad (1)$$

where $R(\omega) = R_o r(\omega)$ and $A(\omega) = A_o a(\omega)$ are the frequency dependent and known detector response and the absorptivity of the electron system respectively. In equilibrium the spectral emission intensity of a system with absorptivity $A(\omega)$ is given by

$$I(\omega,T) = I_{BB}(\omega,T)\cdot A(\omega) \qquad (2)$$

with I_{BB} the black body emission intensity (Planck-function). Assuming a quasi equilibrium of the electron system at a temperature T_e, we can express the broadband emission from the 2D carrier gas by $I(\omega,T_e)$.

The absorptivity can be expressed for normal incidence according to

$$A(\omega) = \frac{4ReF}{(\sqrt{\varepsilon_s} + 1 + F)^2} \qquad (3)$$

with $F = \sigma(\omega)/\varepsilon_o \cdot c$ and ε_s being the dielectric constant of the substrate. For $\sigma(\omega)$ a Drude type frequency behavior is assumed.

The unknown parameters in equ. (1) are determined by measuring with two detectors at two different electric fields giving four equations for four unknown factors. Fig. 3 shows the observed detector signal in Volts as a function of electric field for two different samples: a low mobility sample with $n_s = 8.7 \times 10^{11} cm^{-2}$ and $\mu = 1.6 \times 10^3 cm^2/Vs$ (Sample 1) and a high mobility sample with $n_s = 2.4 \times 10^{11} cm^{-2}$ and $\mu = 1.0 \times 10^6 cm^2/Vs$ (Sample 2, dark). It is directly evident that the lower mobility sample shows a considerably higher emission signal.

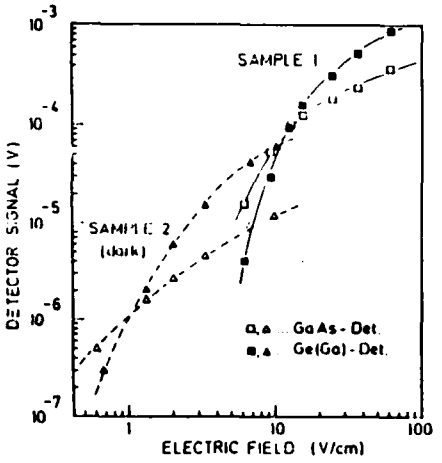

Fig. 3: Detector signals as a function of applied electric field for two different detectors after Ref. 5.
The sample and detector properties are given in the text.

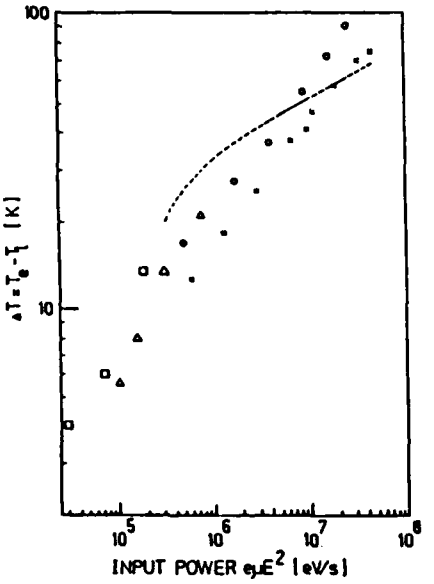

Fig. 4: Electron heating versus input power per electron obtained from the different techniques:
Ref. 3: (Δ) sample described in Fig. 1, (□) N_s=3.5x10^{11}cm^{-2}, μ=7.0x10^{4}cm^2/Vs.
Ref. 5: (x) Sample 1, (o) Sample 2 (see text); dashed curve: data from Ref. 13.

Quantitative values for the electron temperature are determined from the fit of Fig. 3 according to equ. (1) and also plotted as a function of the input power in Fig. 4. The basic behavior of ΔT is the same as determined with the other techniques. The emission data have a somewhat steeper slope than the luminescence data. There is also a weak dependence on density evident in the emission data.

The emission technique seems to be the most appropriate method to determine T_e. However, the analysis requires several assumptions which might introduce sample dependences.

A similar FIR emission technique is the analysis of the emission from 2D plasmon excitations as demonstrated first in Si[27,7] and later in GaAs[28]. In a recent paper Sambe et al.[29] have analyzed the emitted power from 2D plasmon excitation in GaAs and derived electron temperatures as a function of electric field. As mobility on electric field data were not published an inclusion of their data in Fig. 4 is not possible.

The summary of the experimental findings is shown in Fig. 4 as a plot of $\Delta T = T_e - T_L$ over the input power per electron P_e. It is clearly evident that the emission data continue very well the SdH results. The data can be described by a relation $\Delta T \propto \sqrt{e\mu E^2}$ up to electron temperatures of 30 K. For higher temperatures the emission data show a weak, while the luminescence data show a considerably stronger change in slope.

d) Determination of the energy relaxation time

To derive an energy relaxation time from the data an energy balance equation for the average electron energy $\varepsilon(T)$ using Fermi-Dirac statistics with an electron temperature T_e is used:

$$|\varepsilon(T_e) - \varepsilon(T_L)|/\tau_\varepsilon \approx \frac{\pi^2 k_B^2}{6\varepsilon_F}(T_e^2 - T_L^2)/\tau_\varepsilon = e\mu E^2 = P_e \qquad (4)$$

where ε_F is the Fermi energy and μ the electric field dependent mobility. It is directly evident that the expression $\Delta T = T_e - T_L = \text{const.} \sqrt{P_e \cdot \varepsilon_F \cdot \tau_\varepsilon}$ describes the experiments quite well indicating that for a given P_e the product $\varepsilon_F \cdot \tau$ has to be sample independent. As $N_s = D(\varepsilon) \cdot \varepsilon_F$ with $D(\varepsilon) = \text{const.}$ τ_ε is inversely proportional to the 2D carrier density.

The resulting energy relaxation times as a function of density as obtained from Fig. 4 for the range of electron temperatures, where the slope is constant, is plotted in Fig.5. As long as the slope of ΔT over P_e is constant we obtain a τ_ε-value independent of T_e for a given sample. It is clearly evident that the energy relaxation time is a linear inverse function of the density as a consequence of the analysis with equ. (4). Both methods, the SdH oscillations and the emission technique, give within experimental accuracy the same τ_ε-values so that we can be quite confident about the obtained results.

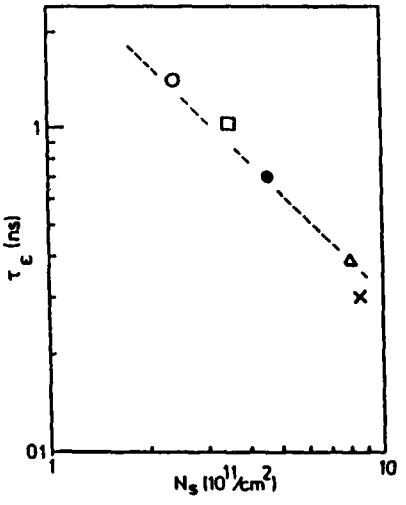

Fig. 5: Calculated energy relaxation time versus 2D electron density for three samples from Ref. 3 (□, ●, Δ) and two samples from Ref. 5 (o, x). The symbols represent the same samples as in Fig. 4.

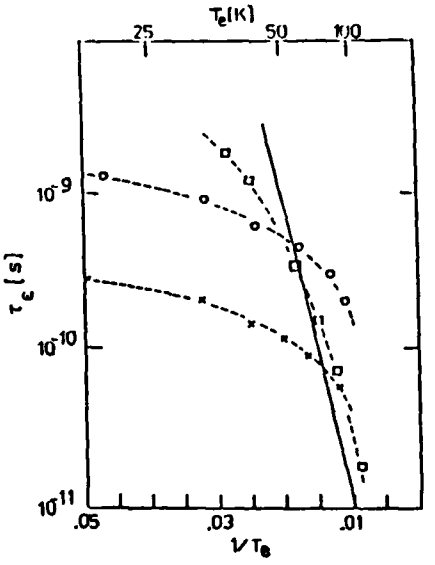

Fig. 6: Energy relaxation times versus electron temperature for Sample 1 (x) and Sample 2 (o) from Ref. 5 and for a sample with $N_s = 3.9 \times 10^{11}$ cm^{-2} and $\mu = 7.9 \times 10^4$ cm^2/Vs from Ref. 3. The full curve represents the loss due to optical phonons[14].

An evaluation of τ_ε over T_e is only meaningful for temperatures above 30 K, where the slope starts changing. But also in the higher temperature range we use equ. (4) to evaluate τ_ε which means that we use degenerate Fermi-Dirac statistics with an electron temperature T_e. The use of the statistics has a strong influence on the results. A plot of τ_ε-values from the emission data for two different samples and for the photoluminescence data is shown in Fig. 6 as a function of the inverse electron temperature (and electron temperature). The energy relaxation times derived from the emission data show a similar behavior for both concentrations: For temperatures above 40 K τ_ε decreases significantly reaching values of a few hundred psec. The analysis of the photoluminescence data gives a considerably stronger dependence of τ_ε on T_e which is already evident in the weaker ΔT over P_e curve. The full curve shows calculations of the energy relaxation rate due to optical phonons for a 3D case[14]. This curve has a slope proportional to the optical phonon energy (36 meV) in GaAs. It is evident from Fig. 6 that for both techniques there is a tendency toward the optical phonon line. However, there is a clear difference in the behavior of the results from the two techniques. The photoluminescence data seem to be more strongly influenced by the optical phonon emission. The reason for this is not clear but might be due to the fact that in the photoluminescence experiment electrons are always excited above the optical phonon energy by the laser excitation.

In Ref. 14 it was argued that the energy loss rate for electrons was considerably smaller than for holes. However, we do not find this result since the energy loss rates shown in Fig. 6 are comparable with loss rates of holes. The difference in the data comes from the analysis. Shah et al.[14] used non-degenerate statistics. The τ_ε-values obtained this way are longer by a factor $\varepsilon_F/\Delta T$. For samples with Fermi energies of the order of 20 meV the use of non-degenerate statistics seems not appropriate.

A critical analysis of the energy relaxation was performed by Tsubaki et al.[30] who analysed transport studies as a function of electric field from several authors. The influence of the used statistics in the evaluation was examined. It is shown that the application of degenerate statistics is meaningful down to ε_F/k_BT-values of 3. However, the obtained τ_ε-values are independent of N_s and are nearly an order of magnitude shorter than the data shown in Fig. 6. At low temperatures the values are comparable, however, the slope of the τ_ε versus T_e plot is considerably steeper (in Ref. 30) than the optical phonon curve (see full curve in Fig. 6).

A theoretical description of the energy relaxation rate for 2D electrons in GaAs in the case of acoustic phonon scattering has been published by Vass[9]. Vass derived an expression for the energy loss rate: $\Delta T = \text{const.} \sqrt{P_e}$ where the calculated value of the constant agrees well with the experimental findings in GaAs and Si[4]. The power loss is dominated by acoustic deformation potential scattering up to temperatures of 40 K. In a recent paper[10] values for the energy relaxation time as a function of electric field and electron concentration were reported including optical phonon emission and electron-electron scattering. The calculated values show the same electric field (or T_e) dependence as the experimental

values but are an order of magnitude to high. The predicted carrier density dependence is also too weak.

Price has investigated the mobility and energy loss rate for piezo-electric and deformation potential acoustic phonon scattering[13]. For temperatures up to 10 K he predicts piezo-electric scattering to be dominant giving a considerably steeper dependence of ΔT on P_e than from equ. (4). For higher temperatures he predicts a linear dependence of ΔT on P_e which is also dependent on the sample concentration. These results are not in agreement with the experimental observations.

ENERGY RELAXATION IN HIGH MAGNETIC FIELDS

A direct way to obtain the energy relaxation rate in the presence of a strong magnetic field is the measurement of the incoherent saturation of the CR transmission. This technique has been applied to bulk n-type InSb and GaAs[31,32]. It was found that an interplay between electron-electron scattering and optical phonon emission governs the energy relaxation. The same technique was applied to GaAs/GaAlAs heterostructures by Helm et al.[19]. A high power cw optically pumped FIR laser was used to perform the experiments. Typical transmission spectra for two different samples are shown in Fig. 7. It is evident that powers below 1 W/cm^2 reduce the transmission already significantly and that the lower density sample saturates stronger. In the analysis rate equations for three Landau levels and a constant relaxation time τ_B was used. Fig. 8 shows the obtained relaxation time τ_B plotted against the total 2D carrier concentration. A systematic decrease of τ_B with N_s is observed even though there is considerable scatter in the data. The dependence of τ_B on N_s indicates that the mechanism may be similar to that found in bulk semiconductors[31]. It is also interesting to note that in the zero magnetic field case a similar dependence is found.

Data on relaxation rates between Landau levels were also reported by Ryan et al.[20] and Hollering et al.[21] using psec photoluminescence techniques. Ryan et al. find relaxation times in the order of 0.3 ns between the first excited and lowest Landau level for MQW samples with $N_s = 5 \times 10^{11}$cm^{-2}. The relaxation times in magnetic fields of 7 and 8 T are longer than without magnetic field. On the other hand Hollering et al. find a considerably shorter time for fields of 20 T as compared to the zero magnetic field case.

The whole behavior seems to be consistent: In fields below 10 T the energy relaxation time derived is increased as compared to the field free case. The data from Fig. 8 have to be compared with τ_ε-values in Fig. 6 at the highest temperatures. This comparison shows that they are somewhat longer in agreement with Ryan's observation on the same sample. The considerably shorter values for 20 T are somewhat surprising. In Ref. 21 they are briefly explained by a reduced screening of the electron LO phonon interaction.

Further experimental and theoretical studies in the magnetic field are necessary to get clear evidence for the relaxation mechanism. In a very recent paper Rodriguez et al.[33] report an intensity dependent CR transmission experiment at rather low

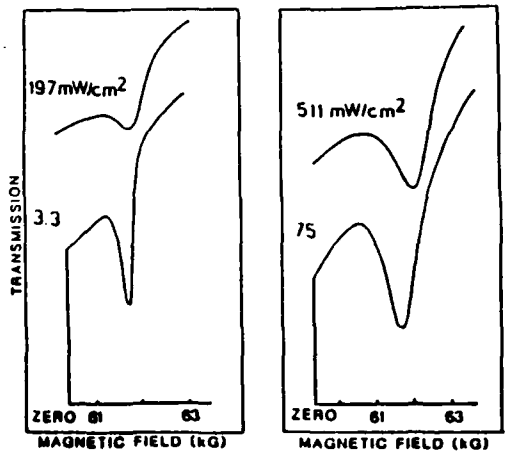

Fig. 7: Cylotron resonance absorption for two different GaAs/GaAlAs heterolayers at 118 μm for different laser intensities: left sample with N_s = $1.2 \times 10^{11} cm^{-2}$, right sample with $N_s = 3.0 \times 10^{11} cm^{-2}$.

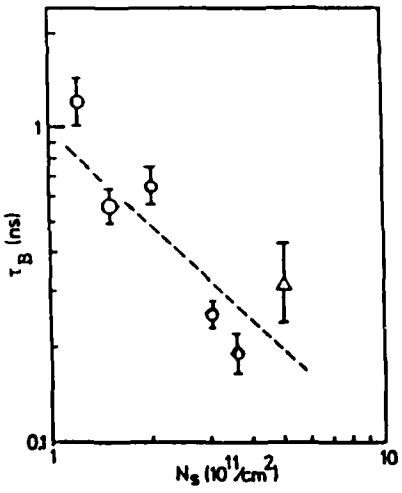

Fig. 8: Calculated lifetimes from saturation behavior as a function of N_s: (o) cyclotron resonance, (Δ) photoluminescence. The dashed curve represent a linear dependence.

frequencies. Saturation is observed at considerably higher intensities than in Ref. 19 for magnetic fields below 4 T. This indicates a non-resonant heating process similar to direct electric field heating. The observed relaxation times in the order of 10 psec probably directly reveal the optical phonon relaxation time. The main reason for this behavior is the nearly equidistant Landau level spacing at low magnetic field. In this situation a resonant saturation of a transition between two levels is not possible. Only if a sufficient amount of nonparabolicity is present the level shifts are larger than the individual Landau level linewidths and a saturation of an individual transition becomes possible as demonstrated in Ref. 19.

ACKNOWLEDGEMENT

This work was partly supported by the European Research Office of the U.S. Army, London, and the Stiftung Volkswagenwerk, Projekt-Nr. I 61 840, Hannover.

REFERENCES

1. K. Hess, T. Englert, T. Neugebauer, G. Landwehr and G. Dorda, Phys. Rev. B 16, 3652 (1977).
2. T. Englert and G. Landwehr, Phys. Rev. B 21, 702 (1980).
3. H. Sakaki, K. Hirakawa, J. Yoshino, S.P. Svensson, Y. Sekiguchi, T. Hotta, S. Nishii and N. Miura, Surf. Sci. 142, 306 (1984).
4. R.A. Höpfel, E. Vass and E. Gornik, Solid State Commun. 49, 501 (1984).
5. R.A. Höpfel, E. Gornik and G. Weimann, Proc. of the 17th Int. Conf. on the Physics of Semiconductors, p. 579, Springer-Verlag (1984); R.A. Höpfel and G. Weimann, Appl. Phys. Lett. 46, 291 (1985).
6. E. Gornik and D.C. Tsui, Solid State Electron. 21, 139 (1978).
7. R.A. Höpfel, E. Vass and E. Gornik, Phys. Rev. Lett. 49, 1667 (1982).
8. R.A. Höpfel and E. Gornik, Surface Science 142, 412 (1984).
9. E. Vass, Solid State Commun. 55, 847 (1985).
10. E. Vass, Physica 134 B, 337 (1985).
11. P.J. Price, J. Appl. Phys. 53, 6863 (1982).
12. P.J. Price, Physica 134 B, 164 (1985).
13. J. Shah, A. Pinczuk, H.L. Störmer, A.C. Gossard and W. Wiegmann, Appl. Phys. Lett. 42, 55 (1983).
14. J. Shah, A. Pinczuk, A.C. Gossard and W. Wiegmann, Physica 134 B, 174 (1985).
15. C.H. Yang and S.A. Lyon, Physica 134 B+C, 305 (1985).
16. S. Das Sarma and B.A. Mason, Physica 134 B+C, 301 (1985).
17. P. Kocevar, Physica Status Solidi (b) 84, 581 (1977).
18. P.J. Price, Phys. Rev. B 30, 2236 (1984).
19. M. Helm, E. Gornik, A. Black, G.R. Allan, C.R. Pidgeon and K. Mitchell, Physica 134 B, 323 (1985).
20. J.F. Ryan, Physica 134 B, 403 (1985); J.F. Ryan, R.A. Taylor, A.J. Turberfield and J.M. Worlock, Physica 134 B, 318 (1985).
21. R.W.J. Hollering, T.T.J.M. Berendshot, H.J.A. Blyssen, P. Wyder, M.R. Leys and J. Wolter, Physica 134 B, 422 (1985).
22. J.P. Maneval, A. Zilberstein and H.F. Budd, Phys. Rev. Lett. 23, 848 (1969).
23. G. Bauer and H. Kahlert, Phys. Rev. 5, 556 (1972); H. Kahlert and G. Bauer, Phys. Rev. B 7, 2670 (1973).
24. T.J. Drummond et al., Electron. Lett. 17, 545 (1981).
25. S. Hiyamizu, T. Fujii, T. Mimura, K. Nanbu, J. Saito and H. Has, Japan. J. Appl. Phys. 20, 455 (1981).
26. M. Inoue, M. Inayama, S. Hiyamizu and Y. Inuishi, Japan. J. Appl. Phys. 22, 357 (1983) Suppl. 22-1.
27. D. Tsui, E. Gornik and R.A. Logan, Solid State Commun. 35, 875 (1980).
28. R.A. Höpfel, G. Lindemann, E. Gornik, G. Stangl, A.C. Gossard and W. Wiegmann, Surf. Sci. 113, 118 (1982).
29. Y. Sambe et al., Ext. Abstract 17th Conf. on Solid State Devices and Materials (Tokyo), 95 (1985).
30. K. Tsubaki, A. Sugimura and K. Kumabe, Appl. Phys. Lett. 46, 764 (1985).
31. E. Gornik, T.Y. Chang, T.J. Bridges, V.T. Nguyen, I.D. Mc Gee and W. Müller, Phys. Rev. Lett. 40, 1151 (1978).
32. G.R. Allan, A. Black, C.R. Pidgeon, E. Gornik, W. Seidenbusch and P. Colter, Phys. Rev. B 31, 3560 (1985).
33. G.A. Rodriguez, R.M. Hart, A.J. Sievers, F. Keilmann, preprint.

Solid-State Electronics Vol. 31, No. 3/4, pp. 759–762, 1988
Printed in Great Britain

0038-1101/88 $3.00 + 0.00
Pergamon Journals Ltd

NEW RESULTS ON STIMULATED EMISSION FROM p-GERMANIUM IN CROSSED FIELDS

M. Helm, K. Unterrainer, E. Gornik

Institut für Experimentalphysik, Universität Innsbruck, A-6020 Innsbruck, Austria

E. E. Haller

Lawrence Berkeley Laboratories, Berkeley, CA 94720, USA

ABSTRACT

The spectrum of the stimulated far infrared emission from p-Germanium in crossed electric and magnetic fields is studied by means of a tunable narrowband GaAs-detector. A multimode spectrum is observed from mirrorless samples and quantitatively explained in terms of waveguide-like modes.

KEYWORDS

Far infrared; laser; p-Germanium; hot holes; crossed fields; mode structure;

INTRODUCTION

During the last three years it has become possible to realize high power far infrared (FIR) semiconductor lasers /1-7/. The stimulated emission is caused by a population inversion between the light and heavy hole bands in lightly p-doped Germanium crystals subjected to crossed electric and magnetic fields. This population inversion builds up, when the heavy holes interact strongly with the optical phonons ("streaming motion"), whereas the light holes accumulate in momentum space /8/. Up to now, lasing has been observed for electric and magnetic fields satisfying the relation $1 \leq \zeta_h \leq 1.9$, where $\zeta_h = \sqrt{2\hbar\omega_{op}/m_h^*}\cdot(B/E) = v_{op}^h B/E$, with the optical phonon energy $\hbar\omega_{op} = 37$ meV and the effective mass of the heavy holes $m_h^* = 0.35\ m_0$. Emission wavelengths between 75 μm and 250 μm have been reported with output powers up to 10 Watts. The radiation has been observed both from mirrorless samples which form a waveguide-like cavity and from samples with external mirrors /7/.

A point not yet clarified is the mode structure of the emitted light. Different authors reported a variety of different spectra /4-7/, and no unambiguous explanation could be given, partly due to insufficient resolution of the spectrometers used in these experiments.

We have studied the spectrum of the stimulated emission from p-Ge by means of an extremely narrowband, magnetic field tunable n-GaAs detector. By analyzing samples with different dimensions, we are able to give a quantitative explanation of the mode structure in the configuration without external cavity. Recent results with external mirrors are also briefly discussed.

EXPERIMENT

Three different samples were used for the experiments, all cut from a Ga-doped Ge-crystal with $p = N_A - N_D = 1.2 \cdot 10^{14}$ cm^{-3}. The sample dimensions are given in table 1:

TABLE 1 Sample dimensions

Sample	d	a	l	(in mm)
1	3.7	2.4	46.9	
2	4.2	3.15	43.1	
3	5.2	3.75	48.4	

The distance between the electrical contacts is d, l is the sample length in the direction of the magnetic field (in our case the (111)-direction), and a is the width. Electrical

contacts were made by evaporating Indium (with some gold) and alloying at 400°C. All faces of the samples were polished and are parallel within 30'', which turned out to be crucial for the achievement of laser oscillation. Voltage pulses of up to 1000 V with 1μs duration were applied to the samples with a low impedance high power pulse generator. The typical current through the samples was 200 A, in accordance with the relation $j=\frac{1}{4}pev^{h}_{op}$, where j is the current density, and $\frac{1}{4}v^{h}_{op}$ is the approximate drift velocity of the heavy holes under "streaming motion" conditions /8/. The pulse repetition rate was chosen to be around 5Hz. For rates higher than 10Hz lasing breaks down due to the sample heating. The experiments were performed at 4.2K, so the sample was immersed in liquid He at the center of a superconducting solenoid. To check the range of electric and magnetic fields where lasing can be achieved, the radiation was detected with a broad band Ge:Ga-detector with peak sensitivity at about 110 μm. A magnetic field tunable narrowband GaAs-detector was used for the detailed analysis of the emission spectrum. It was placed in the center of a second magnet in the cryostat below the sample. The Zeeman-split 1s-2p+ shallow donor line is used for detection /9/. This line is tunable between 45 cm^{-1} and 130 cm^{-1} for magnetic fields of 1 T to 6.5 T. Due to the fact that the GaAs contains only one chemical species of shallow donors, the absorption line is extremely narrow (0.25 cm^{-1}), and the GaAs can be used as a high resolution spectrometer.

RESULTS AND DISCUSSION

Figure 1 shows typical traces of stimulated emission from sample 2, recorded with a Ge:Ga-detector. The detector signal due to stimulated emission is a factor of 10^2-10^3 above the level of spontaneous emission. The region of lasing extends from somewhat less than B=1 T for the lowest electric field of E ≃ 1000 V/cm up to more than 2 T for E ≃ 2000 V/cm. This corresponds to $1.3 \lesssim \zeta \lesssim 2.4$. We observe lasing at somewhat higher magnetic fields, that is for larger values of ζ, and also in a wider range of ζ than has been reported previously /1-5/. A possible explanation of this discrepancy is the effective inhomogeneity of the magnetic field in the sample. However, this is only about 10% over the whole sample length. Another reason could be the crystallographic direction of the electric field, which is not known in our experiment. Comparing the magnitude of the signal with the signal obtained from a FIR gas laser and a InSb-Landau source, the emitted power was estimated to reach 100 mW.

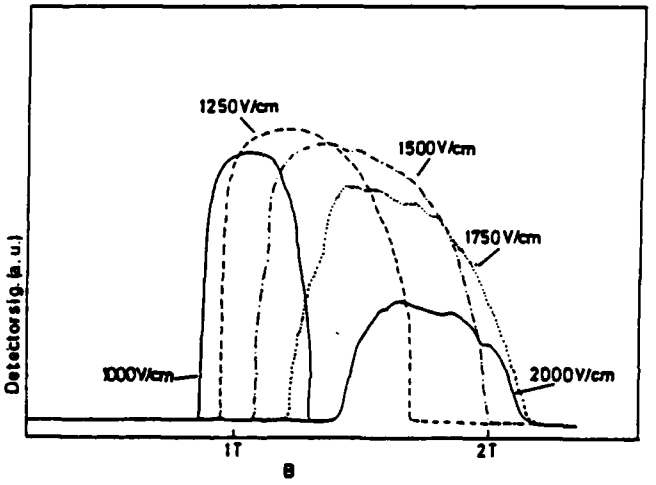

Fig. 1: Ge:Ga-detector signal from sample 2 as a function of magnetic field for different electric field values.

To analyze the spectrum of the stimulated emission the electric and magnetic fields applied to the sample were set to a fixed value, while the magnetic field of the GaAs-detector was tuned. Using the 1s-2p+ shallow donor transition, the frequency of the detected radiation is linearly related to the magnetic field over a wide range. Figure 2 shows three spectra from sample 2, for three different values of the electric and magnetic field. The spectra consist of 10 - 20 lines with a regular mode spacing of about 1.4 cm^{-1}. Their positions remain fixed with changes in the applied fields. In the high-gain region some additional lines appear, disturbing the regular structure. The measured widths are about 0.4 cm^{-1}. We conclude that the real line width of the emission is of the same order of magnitude as the detector linewidth (0.25 cm^{-1}). By varying the electric and magnetic fields it is possible to obtain lasing between 75 μm and 110 μm. There is a general trend towards emission at shorter wavelengths for both higher E- and B-fields (see Fig.2). In contrast to Andronov's /6/ and Komiyama's /5/ work, no long-wavelength-lasing (150 - 250 μm) could be found, not even at lower magnetic fields.

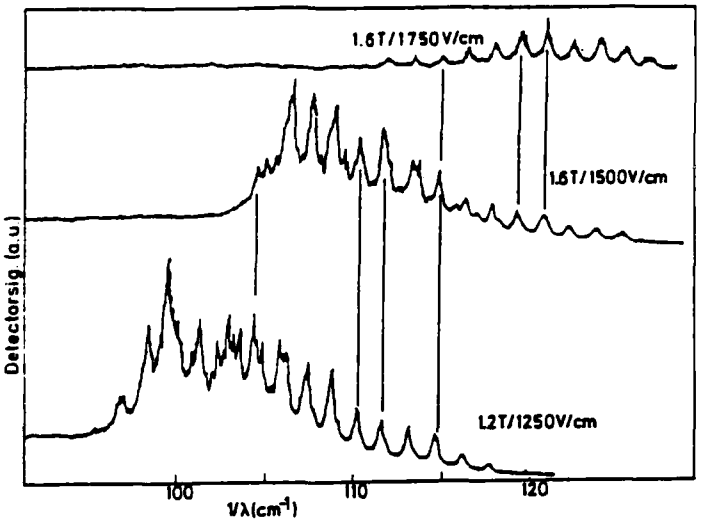

Fig. 2: Spectrum of stimulated emission from sample 2 for different electric and magnetic fields.

Andronov et al. /1/ and Komiyama et al. /2/ suggested that the lasing modes are due to total reflections at the sample surface, since without mirrors the quality factor of the cavity is far to low to allow longitudinal or transverse modes to oscillate (reflectivity of the surface at normal incidence: 36%). In the following we want to clear up the origin of these modes and their spacing. In order to get more information, we have analyzed two other samples with different dimensions (see Table 1). The characterization was performed in the same way as described above. As expected, a wider mode spacing is observed for the thinner sample and a smaller spacing for the thicker sample; $\Delta\nu$ = 1.7cm^{-1}, 1.4cm^{-1}, and 1.1cm^{-1} for samples 1,2 and 3, respectively. Comparing these values with the dimensions a and d of the samples, it appears to be very likely that the width a is the crucial parameter determining the mode spacing. This is also consistent with the physical reason that the surfaces coated with the electrical contacts are not serving as mirrors as well as the other surfaces.

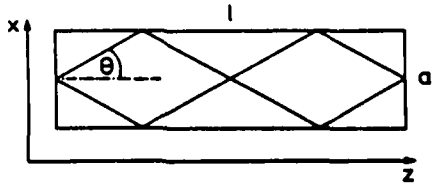

Fig. 3: Sketch of the ray path in the Germanium-crystal.

For the calculation of the mode spacing we consider an electromagnetic wave in the germanium crystal propagating with components of the wavevector in x- and z-directions, according to Fig.3: $\vec{k} = k_x\vec{e}_x + k_z\vec{e}_z$, where $\vec{e}_x$ and $\vec{e}_z$ are the respective unit vectors. The transverse resonance condition is given by /10/

$$k_x n = k\, n \sin\theta = M\pi/a \ , \qquad (1)$$

where n is the refractive index, M is an integer, and θ is indicated in Fig. 3. In addition, we have the geometrical condition

$$\tan\theta = Na/l \qquad (2)$$

(N integer), which ensures that the path of the ray is closed within the sample. This leads to a mode spacing (in wavenumbers)

$$\Delta\nu = (2a\, n \sin\theta)^{-1}. \qquad (3)$$

θ must satisfy the condition $14.5^\circ < \theta < 75.5^\circ$, because 14.5° is the angle of total reflection for Germanium. One can assume that modes with the smallest possible θ have the lowest losses, because they undergo the fewest reflections. Thus, for each sample the mode

spacing is determined first by choosing the angle, θ, with the smallest possible N (Eq. (2)), and then this angle is used in Eq. (3). This procedure gives a mode spacing, $\Delta\nu$, of $1.77cm^{-1}$ (N=6), $1.41cm^{-1}$ (N=5), and $1.13\ cm^{-1}$ (N=4), for sample 1,2 and 3, respectively, in good agreement with the measured values. The additional modes appearing at the high-gain regions can be understood as modes with a larger value of θ. According to Eq. (3), their spacing is smaller than the fundamental spacing, which makes the mode structure in the high-gain region rather complex. The longitudinal resonance condition analogous to Eq. (1) is not considered, because it would yield a very narrow mode structure which is not observed in the experiment.

From the above considerations it appears reasonable to produce a very thin sample in order to obtain a single mode oscillation /6/. We prepared a sample with a = 1 mm, expecting oscillation on two lines. However, it was not possible to achieve lasing from this sample. Probably the losses are too high because of the high order of the modes necessary for this geometry (N>12).

We have also investigated samples with an external semiconfocal resonator. Both mirrors consist of pure Germanium plates. The curved mirror is coated with gold, the plane mirror with a mesh or a Cr-film to yield 90% - 99% reflection. When the reflectivity is about 90%, no lasing can be observed. This is a further proof for the waveguide-like modes discussed above: They are destroyed by attaching the mirrors on both ends. On increasing the reflectivity to 99% lasing occurs again, most likely on longitudinal modes in this case. The analysis of the emission spectrum will be discussed elsewhere /11/.

In summary, we have investigated the emission spectrum of p-Ge lasers with different dimensions. The mode structure of samples without mirrors could be quantitatively explained in terms of waveguide-like modes.

ACKNOWLEDGEMENT

We gratefully acknowledge expert technical help of G. Strasser. This work was supported by the European Research Office of the U.S. Army.

REFERENCES

/1/ A. A. Andronov, I. V. Zverev, V. A. Kozlov, Yu. N. Nozdrin, S. A. Pavlov and V. N. Shastin (1984), Sov. Phys.-JETP Lett. 40, 804
/2/ S. Komiyama, N. Iizuka, and Y. Akasaka (1985), Appl. Phys. Lett. 47, 958
/3/ A. A. Andronov et al., Physica 134B, 210 (1985)
/4/ S. Komiyama and S. Kuroda, Solid State Commun. 59, 167 (1986)
/5/ S. Komiyama, Proc. 18th Int. Conf. Phys. Semiconductors, World Scientific Publishing, Singapore, 1987, p. 1641
/6/ A. A. Andronov et al., Proc. 18th Int. Conf. Phys. Semiconductors, World Scientific Publishing, Singapore, 1987, p. 1663
/7/ S. Komiyama and S. Kuroda, Jap. J. Appl. Phys. 26, L71 (1987)
/8/ S. Komiyama, Adv. Phys. 31, 255 (1982)
/9/ E. Gornik, Physica 127B, 95 (1984)
/10/ M. J. Adams, An Introduction to Optical Waveguides, J. Wiley & Sons, New York, 1981
/11/ K. Unterrainer, M. Helm, E. Gornik, and E. E. Haller, to be published

Mode structure of the *p*-germanium far-infrared laser with and without external mirrors: Single line operation

K. Unterrainer, M. Helm,[a] and E. Gornik
Institut für Experimentalphysik, Universität Innsbruck, A-6020 Innsbruck, Austria

E. E. Haller
Lawrence Berkeley Laboratories, Berkeley, California 94720

J. Leotin
Institut National des Sciences Appliquees, Department de Genie Physique des Materiaux, 31077 Toulouse Cedex, France

(Received 12 October 1987; accepted for publication 9 December 1987)

The mode structure of *p*-Ge far-infrared lasers with and without mirrors is investigated. Without external mirrors a multimode spectrum is observed and quantitatively explained in terms of waveguidelike modes. An external resonator drastically reduces the number of oscillating modes. For the first time single line operation is demonstrated in this configuration.

Recently, it has become possible to realize high-power far-infrared (FIR) semiconductor lasers from *p*-Ge.[1–8] The stimulated emission is due to transitions between the light and the heavy hole bands, which can form an inverted system when the crystal is subject to crossed electric and magnetic fields. Emission wavelengths between 75 and 250 μm have been reported with output powers up to 10 W.[1–5] Several attempts have been made to analyze the spectrum of the emitted radiation and to understand the mode structure, but no unambiguous interpretation of the various spectra observed could be given so far.[4–7]

We have studied the spectrum of the stimulated emission from *p*-Ge by means of an extremely narrowband, magnetic field tunable *n*-GaAs detector. By investigating samples with different dimensions, we are able to give a quantitative explanation of the mode structure in the configuration without external cavity. After attaching mirrors we observe, for the first time in this configuration, a single line oscillation.

For the experiments three different samples were used, all cut from a Ga-doped germanium crystal with $p = N_A - N_D = 1.2\times10^{14}\,\mathrm{cm}^{-3}$. The dimensions are given in Table I. Electrical contacts were made by evaporating indium (with 5% gold) and alloying at 400 °C. All faces of the sample were polished and are parallel within 30 arcseconds. To form a semiconfocal resonator,[7] two external mirrors made of pure Ge are used. The plane mirror consists of a 0.9-mm-thick parallel Ge plate coated with a 1500-Å chromium layer. The reflectivity was determined with a FIR gas laser to be 99%. The curved mirror is produced by depositing 2000 Å gold on the curved face of a plane-convex Ge lens (thickness 1.1 mm) to serve as a 100% reflecting mirror. The radius of curvature is 100 mm, which provides a stable cavity configuration. Both mirrors were attached to the sample with silicone oil and fixed with nail enamel.

Voltage pulses of up to 1200 V with 1 μs duration were applied with a high-power, low-impedance pulse generator. The pulse repetition rate was chosen to be around 5 Hz. For rates higher than 10 Hz, lasing breaks down due to sample heating. The experiments were performed at 4.2 K, so the sample was immersed in liquid helium at the center of a superconducting solenoid. The FIR radiation was guided through a brass light pipe (12 mm bore) to the detectors, which were placed in the same cryostat below the sample in the center of a second superconducting magnet. To check the range of electric and magnetic fields where lasing can be achieved, the radiation was detected with a broadband Ge:Ga detector with peak sensitivity at about 110 μm. A magnetic field tunable GaAs detector was used for the detailed analysis of the emission spectra. The Zeeman-split $1s$-$2p^+$ shallow donor line was used for detection.[9] This line is linearly tunable between 45 and 130 cm^{-1} with magnetic fields between 1 and 6.5 T. The GaAs detector having an intrinsic linewidth of 0.25 cm^{-1} is thus used as a high-resolution spectrometer.

For samples without mirrors, lasing was observed for magnetic fields between 1 and 2 T and electric fields between 1000 and 2500 V/cm. The output power was estimated to reach 200 mW by comparing the magnitude of the signal with the signal obtained from a FIR gas laser and an InSb-Landau source. Figure 1 shows spectra (intensity versus frequency) from two samples for different values of the electric and magnetic fields. The decreasing background level is due to the variation of the detector characteristic with magnetic field. The spectra consist of 10–20 lines with a regular mode spacing. Their positions remain fixed with changes in applied fields. The measured linewidth is about 0.4 cm^{-1}. We

TABLE I. Sample dimensions and observed mode spacings. l is the sample length [(111) direction], d is the distance between the electrical contacts, a is the width, and $\Delta\nu$ is the measured mode spacing.

Sample	l	d	a (mm)	$\Delta\nu$ (cm^{-1})
1	46.9	3.7	2.4	1.74
2	43.1	4.2	3.15	1.40
3	48.4	5.2	3.75	1.20

[a] Present address: Bell Communications Research, Inc., Red Bank, NJ 07701.

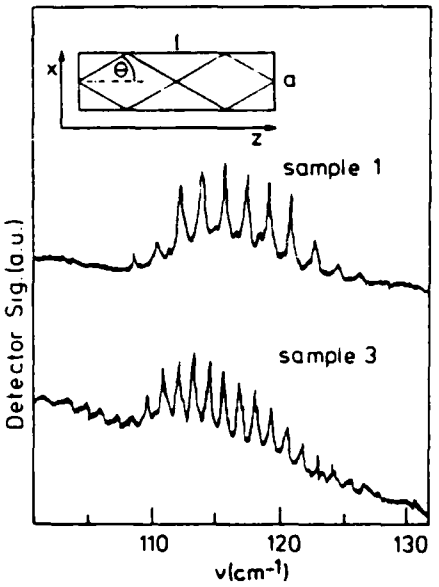

FIG. 1. Spectrum of stimulated emission for different electric and magnetic fields. Sample 1: $E = 1.8$ kV/cm, $B = 1.4$ T. Sample 3: $E = 1.9$ kV/cm, $B = 1.7$ T. The insert schematically shows the ray path in the Ge crystal.

conclude that the real width of the emission is of the same order of magnitude as the detector linewidth (0.25 cm^{-1}). By varying the electric and magnetic fields it is possible to obtain lasing between 75 and 110 μm. There is a general trend towards emission at shorter wavelengths for both higher electric and higher magnetic fields. In contrast to Andronov *et al.*[6] and Komiyama,[5] no long wavelength lasing (150–250 μm) could be found in our samples, which is probably because of the somewhat higher carrier concentration. Andronov *et al.*[1] and Komiyama *et al.*[2] suggested that the lasing modes are due to total reflections at the sample surfaces, since without mirrors the quality factor of the cavity is far too low to allow longitudinal or transverse modes to oscillate (the Ge surface has 36% reflectivity at normal incidence). According to Fig. 1 the observed mode spacings are 1.74 and 1.20 cm^{-1} for samples 1 and 3, respectively, and 1.40 cm^{-1} for sample 2 (not shown). Comparing the spacings with the dimensions of the samples, it appears to be very likely that the width, a, is the crucial parameter determining the mode spacing (see Table I).

The mode spacings can be explained by considering an electromagnetic wave in the germanium crystal (see insert in Fig. 1) propagating with components of the wave vector in the direction of l (z direction) and a (x direction): $\mathbf{k} = k_x \mathbf{e}_x + k_z \mathbf{e}_z$, where $\mathbf{e}_x$ and $\mathbf{e}_z$ are the respective unit vectors. The transverse resonance condition is given by[10] $k_x n = kn \sin\theta = M\pi/a$, where n is the refractive index, M is an integer, and θ is the angle between $\mathbf{k}$ and the longitudinal axis of the crystal. The analogous longitudinal resonance condition is not considered, because it would yield a very narrow mode structure which is not observed in the experiment. In addition, we have the geometrical condition $\tan\theta = Na/l$ (N integer), which ensures that the path of the ray is closed within the sample. This leads to a mode spacing (in wave numbers) $\Delta\nu = (2an \sin\theta)^{-1}$. θ must satisfy the condition $14.5° < \theta < 75.5°$, because 14.5° is the angle of total reflection for germanium. One can assume that modes with the smallest possible θ have the lowest losses, because they undergo the fewest reflections. Thus, for each sample the mode spacing is determined first by choosing the angle θ with the smallest possible N, and then this angle is used in the expression for $\Delta\nu$. This procedure gives a mode spacing $\Delta\nu$ of 1.77 cm^{-1} ($N = 6$), 1.41 cm^{-1} ($N = 5$), and 1.14 cm^{-1} ($N = 4$), for samples 1, 2, and 3, respectively, in good agreement with the measured values. This interpretation is confirmed by the work of Andronov *et al.*,[6] who reported emission of a single line by using a very thin ($a = 0.7$ mm) sample, where the mode spacing is as wide as the gain region.

After attaching external mirrors to sample 3 (see insert in Fig. 2), the region of electric and magnetic fields where lasing occurs stays roughly the same. The detector signal is also of the same order of magnitude with and without mirrors, in contrast to Komiyama and Kuroda,[7] because our light pipe is only 24 cm long and therefore the attenuation of the radiation is negligible also for the strongly deflected light from the mirrorless samples. The observed spectra, however, exhibit a dramatic change. Figure 2 shows spectra of sample 3 for different electric and magnetic fields, recorded with the GaAs detector. A considerably reduced number of lines appears with wider mode spacing and higher amplitude, accompanied by some other less dominant structure. Varying the electric and magnetic fields allows us to switch on and off lines on the long or short wavelength side of the spectrum due to a change in the gain spectrum. In this way it was possible to obtain operation of a single line (lower part of Fig. 2). This is the first report on forcing a multimode p-Ge laser to oscillate on a single line by attaching external mirrors. The emission wavelength is 87.3 μm (114.5 cm^{-1}), the

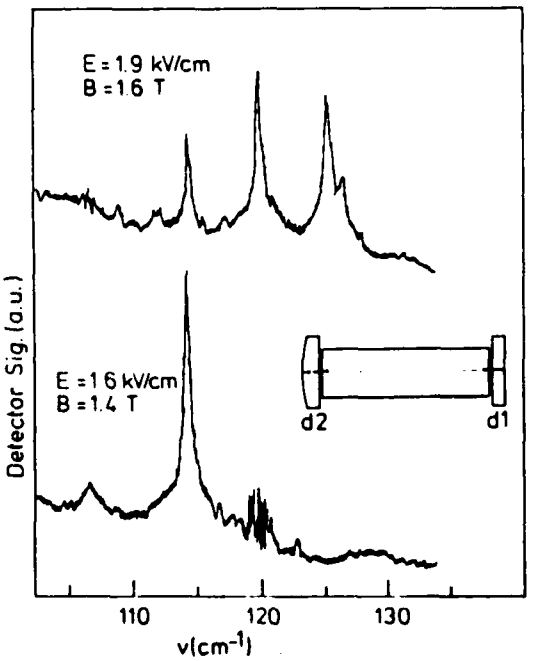

FIG. 2. Emission spectra from sample 3 after attaching external mirrors for different electric and magnetic fields. The insert shows the cavity configuration.

adjacent line at 83.3 μm (120.0 cm^{-1}) is just at threshold. As is seen from Fig. 2 the single line contains approximately the same total intensity as the three lines together. However, one cannot exclude the coexistence of several cavity modes within this line, because their spacing would be below the resolution of the detector. The spectra observed by Andronov *et al.*[6] from samples with external mirrors showed a very irregular and complicated structure. Komiyama and Kuroda[7] reported some changes in the spectrum and were able to reduce the number of oscillating lines by sandwiching a thin layer of poly-4-methylpent-1-ene (manufactured under the trade name TPX by Imperial Chemical Industries) between the sample and one mirror.

The mode spacing in Fig. 2 is equal to $\Delta\nu = 5.5\ cm^{-1}$, which is too large for fundamental longitudinal or transverse cavity modes. A possible explanation is the formation of an intracavity interference filter by the two Ge plates: Since they are not subject to the electric field like the sample, they are expected to have a slightly different index of refraction and also the thin layer between sample and mirror induces a change of the refractive index, which provides the possibility of Fabry–Perot like reflections. Thicknesses of $d_1 = 0.9$ mm and $d_2 = 1.1$ mm (the slight curvature of the convex plate is neglected) would give a spacing of only 1.4 and 1.1 cm^{-1}, respectively. If, however, the combined resonance condition for both plates is considered, the spacing is calculated to 5.5 cm^{-1}. This result is based upon a ratio of d_2/d_1 equal to 5/4. Considering an uncertainty of the measured thicknesses of 0.05 mm and a low finesse of the Fabry–Perots, one gets spacings between 4 and 6 cm^{-1}. A definitive explanation of the present spectra would require knowledge about the refractive index of the lasing sample as well as the influence of the thin layer between sample and mirrors. The investigation of different mirror configurations, especially with different thicknesses, appears necessary.

We also checked the emission when the plane mirror had a reflectivity of only 90%. In this case no lasing was achieved, which confirms the interpretation as waveguidelike modes in the mirrorless configuration: These modes are destroyed by attaching mirrors, which prevents total reflection on both end faces. Considering only the mirror output and no other losses the gain is calculated to be about $5 \times 10^{-3}\ cm^{-1}$, which indicates that a high-quality factor of the cavity is necessary.

In summary, we have quantitatively explained the mode structure of *p*-Ge lasers without external mirrors in terms of waveguidelike modes. With external mirrors laser operation on a single line is demonstrated.

We would like to thank R. A. Höpfel for helpful discussions and gratefully acknowledge technical assistance of G. Strasser. This work was supported by the European Research Office of the U.S. Army.

[1] A. A. Andronov, I. V. Zverev, V. A. Kozlov, Yu. N. Nozdrin, S. A. Pavlov, and V. N. Shastin, Sov. Phys. JETP Lett. **40**, 804 (1984).
[2] S. Komiyama, N. Iizuka, and Y. Akasaka, Appl. Phys. Lett. **47**, 958 (1985).
[3] A. Andronov, A. Belyantsev, E. Dodin, V. Gavrilenko, Y. Ivanov, V. Kozlov, Z. Krasil'nik, L. Mazov, A. Muravjov, I. Nefedov, V. Nikanorov, Y. Nozdrin, S. Pavlov, V. Shastin, V. Valvo, and Y. Vasil'ev, Physica B **134**, 210 (1985).
[4] S. Komiyama and S. Kuroda, Solid State Commun. **59**, 167 (1986).
[5] S. Komiyama, in *Proceedings of the 18th International Conference on the Physics of Semiconductors* (World Scientific, Singapore, 1987), p. 1641.
[6] A. Andronov, A. Muravjev, I. Nefedov, Y. Nozdrin, S. Pavlov, V. Shastin, Y. Mityagin, V. Murzin, S. Stoklitsky, I. Trofimov, and A. Chebotarev, in *Proceedings of the 18th International Conference on the Physics of Semiconductors* (World Scientific, Singapore, 1987), p. 1663.
[7] S. Komiyama and S. Kuroda, Jpn. J. Appl. Phys. **26**, L71 (1987).
[8] M. Helm, K. Unterrainer, E. Gornik, and E. E. Haller, at the 5th Int. Conf. on Hot Carriers in Semiconductors, Boston, 1987, to be published in Solid-State Electronics.
[9] E. Gornik, Physica B **127**, 95 (1984).
[10] M. J. Adams, *An Introduction to Optical Waveguides* (Wiley, New York, 1981).

HOT CARRIER QUANTUM DISTRIBUTION FUNCTION IN CROSSED ELECTRIC AND MAGNETIC FIELDS

M.Helm[+], K.Unterrainer and E.Gornik

Institut für Experimentalphysik, Universität Innsbruck,

A-6020 Innsbruck, Austria

ABSTRACT

The problem of the hot carrier distribution function in crossed electric and magnetic field is treated for free carriers in a parabolic band. To account for the discrete structure of the energy spectrum (Landau levels) a fully quantum mechanical treatment is employed. The master equation for the diagonal elements of the density operator is solved for three Landau levels considering optical and acoustic deformation potential scattering. Numerical results are presented for the case of the light holes in p-Germanium. The total populations of the different Landau levels are discussed as well as the one-dimensional distribution functions in the Landau levels, and their dependences on electric and magnetic field strengths are studied. Special attention is paid to the occurrence of a population inversion between Landau levels and to a comparison of the present approach to the classical picture of streaming motion.

[+]Present address: Bell Communications Research, Inc., Red Bank, New Jersey 07701

PACS 72.20 My, 72.20 Dp

1. INTRODUCTION

The transport problem of carriers in semiconductors under presence of crossed electric and magnetic fields has been discussed in the literature for many years (for review articles see Refs. 1 and 2). In most of the previous work the electric field was assumed to act as a weak perturbation, i.e. its main role was to probe the system. According to this, the central aim was to calculate the diagonal part of the conductivity , σ_{xx} , using the equilibrium carrier distribution function. In this way it was, for example, possible to explain magnetophonon oscillations successfully[3]. Another part of the work published in the past was devoted to hot electron transport in crossed fields[4-9], which means the presence of a rather high electric field and requires the calculation of the nonequilibrium distribution function. Most of the authors assumed a very small magnetic field to justify the use of a classical distribution function, calculated by means of the Boltzmann equation[7] or Monte Carlo techniques[8,9]. The other limiting case, the extreme magnetic quantum limit, has been studied in the frame of quantum transport equations[10]. In this situation only the lowest Landau level (LL) is assumed to be occupied. Only very little attention has been paid to the intermediate range, where several LL's are occupied, but the discrete structure of the energy spectrum is nonetheless important[11,12].

Very recently, this case turned out to be of great practical interest due to the observation of population inversion between LL's and stimulated cyclotron resonance emission in p-Germanium[13]. This phenomenon (also discussed as negative dynamic conductivity) has been

predicted already fifteen years ago[14-17]. The build-up of an inverted distribution function has been described in terms of streaming motion and accumulation of carriers in momentum space[18]. This concept is based on the classical motion of carriers in crossed fields considering a sufficiently strong interaction with optical phonons. The classical trajectories of the carriers are circles in velocity space centered at v=-E/B. The energy of the optical phonons, $\hbar\omega_{op}$, is represented by another circle, $v = v_{op} = \sqrt{2\hbar\omega_{op}/m^*}$ (m^*...effective mass), centered at the origin v=0. For high electric fields, $E/B \gg v_{op}$, all carrier trajectories cross the circle $v=v_{op}$, so the carriers continuously get accelerated and scattered back by the emission of an optical phonon (streaming motion). For higher magnetic fields ($E/B \lesssim v_{op}$) a part of the trajectories is closed without crossing the circle $v=v_{op}$. The corresponding carriers are not affected by optical phonon scattering and accumulate in a limited area of v- or momentum space, because they can be removed from there only by acoustic phonon or impurity scattering, which are both much slower than the optical mode scattering. It has been shown that a torus-type distribution function can arise in this accumulation area[16], which corresponds to a population inversion between LL. Fig.1 shows electron trajectories in velocity space. The accumulation area is bounded near the second circle. The circles can also be regarded as Landau levels, then the n=0 and n=1 LL's lie in the accumulation area, whereas the carriers in all higher LL's interact strongly with optical phonons (streaming; indicated by the dashed part of the cycles). Up to now, most of the calculations analyzing this situation dealt with the limit of nonquantizing magnetic fields; that means the use of a classical distribution function and the use of the zero magnetic field

scattering rates[7-9]. Although much physical insight can be gained by this approach, it would be interesting to illuminate the problem from the opposite side by calculating the occupation of LL's in the frame of quantum mechanical transport theory. A first attempt has been made by Helm and Gornik[12], who solved the quantum mechanical transport equation for three LL's, though neglecting the k_z- dependence (z..direction of magnetic field) of the distribution function.

In this paper we want to extend this approach by solving the master equation for the density operator including the k_z- dependence of the distribution function. We calculate, for the first time, the hot carrier quantum distribution function in crossed electric and magnetic fields for three LL without any weak-electric field approximation. The basic equations and the way of their solution will be presented in Sec.2. Analytical results of the scattering rates for acoustic and optical deformation potential interaction are given. In Sec.3 the numerical results are shown for the case of the light holes of p-Germanium. The total populations of the different LL's are discussed as well as the one-dimensional distribution functions in the LL's, and their dependences on electric and magnetic fields and phonon coupling strengths are studied. Special attention is paid to a comparison of the quantum mechanical picture with the classical picture of streaming motion.

2. THEORY

(a) Basic expressions

We consider the Hamiltonian for a carrier with charge e and effective mass m^* in crossed electric and magnetic fields interacting with phonons[6,10]:

$$H = \frac{1}{2m^*}(\vec{p}-e\vec{A})^2 - e\vec{E}\cdot\vec{r} + H_{ph} + H_{el-ph} \qquad (1)$$

Here H_{ph} is the free phonon term:

$$H_{ph} = \sum_{\vec{q}} \hbar\omega_q \, (b_q^+ b_q + \tfrac{1}{2}) \qquad (2)$$

where the b_q^+ and b_q are the phonon creation and destruction operators, respectively, and H_{el-ph} is the electron- (hole-) phonon coupling:

$$H_{el-ph} = i \sum_{\vec{q}} C(\vec{q}) \, (b_q \, e^{i\vec{q}\vec{r}} - b_q^+ \, e^{-i\vec{q}\vec{r}}) \qquad (3)$$

C(q) depends on the specific nature of the electron-phonon coupling. Eigenvalues and eigenfunctions of the electronic part of the Hamiltonian ($\vec{B}$ in z-direction, $\vec{E}$ in x-direction) are given by

$$E_\nu = (n+\tfrac{1}{2}) \, \hbar\omega_c + \hbar^2 k_z^2/2m^* - eEX + \tfrac{1}{2} \, m^*(E/B)^2 \qquad (4)$$

where the index ν summarizes the quantum numbers n, k_y, and k_z, $\omega_c = |e|B/m^*$, and $X = (\hbar k_y/eB + m^*E/eB^2)$.

$$\Psi_\nu(\vec{r}) = e^{ik_y y} \, e^{ik_z z} \, \phi_n\left(\frac{x-X}{l}\right) \qquad (5)$$

where $l = \sqrt{\hbar/|e|B}$ and $\phi_n\left(\frac{x-X}{l}\right)$ is the n-th harmonic oscillator wave

function. The basic quantum transport equation is the equation of motion for the density operator, the Liouville - von Neumann equation

$$i\hbar \frac{\partial \rho}{\partial t} = [H, \rho] \qquad (6)$$

Here, ρ is the density operator of the total electron - phonon system. The electron distribution function is given by the diagonal elements of the reduced density operator, f , which is obtained by taking the trace over the phonon states:

$$f_\upsilon = Tr_{ph} \langle \upsilon | \rho | \upsilon \rangle \qquad (7)$$

Assuming no correlation between electron and phonons in the diagonal elements of ρ and a weak electron - phonon coupling the Pauli master equation can be derived for the diagonal elements of the reduced density operator (neglecting the Pauli exclusion principle)[10,19,20]

$$\frac{\partial f}{\partial t}\upsilon = \sum_{\upsilon'} f_\upsilon W_{\upsilon'\upsilon} - f_\upsilon W_{\upsilon\upsilon'} \qquad (8)$$

The $W_{\upsilon\upsilon'}$ are the scattering probabilities from state υ to state υ' according to Fermi's golden rule :

$$W_{\upsilon\upsilon'} = \frac{2\pi}{\hbar} \sum_{\vec{q}} |\langle \upsilon | C(\vec{q})\ e^{i\vec{q}\vec{r}} | \upsilon' \rangle|^2 \left[N_q \delta(E_\upsilon - E_{\upsilon'} + \hbar\omega_q) + (N_q + 1)\delta(E_\upsilon - E_{\upsilon'} - \hbar\omega_q)\right]$$

N_q is the Planck distribution for the phonons, the matrix elements are given by (see e.g. Ref. 21)

$$|\langle \upsilon | e^{i\vec{q}\vec{r}} | \upsilon' \rangle|^2 = |J_{nn'}(q_x, q_y)|^2 \, \delta_{k_z', k_z - q_z} \, \delta_{k_y', k_y - q_y} \qquad (9)$$

with $|J_{nn'}(\xi)|^2 = \frac{n!}{n'!} \xi^{n'-n} e^{-\xi} [L_n^{n'-n}(\xi)]^2 \qquad (n \leq n')$.

and $\xi = l^2(q_x^2 + q_y^2)/2$. The $L_n^{n'-n}$ are associated Laguerre polynomials[22]. It is worth noting that the electric field only appears in the energy conserving δ-function and not in the squared matrix elements.

(b) Steady state solution

We now proceed to get a steady state solution of the master equation (8) which then reads

$$0 = \sum_{\upsilon'} f_{\upsilon'} W_{\upsilon'\upsilon} - f_{\upsilon} W_{\upsilon\upsilon'} \qquad (11)$$

In the following we want to consider the situation where the current through the sample is constant. Therefore we assume a spatially homogeneous distribution function. Thus, the f_{υ} have to be independent of X, and therefore of k_y[6,10]. This enables us to perform the summation over k_y directly and we are left with a system of N coupled integral equations (for N LL) in the variable k_z:

$$0 = \sum_{n'} \int dk_z' \, f_{n'}(k_z') \, W_{n'n}(k_z', k_z) - f_n(k_z) \, W_{nn'}(k_z, k_z') \qquad (12)$$

The rates $W_{nn'}(k_z, k_z')$ are now also k_y-integrated. The distribution functions for the different LL's can be expressed as

$$f_n(k_z) = \frac{1}{\sum_{n'} W_{nn'}(k_z)} \sum_{n'} \int dk_z' \, f_{n'}(k_z') \, W_{n'n}(k_z', k_z) \, , \qquad (13)$$

where $W_{nn'}(k_z) = \int dk_z' \, W_{nn'}(k_z, k_z')$.

The proper normalization condition is $\sum_n \int dk_z f_n(k_z) = 1$.

(c) Transition rates

Regarding the explicit calculation, we restrict ourselves to three Landau levels. A larger number would be desirable, but since the integrals are not symmetric concerning q_x and q_y due to the electric field, no simple general expression for the transition rates $W_{nn'}(k_z, k_z')$ could be found. However, three LL's should be enough to show some interesting features of the carrier distribution.

For the sake of simplicity, we consider acoustic and optical deformation potential interaction in the calculation, which is appropriate i.e. for the light holes of p-Germanium. The polar-optical phonon interaction would also be of interest in order to treat the electrons of GaAs or InSb, but the different momentum dependence needs a numerical evaluation of the scattering rates in this case. The coupling constants are given by (see e.g. Ref.23)

$$|C^{ac}(q)|^2 = \frac{\hbar \, D^2 \, q}{2V \, \rho \, s} \, , \quad |C^{op}(q)|^2 = \frac{\hbar^2 (D_t K)^2}{2V \, \rho \, \hbar\omega_{op}} \qquad (14)$$

where $\hbar\omega_{op}$ is the optical phonon energy, D is the acoustic deformation

potential, D_tK characterizes the optical deformation potential, ρ is the mass density, s is the sound velocity, and V is the crystal volume. We adopt three more approximations for the carrier-phonon interaction:

(1) We consider only the spontaneous emission of optical phonons ($N_{op}= 0$) and

(2) apply the equipartition approximation for acoustic phonons ($1 \ll N_{ac}= kT/\hbar\omega_q$).

(3) Furthermore we regard the scattering by acoustic phonons as elastic ($\hbar\omega_q= 0$ in the energy conserving δ-function).

These approximations can assumed to be valid at intermediate temperatures ($T \simeq 10 - 80$ K). As a consequence, the optical and acoustic scattering rates exhibit the same q-dependences. The explicit transition rates between the three lowest LL's are then given by (the argument (k_z, k_z') is omitted)

$$
\begin{aligned}
W_{00} &= A\, e^{-\frac{1}{2}\epsilon^2} \\
W_{10(01)} &= A\,(1/2)\,(1+\epsilon^2)\, e^{-\frac{1}{2}\epsilon^2} \\
W_{11} &= A\,(1/4)\,(3-2\epsilon^2+\epsilon^4)\, e^{-\frac{1}{2}\epsilon^2} \\
W_{20(02)} &= A\,(1/8)\,(3+2\epsilon^2+\epsilon^4)\, e^{-\frac{1}{2}\epsilon^2} \\
W_{21(12)} &= A\,(1/16)\,(7+9\epsilon^2-5\epsilon^4+\epsilon^6)\, e^{-\frac{1}{2}\epsilon^2} \\
W_{22} &= A\,(1/64)\,(41-52\epsilon^2+50\epsilon^4-12\epsilon^6+\epsilon^8)\, e^{-\frac{1}{2}\epsilon^2} \,.
\end{aligned}
\qquad (15)
$$

Here ϵ is the respective difference of energies in state ν and ν' divided by eEl for each transition rate, which is

$$
\begin{aligned}
&\hbar^2(k_z'^2-k_z^2)/2m^* + (\hbar\omega_{op}) \quad \text{for } W_{00},\ W_{11},\ W_{22}, \\
&\hbar^2(k_z'^2-k_z^2)/2m^* - \hbar\omega_c + (\hbar\omega_{op}) \quad \text{for } W_{10},\ W_{21}.
\end{aligned}
$$

$\hbar^2(k_z'^2-k_z^2)/2m^* + \hbar\omega_c + (\hbar\omega_{op})$ for W_{01}, W_{12},

$\hbar^2(k_z'^2-k_z^2)/2m^* - 2\hbar\omega_c + (\hbar\omega_{op})$ for W_{20}, and

$\hbar^2(k_z'^2-k_z^2)/2m^* + 2\hbar\omega_c + (\hbar\omega_{op})$ for W_{02}.

The $\hbar\omega_{op}$ in parentheses applies only for the optical phonon rates. The constant A is different for acoustic and optical scattering, namely

$$A^{ac} = \frac{D^2 kT}{4\pi^2 \rho\, s^2 \hbar^2} \frac{B\sqrt{2\pi}}{E\ l} \quad \text{and} \quad A^{op} = \frac{(D_t K)^2}{8\pi^2 \rho\, \hbar\omega_{op}} \frac{B\sqrt{2\pi}}{E\ l} \quad . \tag{16}$$

The crucial quantity in the transition rates (15) is ϵ, the ratio of the energy difference between initial and final state and the electrostatic energy eEl. For weak electric fields the energy difference has to be practically zero to yield a reasonable magnitude of the rates. If this is not the case, the rates go to zero. For higher electric fields the energy conservation is <u>seemingly</u> not that strict; as long as the energy difference is of the order of eEl, there is a considerable probability for the respective transition. Physically, the missing amount of energy is supplied by spatial transitions, which are possible due to the overlap of the wavefunctions[12]: A change of the spatial coordinate X implies a change of the total energy due to the term eEX in Eq.(4). Hence at low electric fields the transitions between Landau levels are dominated by transitions associated with a change of the quantum number k_z; at high electric fields the contribution due to spatial transitions (change of quantum number k_y) becomes more important. Typical transitions $W_{nn'}(k_z, k_z')$ are sketched in Fig.2 for acoustic phonons.

The k_z'-integrated rates, $W_{nn'}(k_z)$, which are needed in Eq.(13), are calculated numerically. The main procedure now is the solution of the three coupled integral equations (13) with the transition rates (15). This is done by simultaneous iteration of the three equations. The convergence is rather fast, the fifth iteration is accurate up to 0.1%.

At the end of this section we want to make some comments on previous work performed on the basis of the master equation (11). Inoue and Yamashita[11] expanded the energy conserving δ-function in Eq.(9) up to second order in the electric field. They omitted the k_z-integration and evaluated instead the integral at the k_z-value which gives the major contribution. This leds to a system of N second order differential equations. Within their approximations they were able to give general expressions for the distribution function in an arbitrary number of LL's. Unfortunately no numerical study was performed.

Calecki et al [10] transformed the master equation (11) into a Fokker-Planck equation and studied the extreme quantum limit (one LL) analytically. They got a Maxwellian distribution function in certain limits and derived an expression for the electron temperature. Moreover, they pointed out that the (stationary) distribution function depends only on ratio of the coupling strengths of different scattering processes[20].

In comparison, we can not include an arbitrary number of LL's, but do not make any approximation concerning the electric field or the

integration, like Inoue and Yamashita. Owing to numerical methods we are able to calculate the distribution functions of a finite number of LL's directly from the master equation.

3. RESULTS AND DISCUSSION

The central quantities obtained from the above calculation are the one-dimensional distribution functions $f_n(k_z)$ for the different LL's. Another interesting quantity, especially regarding the appearance of a population inversion, is the total population in every LL $f_n = \int dk_z\ f_n(k_z)$.

Fig.3 shows the dependence of the populations f_0, f_1, f_2 on the electric field for a constant magnetic field (B = 0.35 T and 1 T). The parameters are chosen suitable for the light holes of Germanium[24]: $m^* = 0.043\ m_0$, $\rho = 5300\ kg/m^3$, $s = 5400\ m/s$, $\hbar\omega_{op} = 37$ meV, D = 4.6 eV, $D_tK = 9 \cdot 10^{10}$ eV/m. According to Fig.3a, one can describe the behavior as follows: At low electric fields all populations are near 0.33, but $f_0 > f_1 > f_2$. This is the case, because we assumed acoustic phonon scattering, which is dominant in this region, to be totally elastic. A finite acoustic phonon energy (in the energy δ-function) would increase the differences in the populations. When the electric field is increased, the carriers in the n=2 LL start to interact with optical phonons, which causes a decrease of f_2. This can be regarded as an onset of streaming motion of the carriers in the n=2 LL, or, in other words, of the carriers on the classical trajectory with the largest radius in k- or v- space. As all LL's are connected by the respective scattering rates, also f_0 and f_1 are influenced and a

population inversion between the n=1 and n=0 LL occurs in a narrow range of E. On further increasing the electric field also the carriers in the n=1 LL start to interact strongly with optical phonons (streaming), and f_1 decreases. For very strong electric fields the carriers in all LL's can emit optical phonons and the three populations again will approach the value 0.33. However, there remains the condition $f_0 > f_1 > f_2$, because phonon emission preferably occurs into lower LL's. The difference $f_0 - f_1$ is also shown in Fig. 3, inversion corresponds to $f_0 - f_1 < 0$. The situation at population inversion turns out to be closely analogous to the classical picture: The n=2 LL corresponds to the streaming carriers, the n=0 and n=1 LL's represent the accumulation area (see Fig.1). Due to the specific nature of the scattering rates an inversion occurs in the accumulation area, that is between the n=1 and n=0 LL.

Fig.3b shows the analogous curves for B = 1 T. The general behavior is similar, but no population inversion occurs any more at this magnetic field. All the features are less pronounced and shifted to higher electric fields.

In the calculation the lattice temperature has been taken 10 K, which is near the lower limit for the validity of the high temperature approximation for acoustic phonons; however, at this low temperature (equivalent to weaker acoustic phonon coupling - see Eq.(16)) all the features, especially population inversion, are more pronounced. It turns out that the relative strengths of optical and acoustic phonon coupling influence critically the possibility of inversion: At a too high or low ratio of coupling strengths no inversion builds up any

AD-A194 101 HOT ELECTRON EMISSION IN SEMICONDUCTORS(U) INNSBRUCK UNIV (AUSTRIA) INST OF EXPERIMENTAL PHYSICS E GORNIK ET AL. 25 MAR 88 R/D-4410-EE-01 2/2

UNCLASSIFIED DAJA45-84-C-0032 F/G 20/12 NL

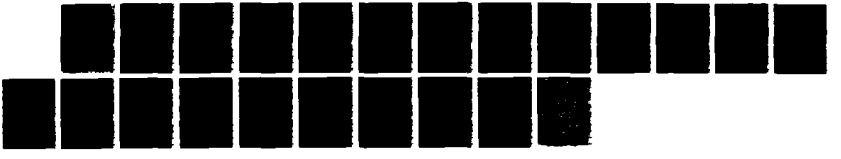

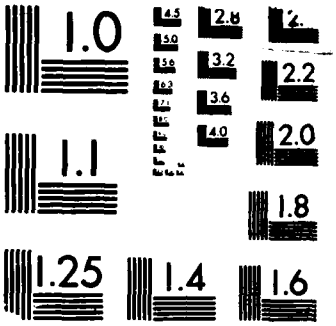

more. By chance, the realistic coupling constants turn out to be nearly optimal.

Let us now turn to the k_z-dependence of the distribution functions. We have calculated $f_n(k_z)$ for magnetic fields of B=0.35T and B=1T, with values of the electric field which appear interesting in view of Fig.3. For B=0.35T (Fig.4), these are E=1kV/cm (acoustic phonon scattering dominant), E=1.9kV/cm (inversion), and E=2.8kV/cm (all LL's streaming). The scale on the abscissa is transformed from k_z to $\hbar^2k_z^2/2m^*$, because in this way a Boltzmann distribution (with carrier temperature T_c) is represented by a straight line (the line in Figs.4 and 5 corresponds to T_c= 50 K). This temperature, however, is not comparable to the temperature derived by Calecki et al[10], because their expressions are valid only in the limit of high lattice temperature ($kT>>\hbar\omega_{op}$) or extremely high electric fields ($eEl>>\hbar\omega_{op}$).

For E=1kV/cm (Fig.4a) most of the carriers are concentrated below a $\hbar^2k_z^2/2m^*$-value of about 20 meV, where the emission of optical phonons starts to become effective. The corresponding kink is observed at energies somewhat below the optical phonon energy (37 meV) because of the possibility of spatial transitions. As the energy is counted from each LL-edge, optical phonon emission from higher LL's is possible at lower k_z-values than from lower LL's (for example the effective energy in the n=2 LL is given by $2\hbar\omega_c + \hbar^2k_z^2/2m^*$). At low energies the distribution function is very hot, because in our approximation the acoustic phonons do not carry energy. At higher energies, where optical phonon emission becomes effective, the distribution is cooled down.

Fig.4b shows $f_n(k_z)$ for 1.9 kV/cm, where according to Fig.3 the inversion is strongest. This "total" inversion is reflected by a "local" inversion in k_z-space near $k_z = 0$. It should be pointed out, however, that a local inversion near the band edge can appear, even if the total populations are not inverted (see below). In connection with a sufficient amount of nonparabolicity in a real system, this could lead to light amplification, too. (Also for a total inversion nonparabolicity is necessary to get amplification, because in the parabolic case the ratio of induced absorption to emission is always (n+1)/n for carriers in the n-th LL.) The fact that the carrier distributions are inverted for large k_z-values ($\hbar^2 k_z^2/2m^* > 25$ meV) is not essential, because the distribution function there is at least three orders of magnitudes smaller than at the band edge. Since the distributions are roughly parallel to the straight line, a mean temperature of about 50 K can be found for them in spite of the inversion. At E = 2.8 kV/cm (Fig.4c) all carriers can interact strongly with optical phonons (streaming). The k_z-distributions are hotter and near to being thermal ($T_c \approx 80$ K).

Fig.5 shows the distribution functions for B = 1 T and E = 2, 3 and 4 kV/cm. 2kV/cm (Fig.5a) represents the low electric field region. The higher magnetic field compared to Fig.4 is reflected by the larger energetic distance of the optical phonon kink in different LL's. At 3 kV/cm (Fig.5b) there appears a local inversion between the n=1 and n=0 LL near $k_z=0$. Fig.5c shows the situation for E=4kV/cm, when the distributions are nearly thermalized by the optical phonon interaction.

In this paper we have calculated the hot carrier distribution function in crossed electric and magnetic fields using the Pauli master equation. Since we take into account three LL's, our approach bridges the gap between the extreme quantum limit and quasiclassical calculations. The total populations of the different LL's have been discussed as well as the one dimensional distribution functions within the LL's.

At low magnetic fields ($B \lesssim 0.35$ T) we find an inversion in a certain range of electric fields, where the motion of the carriers in the two lower LL's is dominated by acoustic phonon scattering, whereas the carriers in the third (n=2) LL already interact strongly with optical phonons. However, the populations are sensitive to the relative coupling strength of acoustic and optical phonon interaction. At low electric fields the one dimensional distribution funtions in the different LL's show a sudden decrease at a certain energy level due to the onset of optical phonon emission. At higher fields, when all carriers in one LL can emit optical phonons, the distribution function is nearly thermal. Therefore a common electron temperature can be defined in this case.

The predictions, however, are not claimed to be quantitatively reliable, because in the real p-Ge System also the heavy holes (which we have neglected) will influence the distribution of the ligth holes. For further improvement of the theory it will be necessary to include a larger number of LL's, especially at lower magnetic fields. Nevertheless the present approach is the first rigorous solution of the master equation in the crossed field situation and shows the appearence of a population inversion, which is due to the interplay of

different scattering mechanisms.

ACKNOWLEDGEMENT: This work was supported by the European Research Office of the U.S.-Army.

REFERENCES

1. R.Kubo, S.J.Miyake, and N.Hashitsume, in "Solid State Physics" Vol.17, Ed. F.Seitz and D.Turnbull (Academic Press, New York, 1965), p.270
2. L.M.Roth and P.N.Argyres, in "Semiconductors and Semimetals" Vol.1, Ed. R.K.Willardson and A.C.Beer (Academic Press, New York, 1966), p.159
3. R.L.Peterson in "Semiconductors and Semimetals" Vol.10, Ed. R.K.Willardson and A.C.Beer (Academic Press, New York, 1975), p.221
4. E.Yamada and T.Kurosawa, J.Phys.Soc.Japan 34, 603 (1973)
5. H.Partl, W.Müller, F.Kohl, and E.Gornik, J.Phys.C 11, 1091 (1978)
6. H.F.Budd, Phys.Rev.175, 271 (1968)
7. F.Brosens and J.T.Devreese, Solid State Commun.44, 597 (1982)
8. P.Warmenbol, F.M.Peeters, and J.T.Devreese, Phys.Rev.B 33, 1213 (1986)
9. F.Abou El-Ela and B.K.Ridley, at the "5th Int Conf. on Hot Carriers in Semiconductors, Boston 1987", to be published in Solid State Electronics
10. D.Calecki, C.Lewiner, and P.Nozieres, J.Phys. (Paris) 38, 169 (1977)
11. S.Inoue and J.Yamashita, Progr.Theor.Phys.42, 158 (1969)
12. M.Helm and E.Gornik, Phys.Rev.B 34, 7459 (1986)
13. Yu.B.Vasil'ev and Yu.L.Ivanov, in "Proceedings of the 18th Int Conf. on the Physics of Semiconductors, Stockholm, 1986", Ed. O.Engström (World Scientific Publishing, Singapore, 1987) p.1659
14. H.Kaeda and T.Kurosawa, in "Proceedings of the 11th Int. Conf. on

the Physics of Semiconductors, Warsaw, 1972", Ed. Polish Academy of Sciences (PWN-Polish Scientific Publishers, Warsaw, 1972), p.602

15. Ya.I.Al'ber, A.A.Andronov, V.A.Valov, V.A.Kozlov, and I.P.Ryazantseva, Solid State Commun. 19, 955 (1976)
16. T.Kurosawa, Solid State Commun. 24, 357 (1977)
17. A.A.Andronov, V.A.Valov, V.A.Kozlov, and L.S.Masov, Solid State Commun.36, 603 (1980)
18. S.Komiyama, Adv.Phys. 31, 255 (1981)
19. L. Van Hove, Physica 21, 517 (1955); 23, 441 (1957)
20. D.Calecki, in "Physics of Nonlinear Transport in Semiconductors", Ed. D.K.Ferry, J.R.Barker, and C.Jacoboni (Plenum Press, New York, 1980), p.289
21. J.R.Barker, J.Phys.C 5, 1657, (1972)
22. I.S.Gradsteyn and I.M.Ryzhik, "Tables of Integrals, Series and Products" (Academic Press, New York, 1965)
23. L.Reggiani in "Hot Electron Transport in Semiconductors", Ed. L.Reggiani, Topics in Applied Physics 58 (Springer, Berlin, 1984), p.7
24. "Semiconductors", Ed. O.Madelung, M.Schulz, and H.Weiss, Numerical Data and Functional Relationships in Science and Technology, Landolt-Börnstein Series, Group III, Vols. 17a and 17b (Springer, Berlin, 1982)

FIGURE CAPTIONS

Fig.1: Trajectories of electrons in velocity space in crossed electric and magnetic fields ($\vec{E}$ in x-direction, $\vec{B}$ in z-direction). The circle centered at v=0 represents the optical phonon energy. The dashed part of the trajectories indicates the emission of an optical phonon.

Fig.2: The energies of two LL's are plotted versus k_z and the carrier position along the electric field. The mechanism of acoustic phonon transitions is illustrated.

Fig.3: The populations f_n of the n=0 (solid line), n=1 (dashed) and n=2 LL (dashed-dotted) and the population difference f_0-f_1 (dotted) as a function of the electric field for (a) B=0.35T and (b) B=1T.

Fig.4: The one-dimensional distribution functions $f_n(k_z)$ in the n=0 (solid line), n=1 (dashed) and n=2 LL (dashed-dotted) are plotted versus $\hbar^2k^2/2m^*$ for B=0.35 T and (a) E=1kV/cm, (b) E=1.9kV/cm, (c) E=2.8kV/cm. The dotted straight line represents a Boltzmann distribution with T_c=50K.

Fig.5: Same as Fig.4, but for B=1T and (a) E=2kV/cm, (b) E=3kV/cm, (c) E=4kV/cm.

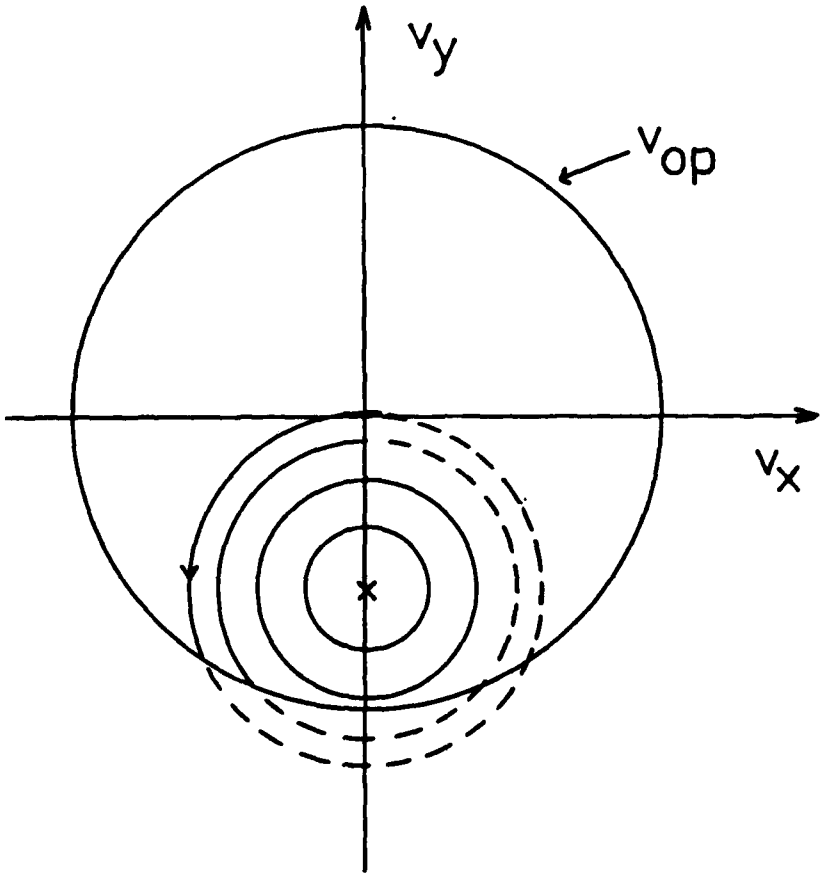

Fig 1 Hklim et al

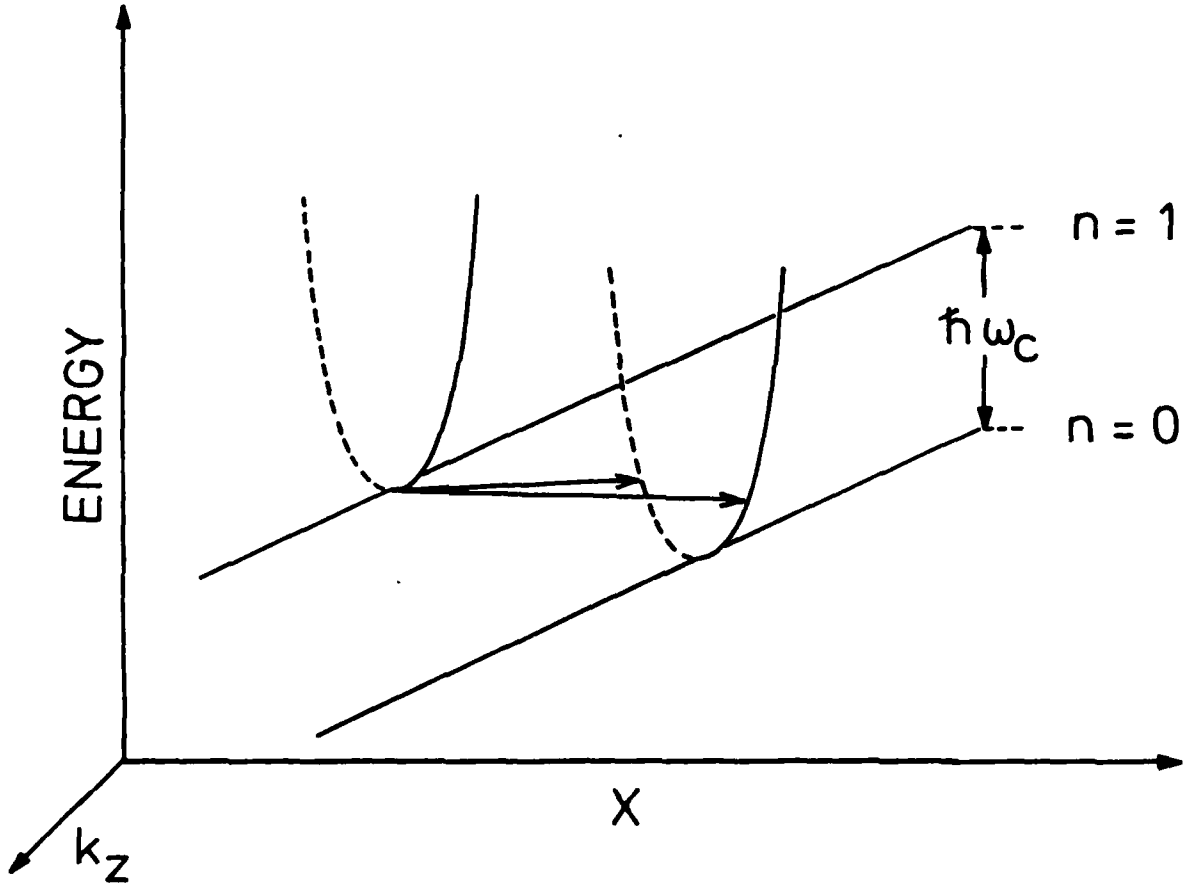
ENERGY
n = 1
ħω_c
n = 0
X
k_z

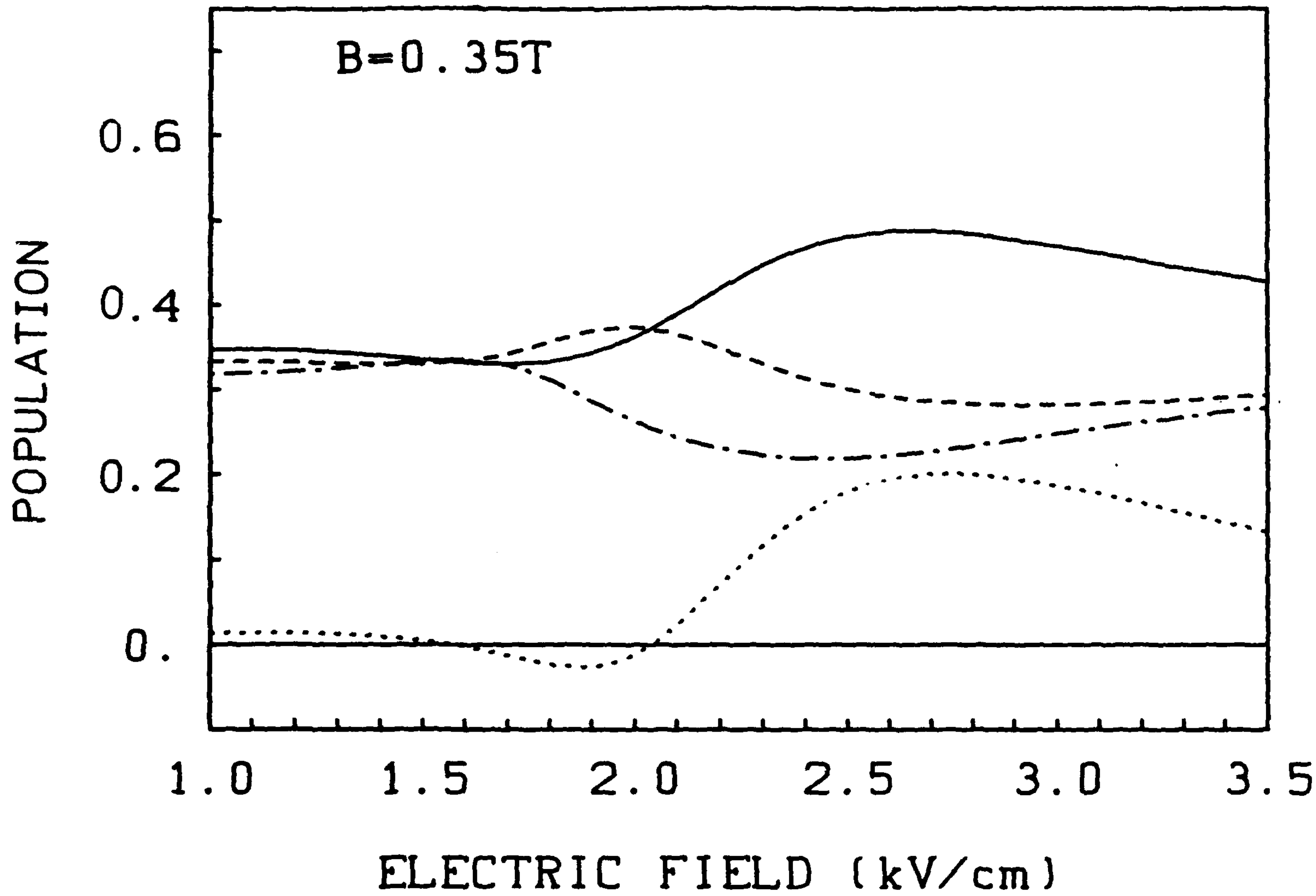
B=0.35T
POPULATION
0.6
0.4
0.2
0.
1.0
1.5
2.0
2.5
3.0
3.5
ELECTRIC FIELD (kV/cm)

Fig. 2a

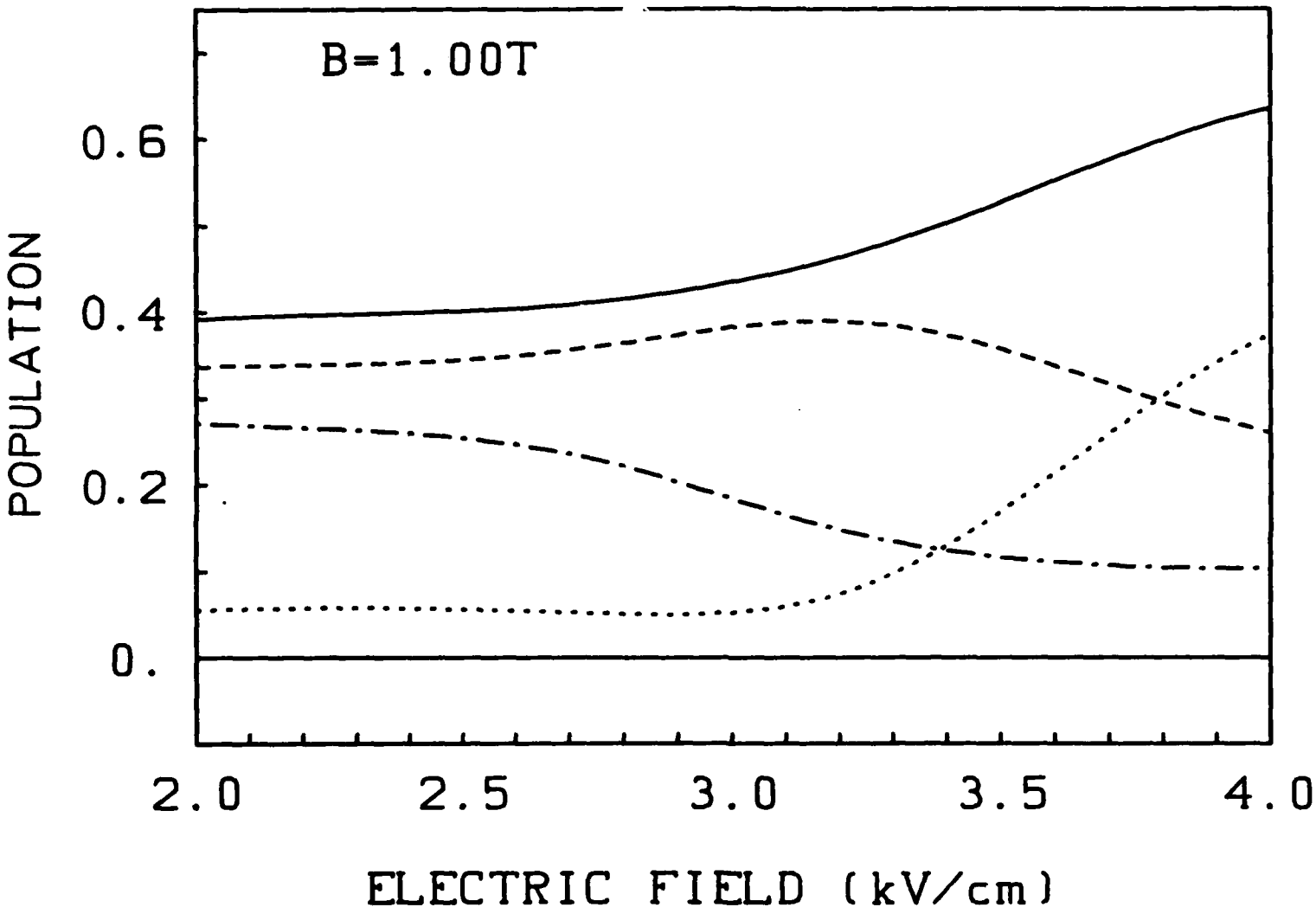

Fig 3(Klein et al

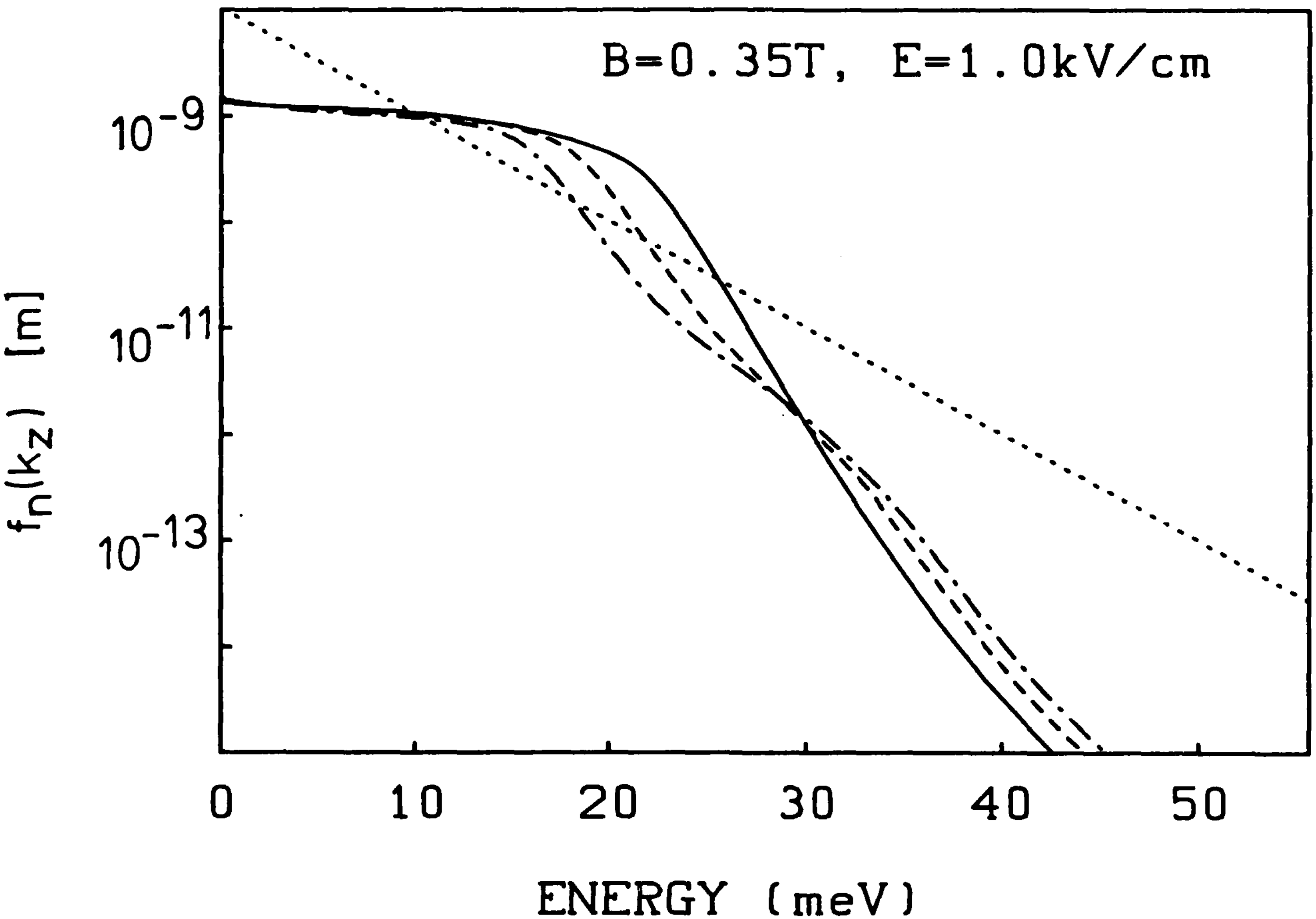
B=0.35T, E=1.0kV/cm
10^{-9}
10^{-11}
10^{-13}
$f_n(k_z)$ [m]
0
10
20
30
40
50
ENERGY (meV)

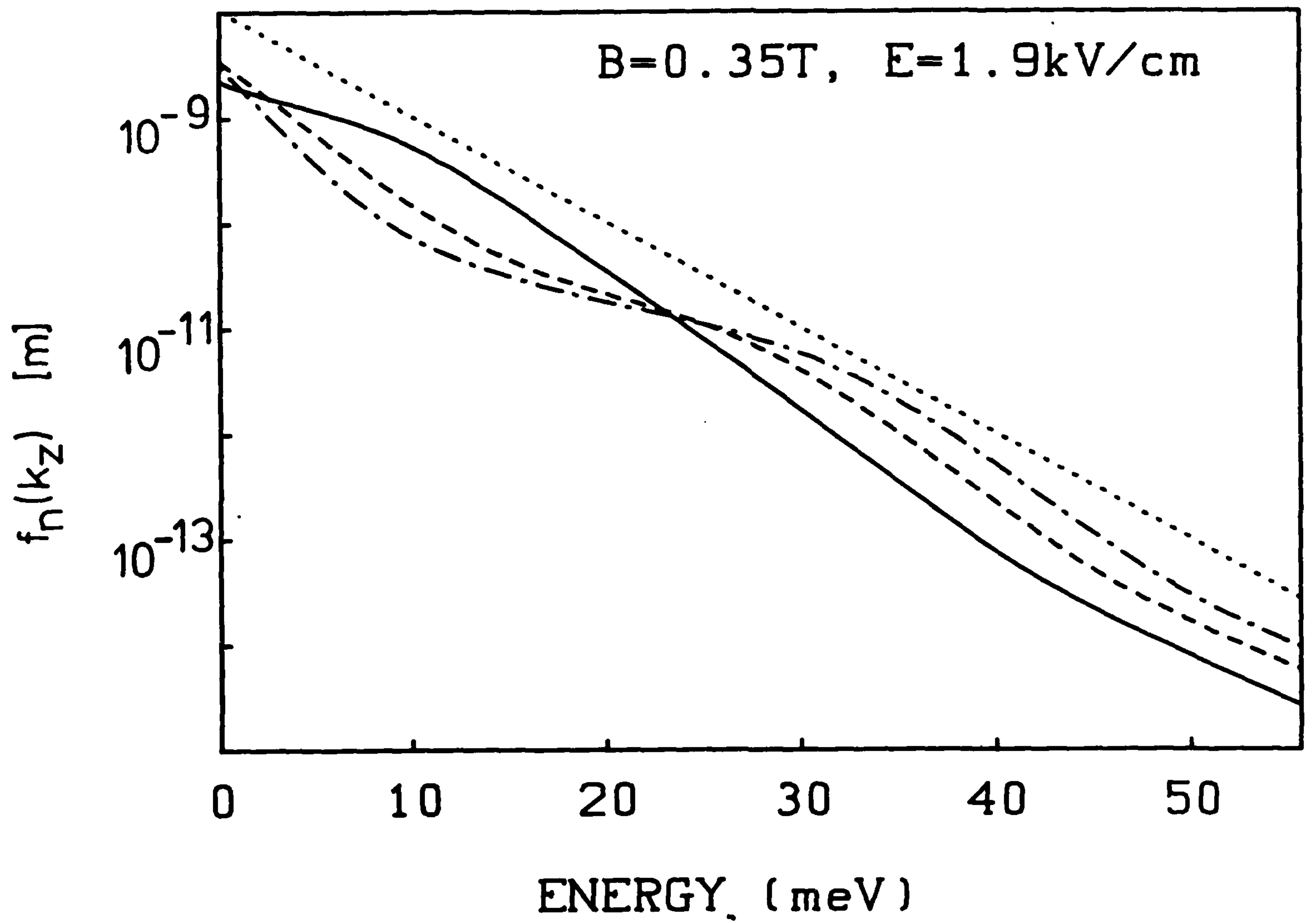

Fig 4b

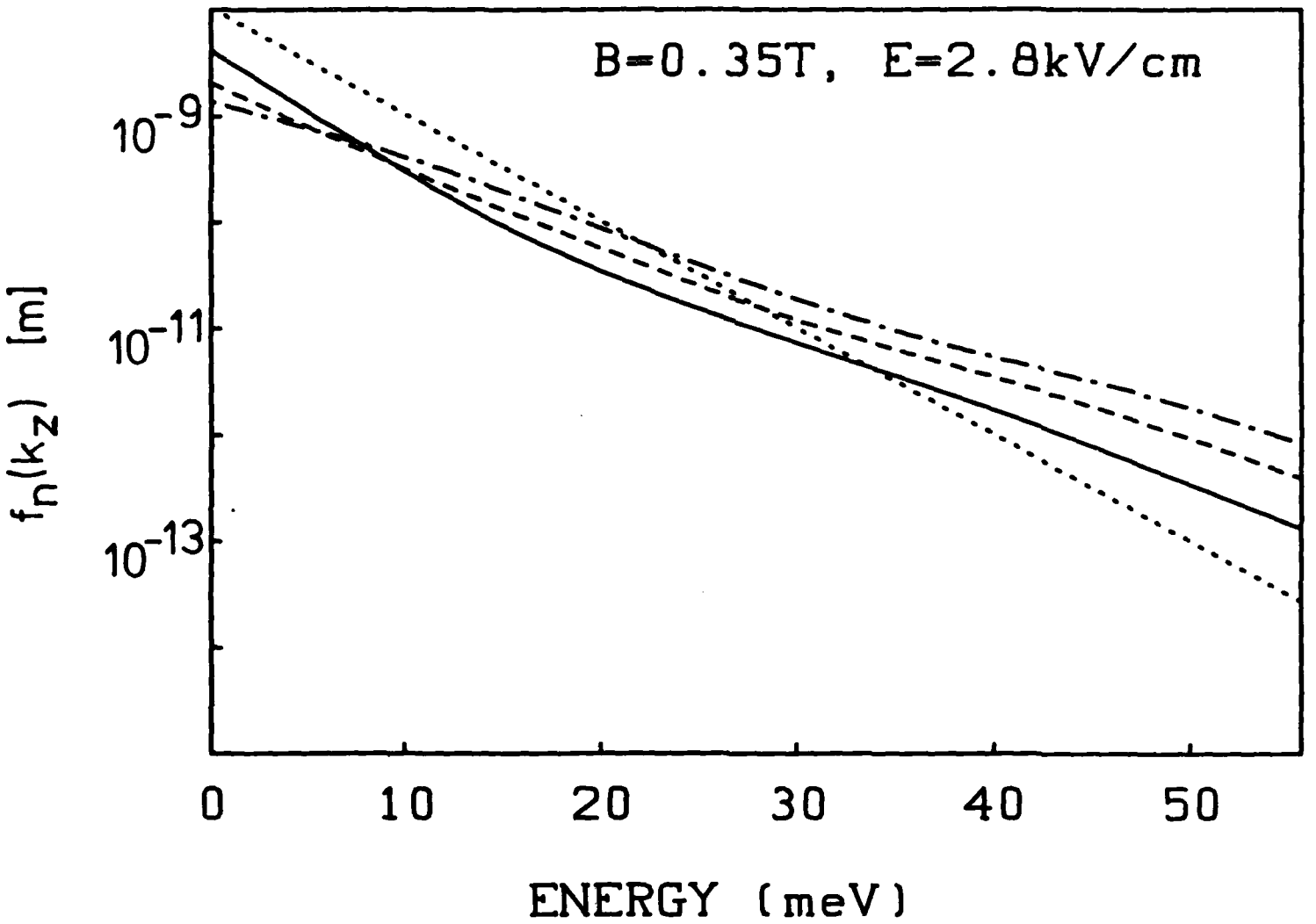

Fig 4c

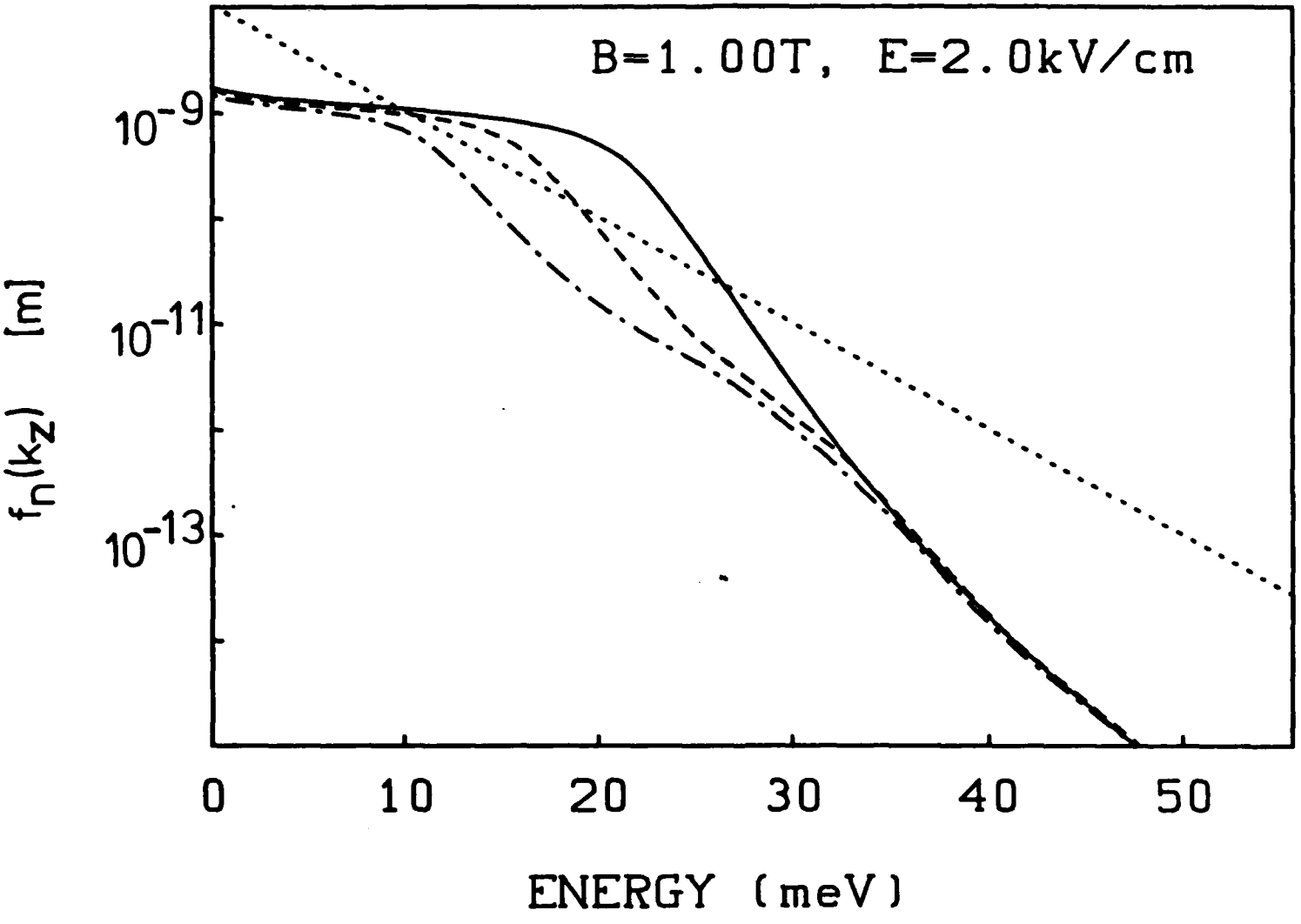

Fig 5a Holm et al

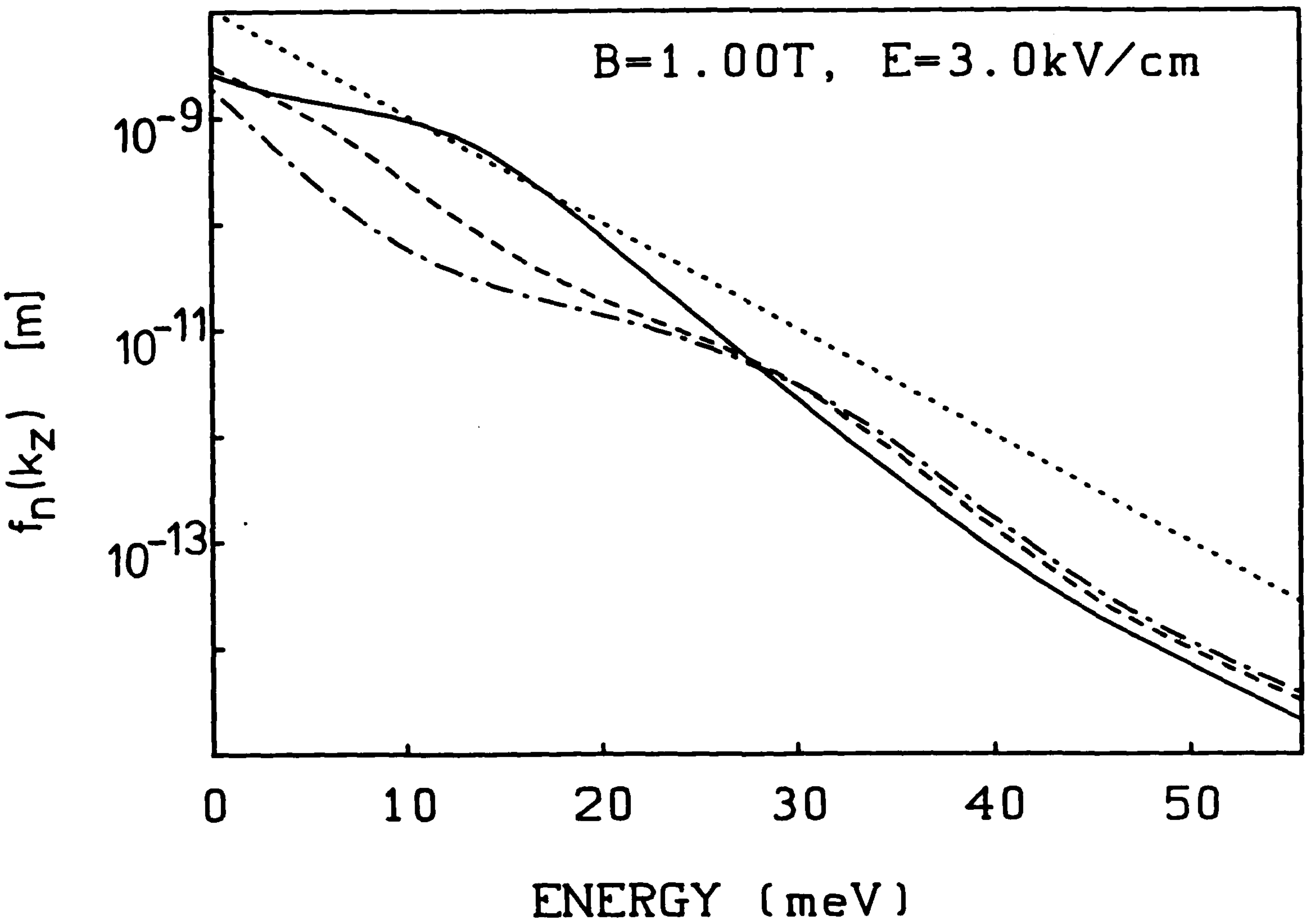

Fig 5E Helm et al

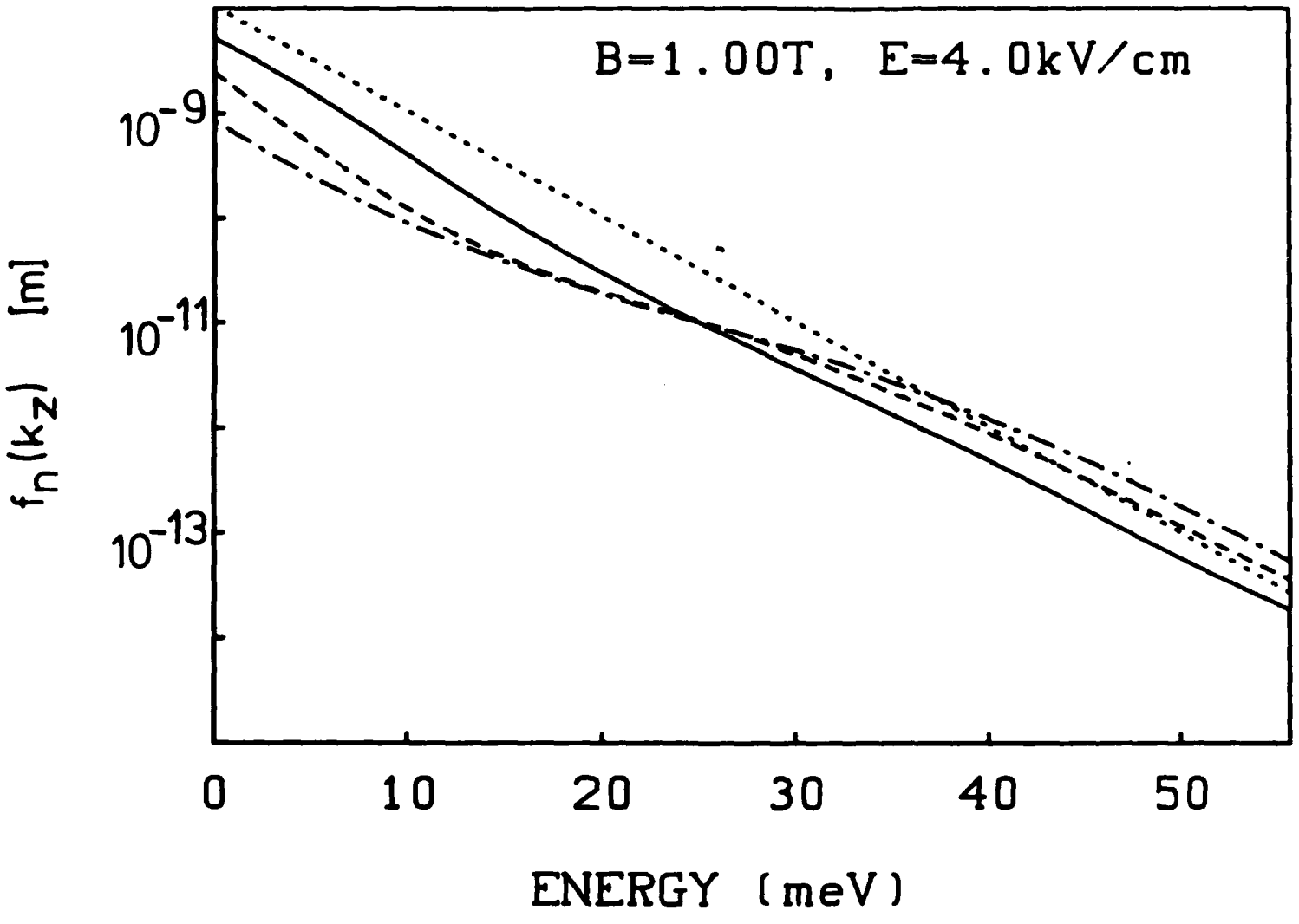

Fig 5c

Solid-State Electronics Vol. 31, No. 3/4, pp. 751–754, 1988
Printed in Great Britain

0038-1101/88 $3.00 + 0.00
Pergamon Journals Ltd

ANALYSIS OF CARRIER DISTRIBUTION FUNCTION THROUGH SMITH-PURCELL EFFECT IN GaAs/GaAlAs HETEROSTRUCTURES

E. Gornik, R. Christanell, R. Lassnig,
W. Beinstingl, K. Berthold
Institut für Experimentalphysik, Universität Innsbruck
A-6020 Innsbruck, Austria

G. Weimann
Forschungsinstitut der Deutschen Bundespost
D-6600 Darmstadt, Germany

ABSTRACT

We have observed for the first time the Smith-Purcell effect in GaAs-GaAlAs-heterostructures. A grating structure induces far infrared (FIR) emission from drifted carrier distributions, which is angle dependent and allows the determination of intrinsic carrier properties.

INTRODUCTION

The two-dimensional electrons in selectively doped GaAs/GaAlAs heterojunctions exhibit extremely high mobilities at low temperatures /1-3/. The electrons are easily heated up in an external electric field leading to a rapid rise in electron temperature /4-6/ and a reduction of electron mobility /7/. No detailed analysis of the form of the distribution function has been performed for extremely high mobilities. In this case normal Fermi distributions cannot be used since drift energies comparable with the Fermi energy can be achieved already at low electric fields.

In this paper we present a direct analysis of the electron distribution function for extremely high mobility samples as a function of the external electric field. The Smith-Purcell effect /8/ is measured in a semiconductor for the first time: A periodic potential of period L induces an energy loss of a drifting carrier distribution via photon emission. The angle between the drift and the grating momentum is varied by using different sample geometries. The geometry-dependent emission spectra are monitored through a magnetic-field-tuned InSb-detector /9/.

Through the selective momentum transfer ($\pm q = 2\pi/L$) the spectral analysis of the energy loss yields detailed information on the drifted electron distribution function. For a momentum transfer much smaller than the electron momentum, the frequency ω of the emitted light is directly proportional to the particle wavevector k:

$$\omega = \hbar kq/m^* = v_k q \qquad (q \ll k). \tag{1}$$

m^* is the electron mass. Thus the emitted spectra reflect directly the distribution of the carrier velocities v_k. In the following analysis the electron distribution function will be described as a shifted Fermi function:

$$f(E) = 1/(1 + \exp(\hbar^2 (k - k_D)^2/2m^* - \mu)/T_e), \tag{2}$$

introducing the drift momentum k_D and the drift-dependent electron temperature T_e as phenomenological parameters. Our model assumes that the distribution function is stationary, depending only on the electric field and the sample mobility. The FIR coupling represents only a negligible cooling process.

THEORY OF THE EMISSION PROCESS

FIR emission from a free electron system requires a second scattering process for momentum conservation, which can be either impurity or phonon scattering /10/. An electromagnetic calculation of the FIR emission from heated carriers through a grating was recently performed in ref. 4. For the electric field driven electrons, the lateral potential modulation $U_o \cos(qx)$ represents a coherent scattering source (the lattice vector has been taken in the x direction). Formally, it can be described as one "extended" impurity, scattering the electrons by $\pm q$. The emission

spectrum of a drifted electron distribution depends on the angle between the lateral structure and the electric field and thus the current direction.

We calculate the emission rate in the lowest order, including only the scattering processes shown in Fig. (1a). This diagrammatic approximation can be controlled analytically also for "badly" shaped electron distributions. Static screening is included in the impurity potential. Evaluating the diagrams Fig. (1a) and performing the sum over the photons the energy loss rate is obtained as:

$$\frac{dW}{dt} = \frac{e^2 U_0^2 q^2}{4\pi^2 m^* c^3 \hbar^4} \sum_{\pm} \frac{1}{|k_x^{\pm}|} \int_{-\infty}^{\infty} dk_y f(k_x^{\pm}, k_y) \{1 - f(k_x^{\pm} \pm q, k_y)\} , \qquad (3)$$

$$k_x^{\pm} = \mp\left(\frac{q}{2} + \frac{\omega m^*}{\hbar q}\right) .$$

The sum over (±) describes the two possible momentum transfers, and the k_y-integration has already been performed by exploiting the delta function for energy conservation. The influence of the electron distribution $f(k_x,k_y)$ is contained in the k_y sum, which is evaluated numerically.

Fig. (1b) shows the calculated energy-dependent emission intensity for the parameters of the sample described below, for an electron temperature of 35 K. The curves are weighted by ω in order to account roughly for the detector sensitivity. The full curve describes a carrier distribution which is heated by an electric field normal to the grating wavevector q. In this direction the result is independent of the drift velocity if a shifted Fermi distribution is used. In contrast, the broken line shows the result for the electric field parallel to q, with $v_D = 0.7\, v_F$: A substantial change of the emission characteristics is obtained. The spectrum splits into two broad structures. The shifts to higher and lower energies demonstrate the transition from normal free carrier emission to the Smith-Purcell regime (the low energy side disappears for still higher drift velocities). While the lower part of the spectrum is out of the range of our detector, the change on the high energy side should be observable when changing the orientation of the current with respect to the grating.

EXPERIMENT

We have plasma etched a periodic grating with lattice constant L into the top layer of a GaAs/GaAlAs heterostructure as shown in Fig. (2a). The height of the modulation was of the order of 200 A and the electron density is $2.8 \times 10^{11}/cm^2$. The modulation induces a periodic potential acting on the 2D electrons, which is evident from Shubnikov-de Haas (SdH) oscillations. At 4.2 K the samples had a zero field mobility of $2.0 \times 10^6 cm^2/Vs$ before plasma etching, and very narrow minima in σ_{xx}. After etching the mobility was only reduced to $1.5 \times 10^6 cm^2/Vs$, however the minima became much broader. We interpret this broadening as the appearance of a sinusoidal potential, leading to a local variation of the electron density. From the width increase of the SdH oscillation we estimate the size of the periodic potential to be of the order of 1 meV.

Two different sample geometries were realized: Sample 1 had the grating grooves parallel to the contacts (Fig. 2b), and as a result q//j. In sample 2 both geometries (q//j and q⊥j) are realized. The drift velocity and mobility versus the external electric field as derived from direct conductivity measurements of the small sample structure (Fig. 2b) at 4.2 K before and after the plasma etching are shown in Fig. (3). It is evident that the saturation drift velocity is already obtained for electric fields in the order of 100 V/cm. The observed dependences of v_D and μ are in good agreement with the theoretical calculation of Lei et al. /11/, based on a non-Boltzmann balance equation approach and using a drifted Fermi/Dirac distribution with temperature T_e.

The analysis of the emitted radiation in the presence of a periodic potential allows us to answer the question whether the drift velocities are realistic and what is the average temperature of the carrier distribution. Emission spectra for a plasma etched sample 1 (Fig. 2b) for several electric fields are shown in Fig. (4). For the lowest electric field the detector response is only due to broad band thermal emission from the heated electron distribution /4/. Above an electric field of 30 V/cm the emission spectra start to show a structure around a magnetic field of 0.3 T, which develops to a clear but broad peak at 100 and 150 v/cm. The spectra show a clear shift between 50 and 100 V/cm, indicated by the arrow which marks the decay of the signal.

For samples without a grating the spectra show a similar form as the curve for 10 V/cm for all electric fields, but the broad peak around 0.3 T is missing. Consequently the additional structure can be directly attributed to Smith-Purcell type emission.

To demonstrate that the observed emission is due to the grating induced potential we prepared a sample where the grating wavevector q is oriented both parallel and normal to the current direction. In Fig. (5) a comparison of the emission for q//j (dashed curve) and q⊥j (full curve) is shown for an electric field of 100 V/cm. In both orientations radiation due to the Smith-Purcell effect is observed. It is evident that the spectrum for q//j is shifted to higher energies. In the q⊥j case the scattering depends essentially on the carrier temperature, independent of the drift velocity. The emission comes mainly from carriers moving with the Fermi velocity perpendicular to the current direction.

From this experiment it is directly evident that the shift of the spectra is due to the drift of the carriers. The spectra thus show the behaviour predicted by the theory (Fig. 1b). For the given situation the shift can be converted into the drift velocities, although we have to keep in mind that the detector has a rather limited resolution of 1 meV and that the emitted spectrum is quite broad.

As an additional proof that the emission is due to the high carrier velocity we reduced the carrier velocity with an applied magnetic field perpendicular to the 2D-plane. The selective emission and the difference in the spectra between j//q and j⊥q disappeared as shown in Fig. (5) for a magnetic field of 1.5 T.

As a rough estimate we obtain a drift velocity of 1.5×10^7 cm/s for 100 V/cm. This drift velocity is somewhat smaller than that derived from current measurements. In addition we can estimate the carrier temperature: It has to be in the order of 40 - 50 K from a fit of the decaying part of the spectra which are marked by arrows. Our calculations show that for considerably higher temperatures (T_e > 70 K) the spectra become extremely broadened and it would not be possible to observe well-defined structures with the given resolution of the InSb detector.

REFERENCES

/1/ H.L. Störmer, R. Dingle, A.C. Gossard, W. Wiegmann, and M.D. Sturge, Solid State Commun. 29, 705 (1979).
/2/ K. Hirakawa and H. Sakaki, Phys. Rev. B33, 8291 (1986).
/3/ J.J. Harris, C.T. Foxon, D.E. Lacklison, and K.W.J. Barnham, Superlattices and Microstructures 2, 563 (1986).
/4/ R.A. Höpfel and G. Weimann, Appl. Phys. Lett. 46, 291 (1985).
/5/ H. Sakaki, K. Hirakawa, J. Yoshino, S.P. Svensson, Y. Sekiguchi, T. Hotta, S. Nishii, and N. Miura, Surf. Sci. 142, 306 (1984).
/6/ J. Shah, A. Pinczuk, H.L. Störmer, A.C. Gossard, and W. Wiegmann, Appl. Phys. Lett. 42, 55 (1983).
/7/ J. Shah, A. Pinczuk, H.L. Störmer, A.C. Gossard, and W. Wiegmann, Appl. Phys. Lett. 44, 322 (1984).
/8/ S.J. Smith, E.M. Purcell, Phys. Rev. 92, 1069 (1953).
/9/ E. Gornik, W. Müller, F. Kohl, IEEE Transactions on Microwave Theory and Techniques MTT 22, 991 (1974).
/10/ G.D. Mahan, in Many Particle Physics, Plenum Press 1981, p. 707
/11/ X.L. Lei, J.Q. Zhang, J.L. Birman, C.S. Ting, Phys. Rev. B33, 4382 (1986).

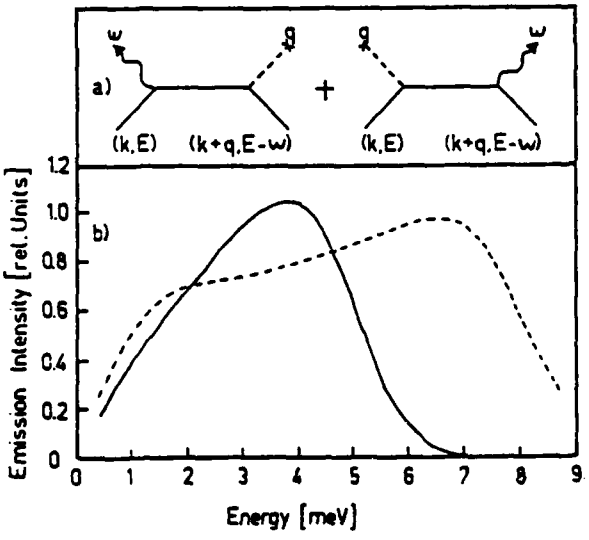

Fig. 1:
(a) Scattering diagrams used for the theoretical calculation.
(b) Calculated emission intensity versus frequency from drifted electron distributions with a temperature of 35 K, comparing j⊥q (full curve) with j//q (broken curve). The spectra are weighted by ω to account roughly for the detector sensitivity.

Fig. 2

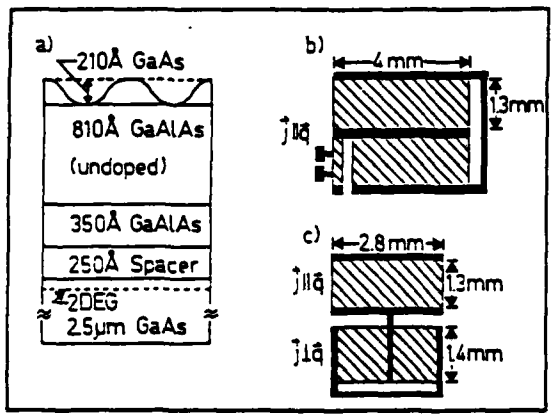

Fig. 4

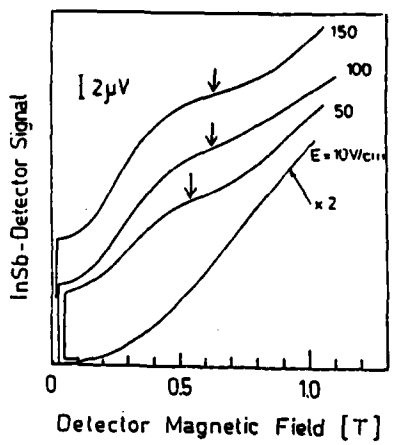

Fig. 3

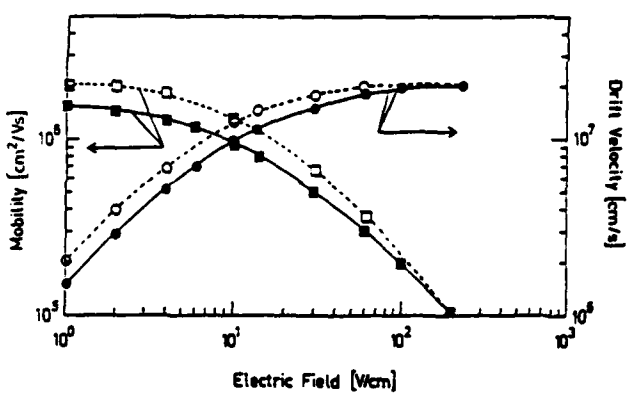

Fig. 5

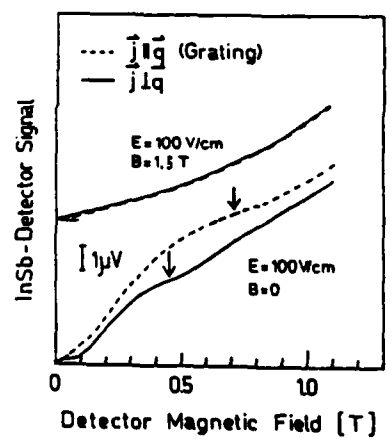

Fig. 2:

Schematical drawing of the GaAs-GaAlAs structures with periodic grating used in the experiments (a). Sample 1 with the contacts parallel to the grating (b) and sample 2 with contacts both parallel and normal to the grating wavevector (c).

Fig. 3:

Mobility and drift velocity of the electrons as a function of the electric field. Open symbols: Before plasma etching. Full symbols: After plasma etching. Due to the high sample mobility the drift velocity saturates already at low electric fields.

Fig. 4:

Emission spectra from drifted electron distributions with j//q, for different electric field strengths. The broad structure appearing at high fields is a consequence of the grating-induced emission.

Fig. 5:

Emission spectra from drifted electron distributions, comparing geometries with j//q and j⊥q. A magnetic field normal to the interface destroys the selective emission.

END

DATE

FILMED

8-88

DTIC